TESTS FOR THE CHARACTERIZATION OF REPLICATED MASONRY AND WALL TIES

Physical Testing and Modelling – Masonry Structures

Rita Esposito, Francesco Messali and Jan Rots

TU Delft

Date April 2016

Editors Jan van Elk & Dirk Doornhof

General Introduction

For the modeling of the seismic response of unreinforced masonry buildings, knowledge of the properties of building material is essential. An experimental program to test the properties of the building materials used in the Groningen area was therefore executed. This included measurements of material in existing buildings (Ref. 1) and in laboratories.

This report describes experiments for the characterization of replicated masonry wall elements of calcium silicate and clay bricks. Especially, the impact of the wall ties (spouwanker) between the front and back walls of cavity wall elements has been investigated. Testing procedures are presented and results discussed. The result of these experiments, together with those of other experiments, have been compiled in summary documents of material properties (Ref. 2 and 3).

The results of these experiments, material properties for masonry building materials, have been used in the modelling of the seismic response of masonry buildings (Ref. 4 and 5).

References

1. In-situ testing of URM houses (building unit: Loppersum, Zijlvest 25), Eucentre (F. Graziotti, A. Rossi, I. Senaldi, S. Peloso), 5th December 2014.
2. Material Characterisation – Version 1.3, Eucentre, P&P, TU-Delft, TU-Eindhoven, October 2015.
3. Summary report for the characterisation of original Groningen masonry, TU Delft (S. Safari, J. Rots), 18th December 2015.
4. URM Modelling and Analysis Cross Validation – Arup, Eucentre, TU Delft, Reference 229746_032.0_REP127_Rev.0.03 April 2015.
5. Eucentre Shake-table Test of Terraced House Modelling Predictions and Analysis Cross Validation, staff from ARUP, Eucentre (Pavia) and TU Delft, November 2015 [this document also includes; (1) Instruments full-scale test-house Eucentre Laboratory, (2) Protocol for Shaking Table Test on Full Scale Building (Eucentre) V_1, and (3) Selection of Acceleration Time-Series for Shake Table Testing of Groningen Masonry Building at the EUCENTRE, Pavia, all three by staff from Eucentre (Pavia)].

<table>
<tr><td rowspan="2">Title</td><td rowspan="2" colspan="2">TESTS FOR THE CHARACTERIZATION OF REPLICATED MASONRY AND WALL TIES
Physical Testing and Modelling – Masonry Structures</td><td>Date</td><td>April 2016</td></tr>
<tr><td>Initiator</td><td>NAM</td></tr>
<tr><td>Autor(s)</td><td>Rita Esposito, Francesco Messali and Jan Rots</td><td>Editors</td><td colspan="2">Jan van Elk and Dirk Doornhof</td></tr>
<tr><td>Organisation</td><td>TU Delft</td><td>Organisation</td><td colspan="2">NAM</td></tr>
<tr><td>Place in the Study and Data Acquisition Plan</td><td colspan="4"><u>Study Theme:</u> Seismic Response of Buildings (URM)
<u>Comment:</u>
For the modeling of the seismic response of unreinforced masonry buildings, knowledge of the properties of building material is essential. An experimental program to test the properties of the building materials used in the Groningen area was therefore executed. This included measurements of material in existing buildings (Ref. 1) and in laboratories. This report describes experiments for the characterization of replicated masonry wall elements of calcium silicate and clay bricks. Especially, the impact of the wall ties (spouwanker) between the front and back walls of cavity wall elements has been investigated. Testing procedures are presented and results discussed. The result of these experiments, together with those of other experiments, have been compiled in summary documents of material properties (Ref. 2 and 3).
The results of these experiments, material properties for masonry building materials, have been used in the modelling of the seismic response of masonry buildings (Ref. 4 and 5).</td></tr>
<tr><td>Directliy linked research</td><td colspan="4">(1) Building Material properties
(2) Shake table tests
(3) Fragility curves for building typologies (URM)
(4) Risk Assessment</td></tr>
<tr><td>Used data</td><td colspan="4">Experiments</td></tr>
<tr><td>Associated organisation</td><td colspan="4">NAM</td></tr>
<tr><td>Assurance</td><td colspan="4">TU Delft</td></tr>
</table>

Project number	C31B60
Report number	
Date	April 18, 2016
Version	8
Status	Final

TESTS FOR THE CHARACTERIZATION OF REPLICATED MASONRY AND WALL TIES

Physical Testing and Modelling – Masonry Structures

Client: Nederlandse Aardolie Maatschappij B.V.

Authors Rita Esposito
R.Esposito@tudelft.nl
Francesco Messali
F.Messali@tudelft.nl
Jan Rots
J.G.Rots@tudelft.nl

Lab collaborators Roy Crielaard
Matteo Maragna

Address Delft University of Technology
Faculty of Civil Engineering and Geosciences
Stevinweg 1, 2628 CN, Delft

Liability statement
TU Delft and those who have contributed to this publication did exercise the greatest care in putting together this publication. However, the possibility should not be excluded that it contains errors and imperfections. Any use of this publication and data from it is entirely on the own responsibility of the user. For everybody who has contributed to this publication, TU Delft disclaims any liability for damage that could result from the use of this publication and data from it, unless the damage results from malice or gross negligence on the part of TU Delft and/or those who have contributed to this publication.

Table of Contents

1 Introduction

The NAM Hazard & Risk work stream as well as the NAM Structural Upgrading work stream heavily depend on non-linear finite element (FEM) analysis for masonry. In addition to non-linear static push-over analyses, non-linear dynamic time domain analyses become increasingly popular in order to assess the seismic capacity of Groningen buildings. These high-end analyses give direct engineering answers, but also serve as validation to simplified approaches that can then be inserted in large-scale probabilistic fragility studies or structural design.

Non-linear FEM codes employ constitutive models that describe the material behaviour. The constitutive models require input material parameters for stiffness, strength and ductility in compression, tension and shear. Subsets of those material parameters are also required for other purposes, like serving analytical structural models, and serving linear lateral force methods or linear response spectrum analyses where results in terms of generalized forces for masonry piers and spandrels have to be judged against material capacities.

The need for benchmarks to validate numerical models led to the set-up of a large scale testing program on replicated masonry. The campaign investigates the behaviour of masonry at material, connection, component and assemblage level. The focus was on typical masonry house typologies from the period 1960-1980. The selected case study was a two-story high terraced house characterised by: 1) cavity walls composed of an inner leaf in calcium silicate masonry and an outer leaf in clay masonry connected by masonry wall ties, 2) solid pre-fabricated concrete floor having a dry connection with the loadbearing masonry walls.

In this report, the attention is focussed on the material and connection characterisation related to the selected assemblage case study.
For both calcium silicate and clay masonry, the material properties as well as their behaviour under compression (Section 6), bending (Section 7 and 8) and shear (Section 9) loading are provided, together with information related to masonry constituents (mortar and masonry units, Sections 4 and 5).
The behaviour of connections is studied by performing friction tests on the floor-to-wall connection (Section 10 and 11) and test on masonry wall ties (Section 12).
A comparison between the experimental results and the material properties defined in design standard is presented in Section 13.
Eventually, a summary and an overview of the material properties are reported in Section14.

2 Nomenclature

2.1 Symbols

This report adopts mainly the nomenclature used in Eurocode 6 [1]. In addition, symbols used in the codes for testing are adopted.

α	Masonry (bed joint) angle of internal friction
α^*	Angle of internal friction of the dry connection (mortar bed joint) between concrete floor and masonry wall
α_{res}	Masonry (bed joint) residual angle of internal friction
α^*_{res}	Residual angle of internal friction of the dry connection (mortar bed joint) between concrete floor and masonry wall
ν	Poisson ratio of masonry
μ	Masonry (bed joint) shear strength coefficient
μ^*	Shear strength coefficient of bed joint between concrete and masonry
μ_{res}	Masonry (bed joint) residual shear strength coefficient
μ^*_{res}	Residual shear strength coefficient of bed joint between concrete and masonry
d_1	Distance between bearing supports
d_2	Distance between loading supports
d_3	Distance between the loading and bearing supports (four-point bending test)
f_b	Compressive strength of masonry unit
f_{bt}	Flexural strength of masonry unit
f_{cc}	28-day cubic compressive strength of concrete
f_{ik}	Characteristic value of the *i*-th property
$f_{ik,EC6}$	Characteristic value of the *i*-th property as prescribed by Eurocode 6
$f_{ik,NPR}$	Characteristic value of the *i*-th property as prescribed by NPR 9096-1-1:2012
f_m	Compressive strength of masonry mortar
f_{mt}	Flexural strength of masonry mortar
f'_m	Compressive strength of masonry in the direction perpendicular to the bed joints
$f'_{m,h}$	Compressive strength of masonry in the direction parallel to the bed joints
f_p	Applied lateral pre-compression stress
f_{x1}	Masonry flexural strength with the moment vector parallel to the bed joints and in the plane of the wall, which generates a plane of failure parallel to the bed joints
f_{x2}	Masonry flexural strength with the moment vector orthogonal to the bed joints and in the plane of the wall, which generates a plane of failure perpendicular to the bed joints
f_{x3}	Masonry flexural strength with the moment vector orthogonal to the plane of the wall
f_{v0}	Masonry (bed joint) initial shear strength
f^*_{v0}	Initial shear strength of the dry connection (mortar bed joint) between concrete floor and masonry wall

$f_{v0,res}$	Masonry (bed joint) residual initial shear strength
$f^{*}_{v0,res}$	Residual initial shear strength of the dry connection (mortar bed joint) between concrete floor and masonry wall
f_w	Masonry uniaxial bond strength between the masonry unit and the mortar
l_j	Length of the mortar bed joint in a masonry specimens
l_m	Length of the mortar specimen
l_s	Length of the masonry specimen as built
l_p	Length of the loading plate for compression tests on mortar specimens
l_u	Length of the masonry unit as used in the construction of masonry
h_m	Height of the mortar specimen
h_s	Height of the masonry specimen as built
h_u	Height of the masonry unit as used in the construction
t_s	Thickness of the masonry specimen as built
t_m	Thickness of the mortar specimen
t_u	Thickness of the masonry unit as used in the construction of masonry
$s_{F_{c,0}}$	Slip of the tie corresponding to the maximum compressive force $F_{c,0}$
$s_{F_{c2}}$	Slip of the tie corresponding to the maximum compressive force $F_{c,2}$
$s_{F_{po,0}}$	Slip of the tie corresponding to the maximum tensile force $F_{po,0}$
$s_{F_{po,1}}$	Slip of the tie corresponding to the maximum tensile force $F_{po,1}$
$s_{F_{po,2}}$	Slip of the tie corresponding to the maximum tensile force $F_{po,2}$
v_{el}	Vertical displacement corresponding to the load F_{el}
w_j	Width of the mortar bed joint in a masonry specimen
A_s	Cross sectional area of the specimen parallel to the bed joints (shear test)
E_{bt}	Elastic modulus of masonry unit
E_1	Secant elastic modulus of masonry subject to a compressive loading perpendicular to the bed joints, evaluated at 1/3 of the maximum stress
E_2	Secant elastic modulus of masonry subject to a compressive loading perpendicular to the bed joints, evaluated at 1/10 of the maximum stress
E_3	Chord elastic modulus of masonry subject to a compressive loading perpendicular to the bed joints, evaluated at between 1/10 and 1/3 of the maximum stress
$E_{1,h}$	Secant elastic modulus of masonry subject to a compressive loading parallel to the bed joints, evaluated at 1/3 of the maximum stress
$E_{2,h}$	Secant elastic modulus of masonry subject to a compressive loading parallel to the bed joints, evaluated at 1/10 of the maximum stress
$E_{3,h}$	Chord elastic modulus of masonry subject to a compressive loading parallel to the bed joints, evaluated at between 1/10 and 1/3 of the maximum stress
F_1	Applied vertical load (bond-wrench test)
F_2	Vertical load due to the weight of the top clamping system (bond-wrench test)
F_3	Vertical load due to the top masonry unit (bond-wrench test)

$F_{c,0}$	Maximum compressive load capacity of tie subject monotonic compressive load
$F_{c,2}$	Maximum compressive load capacity of tie subject fully cyclic load
F_{el}	Selected vertical load value in the linear elastic stage (flexural test of masonry unit)
$F_{\max}$	Maximum vertical load
F_{p}	Applied lateral pre-compression force (shear test)
$F_{po,0}$	Maximum tensile load capacity of tie subject monotonic tension load
$F_{po,1}$	Maximum tensile load capacity of tie subject cyclic tension load
$F_{po,2}$	Maximum tensile load capacity of tie subject fully cyclic load
G_{f-c}	Fracture energy in compression for loading perpendicular to the bed joints
$G_{f-c,h}$	Fracture energy in compression for loading parallel to the bed joints
P_{i}	i-th property (used for comparison)
$M_{\max}$	Maximum bending moment
W	Section modulus

2.2 Abbreviations

Avg.	Average
C.o.V.	Coefficient of variation
CS	Calcium silicate
LVDT	Linear variable differential transformer
St. dev.	Standard deviation

3 Construction of the samples

The masonry specimens were built in the Stevin II laboratory at the Delft University of Technology. Two type of masonry were used: calcium silicate and clay masonry. The former was made of calcium silicate bricks and cement based mortar, while the second one was made of perforated clay bricks and hydraulic lime mortar. The declarations of performance of the materials are reported in Appendix A.
Figure 1 shows the adopted masonry units. Their dimensions are defined considering the orientation of the masonry unit as used in the construction of the masonry. This definition is consistently adopted in this report despite the position of the specimen in the test set-up. A similar consideration is applied to describe the dimensions of masonry specimens.

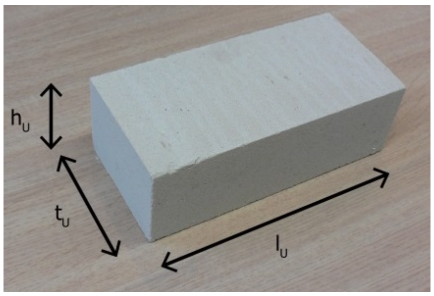

(a)

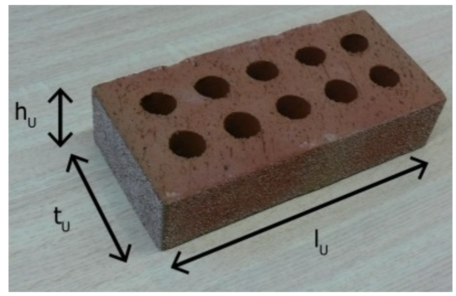

(b)

Figure 1 – Calcium silicate and clay bricks.

In order to ensure quality control, the construction followed the prescription as reported in the construction protocol [2]:

- The bags of mortar mix have been stored dry and separated from the soil;
- The mortar mix has been used within 18 months after production;
- The mortar has been mixed with clean water;
- The mortar has been prepared using a fixed water content;
- The flow of the mortar should be determined in agreement with EN 1015-3:1999 [3].
- At least three samples of mortar (size 160x40x40-mm^3) should be made at every start of the day during construction of masonry for testing the properties. The samples will be tested under flexural and compressive loading in agreement with EN 1015-11:1999 [4];
- The mortar has been prepared and used between 5 and 25 degrees;
- The mortar has been used within 2 hours after preparation;
- No additives have been mixed after preparation of the mortar;
- Bricks have been covered against moisture;
- Bricks were clean before use;
- Bricks have not been wetted before use;

The mortar was prepared with fixed water content per bag of mix (25 kg): 2.8 l/bag for calcium silicate masonry and 3.7l/bag for clay masonry.

4 Flexural strength of masonry unit

The flexure strength of the masonry unit was determined with the three-point bending test following NEN 6790:2005 [5]. The test was also used to determine the elastic modulus of the masonry unit.

4.1 Testing procedure

The masonry units were tested by having the bed joint plane parallel to the loading direction (Figure 2). The specimen was supported by two roller bearings, which were placed 10 mm from the end of the specimen. A third roller was used to apply load to the specimen at mid-span. Table 1 lists the dimensions of the masonry units and the distance between the supports.

The test was carried out by a displacement controlled apparatus including a hydraulic jack with 100 kN capacity. A spherical joint, between the upper roller and hydraulic jack, was used to minimise load eccentricity. To obtain the failure of the specimen in 30 to 90 s, a displacement rate of 0.02 mm/s was adopted. The applied load was recorded from the load cell attached to the hydraulic jack.

Two LVDTs were attached to the specimens to measure horizontal and vertical displacements. On the front side, a horizontal LVDT measured the elongation between two points on the masonry unit. On the back side the vertical displacement at mid-span of the masonry unit, relative to its supports, was measured. The LVDTs had a measuring range of 10 mm with an accuracy of 0.5%.

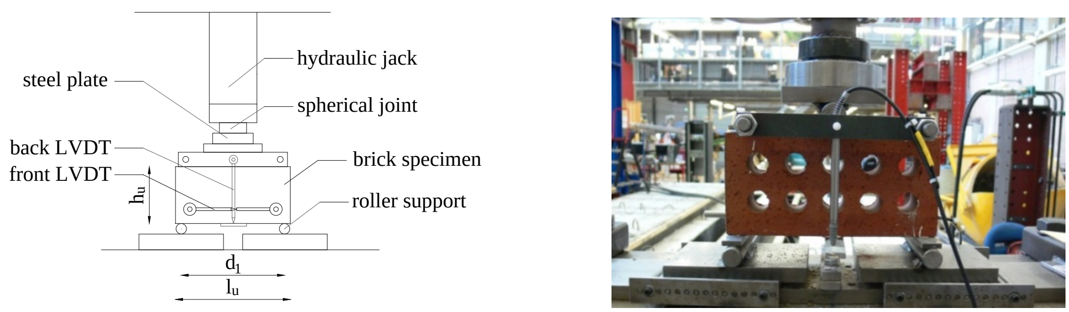

(a) (b)

Figure 2 – Three-point bending test on masonry unit.

Table 1 – Dimensions of the masonry units and distance d_1 between the bearing supports.

Masonry type	Sample name	l_u	t_u	h_u	d_1
		mm	mm	mm	mm
Calcium silicate bricks	TUD_MAT-B11a	212	106	72	192
	TUD_MAT-B11b	212	104	70	192
	TUD_MAT-B11c	212	104	70	191
	TUD_MAT-B11d	213	101	70	192
	TUD_MAT-B11e	213	104	70	192
	TUD_MAT-B11f	212	102	71	189
Clay bricks	TUD_MAT-B21a	212	102	50	193
	TUD_MAT-B21b	214	103	52	192
	TUD_MAT-B21c	213	103	51	192
	TUD_MAT-B21d	213	103	50	193
	TUD_MAT-B21e	209	101	48	189
	TUD_MAT-B21f	213	102	50	191
	TUD_MAT-B21g	210	100	49	190

4.2 Experimental results

The flexural strength of the masonry unit f_{bt} was determined as [3]:

$$f_{bt} = \frac{3}{2}\frac{F_{max} d_1}{h_u t_u^2} \tag{1}$$

where F_{max} is the maximum load, d_1 is the distance between the supports, h_u is the height of the masonry unit, t_u is the thickness of the masonry unit.
Assuming a linear stress distribution over the height of the brick's cross-section, the elastic modulus E_b of the masonry units can be determined as follows:

$$E_b = \frac{F_{el} d_1^3}{48 v_{el} I} \tag{2}$$

where F_{el} and v_{el} are the load and vertical displacement in the linear elastic stage, respectively and I is the moment of inertia of the masonry unit along the cross-section. In the case perforated masonry units, the reduced moment of inertia was considered.

Figure 3 shows the typical displacement-force diagrams for the two types of bricks. The bricks presented a brittle failure when the maximum force was reached. The behaviour was linear approximatively until 90% of the peak load, while some nonlinearity occurs just before the peak.
Table 2 lists the results in terms of flexural strength and elastic modulus.
The *calcium silicate bricks* showed a low variation in strength with an average flexural strength of 2.74 MPa. A symmetric crack pattern was observed (Figure 4a). The calcium silicate bricks used for replicated masonry show a lower flexural strength with respect to brick extracted from existing buildings, which presented strength values of 3.9 MPa for “poor” quality masonry and 4.8 MPa for “good” quality masonry [6]. This variation can be mainly correlated to the properties of the raw material and the porosity of the bricks. Furthermore, the environmental conditions and the long term loading of the bricks in the fields can influence the mechanical property of the brick (e.g. carbonatation).
The *clay bricks* showed a higher variation in strength. In particular samples TUD_MAT-B21e and TUD_MAT-B21g showed strength values of approximatively 6 MPa and an asymmetric crack pattern (Figure 4c), while the majority of the samples showed strength values around 4 MPa and symmetrical crack pattern (Figure 4b). The stronger bricks appeared darker in colour and slightly smaller in dimensions. To understand the representativeness of this subcategory of bricks, dimensions and colour were considered to perform a screening of the perforated clay bricks. Over 900 bricks only 11, corresponding to 1.2%, were identified. As a consequence, this subcategory represents a minority. By excluding this subcategory, the average flexural strength would be lower and approximatively 4.2 MPa.

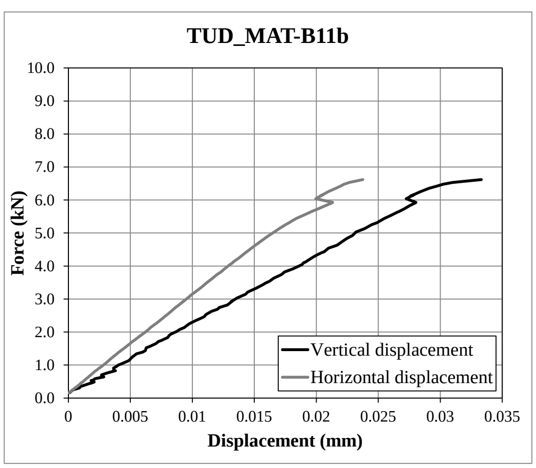

(a)

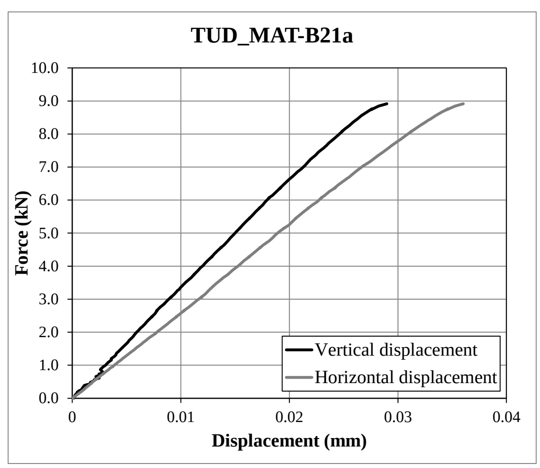

(b)

Figure 3 – Force-displacements curve (LVDTs readings) of three-point bending test on: (a) calcium silicate brick; (b) clay brick.

Table 2 – Flexural strength and elastic modulus for calcium silicate and clay bricks.

Calcium silicate bricks			Clay bricks		
Sample name	f_{bt}	E_{bt}	**Sample name**	f_{bt}	E_{bt}
	MPa	MPa		MPa	MPa
TUD_MAT-B11a	2.70	14080	TUD_MAT-B21a	4.96	14141
TUD_MAT-B11b	2.52	5184	TUD_MAT-B21b	3.81	5405
TUD_MAT-B11c	2.89	8397	TUD_MAT-B21c	4.23	6624
TUD_MAT-B11d	2.97	9921	TUD_MAT-B21d	4.22	4300
TUD_MAT-B11e	2.69	6137	TUD_MAT-B21e*	6.07	10379
TUD_MAT-B11f	2.67	10221	TUD_MAT-B21f	4.11	2912
			TUD_MAT-B21g*	6.03	6714
Average	**2.74**	**8990**		**4.78**	**7211**
Standard deviation	**0.16**	**3202**		**0.94**	**3849**
Coefficient of variation	**0.06**	**0.36**		**0.20**	**0.53**

* asymmetric crack pattern

(a)

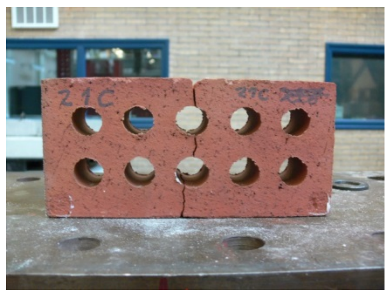

(b)

(c)

Figure 4 – Crack pattern: (a) calcium silicate brick; (b) symmetric crack patter for clay brick; (c) asymmetric crack pattern for clay brick.

5 Flexural and compressive strength of mortar

During the masonry construction, mortar samples were collected and cast in moulds to be tested for the flexural and compressive strength in agreement with EN 1015-11:1999 [4]. The consistency of the mortar was determined in accordance with EN 1015-3:1999 [3].

5.1 Testing procedure

During each day of construction, at least three mortar specimens having a length of l_m = 160 mm, a height of h_m = 40 mm and thickness of t_m = 40 mm were collected. The samples were stored in controlled conditions. The first two days they were placed in a fog room (T = 20 ± 2 °C, RH = 95 ± 5%) with the moulds. After two days, they were unmoulded and kept for other five days in the fog room. Eventually, they were placed in a conditioning room with a temperature of 20 ± 2 °C and a relative humidity of 50 ± 5 % until testing. The test was performed after at least 28 days from construction.

The flexural strength was determined by three-point bending test (Figure 5a). The test set-up is composed by two steel bearing rollers having a diameter of 10 ± 0.5 mm and spaced d_1 = 100 ± 0.5 mm. A third roller is centrally placed on top of the sample to apply the load.

The compression test was performed on the broken pieces obtained from the flexural test, which have at least a length of 40 mm. The specimen is placed between two steel plates with a length of l_p = 40 mm. For the interpretation of the results the specimen is considered to be 40x40x40-mm (Figure 5b).

For both test, the load was applied without shock at a uniform rate so that failure occurred within a period of 30 to 90 s. The maximum load was recorded.

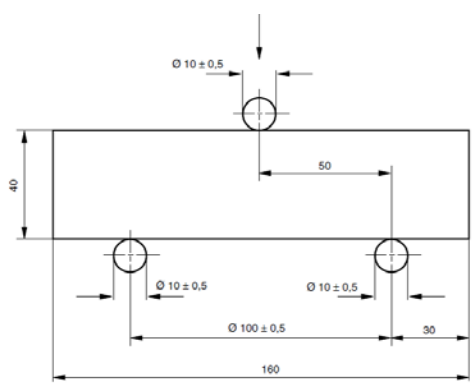

(a)

(b)

Figure 5 – Test on masonry mortar specimens: (a) three-point bending test; (b) compression test.

5.2 Experimental results

The flexural strength f_{mt} of the mortar was calculated as [4]:

$$f_{mt} = \frac{3}{2}\frac{F_{\max} d_1}{t_m h_m^2} \qquad (3)$$

where F_{max} is the maximum load, d_1 is the distance between the supports (100 mm ± 0.5 mm), h_m is the height of the mortar specimen (40 mm) and t_m is the thickness of the mortar specimen (40mm).
The compressive strength f_m of the mortar was calculated as [4]:

$$f_m = \frac{F_{\max}}{t_m l_p} \qquad (4)$$

where F_{max} is the maximum load, t_m is the thickness of the mortar specimen (40 mm) and l_p is the length of the loading plate (40 mm).

5.2.1 Mortar specimens casted during the first construction period

In the first construction period, small-scale specimens and large-scale walls were built during March and April 2015. The first were used to tests the material properties (MAT specimens), while the second to study the in-plane and out-of-plane behaviour of walls (COMP specimens). During this period, the properties of fresh and hardened mortar were measured.

Both mortars showed a similar consistency, which was evaluated with the diameter of the cone obtained by the flow test described in EN 1015-3:1999 [3]. In both cases, the diameter varied between 160 to 180 mm (Table 3).

Figure 6 shows the statistical distribution of flexural and compressive strength of both types of mortar. Tests were performed on randomly selected specimens.

Table 4 lists the results for the *calcium silicate masonry mortar*. Three-point bending tests were performed on 31 specimens and compressive tests on 65 specimens. The mortar has a compressive strength of 6.6 MPa and flexural strength of 2.8 MPa. In both cases, the coefficient of variation is limited to less than 10%.
Table 5 lists the results for the *clay masonry mortar*. Three-point bending tests were performed on 23 specimens and the compressive tests on 48 specimens. The mortar has a compressive strength of 6.1 MPa and flexural strength of 2.4 MPa. In both cases, the coefficient of variation is limited to less than 15%.

Table 3 – Consistency of calcium silicate and clay masonry mortar measured during the first period.

Mortar for calcium silicate masonry			**Mortar for clay masonry**		
Date	**Cast**	**Flow (mm)**	**Day**	**Cast number**	**Flow (mm)**
30-03-2015	1	186	16-04-2015	1	189
	2	179		2	177
31-03-2015	1	169		3	183
	2	177		4	172
	3	178		5	175
	4	178		6	175
02-04-2015	1	162		7	171
	2	174		8	172
	3	162			
	4	179			
	5	172			
Average		**174**			**177**

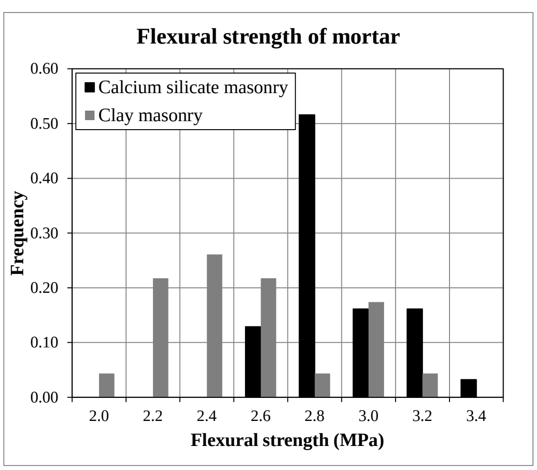

(a)

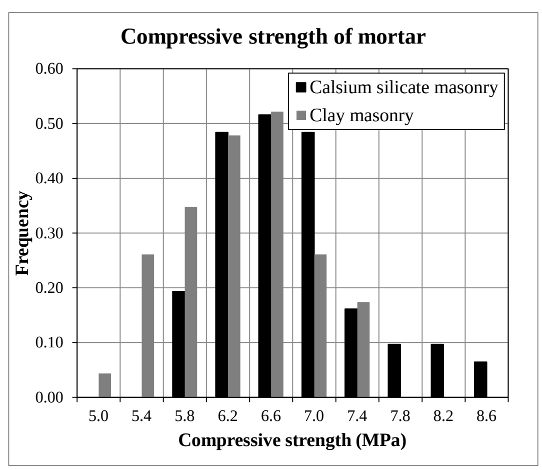

(b)

Figure 6 – Statistical distribution of mortar strength: (a) flexural strength; (b) compressive strength.

Table 4 – Flexural and compressive strength of calcium silicate masonry mortar (first period).

Date	Cast	Flexural tests			Compression test		
		f_{mt} (MPa)	St. Dev.	C.o.V.	f_m (MPa)	St. Dev.	C.o.V.
30-03-2015	1	2.57	0.10	0.04	5.75	0.18	0.03
	2	2.79	0.09	0.03	6.19	0.20	0.03
31-03-2015	1	2.77	0.20	0.07	6.95	0.14	0.02
	2	2.79	0.10	0.04	6.86	0.17	0.02
	3	2.73	0.07	0.02	6.25	0.28	0.05
	4	2.57	0.23	0.09	6.14	0.30	0.05
02-04-2015	1	3.10	0.07	0.02	8.00	0.34	0.04
	2	2.85	0.10	0.03	6.47	0.32	0.05
	3	2.63	0.11	0.04	6.51	0.23	0.04
	4	3.00	0.18	0.06	6.10	0.35	0.06
	5	3.07	0.46	0.15	7.13	0.64	0.09
Average all casts		**2.79**			**6.59**		
Standard deviation		**0.22**			**0.66**		
Coefficient of variation		**0.08**			**0.10**		

Table 5 – Flexural and compressive strength of clay masonry mortar (first period).

Date	Cast	Flexural tests			Compression test		
		f_{mt} (MPa)	St. Dev.	C.o.V.	f_m (MPa)	St. Dev.	C.o.V.
16-04-2015	1	2.46	0.21	0.09	5.40	0.49	0.09
	2	2.71	0.37	0.14	6.15	0.22	0.04
	3	2.06	0.04	0.02	5.50	0.14	0.03
	4	2.52	0.11	0.04	6.52	0.34	0.05
	5	2.64	0.17	0.06	5.77	0.27	0.05
	6	2.72	0.32	0.12	6.61	0.51	0.08
	7	2.16	0.17	0.08	6.77	0.19	0.03
	8	2.06	0.25	0.12	6.19	0.19	0.03
Average all casts		**2.43**			**6.11**		
Standard deviation		**0.32**			**0.57**		
Coefficient of variation		**0.13**			**0.09**		

5.2.2 Mortar specimens casted during the second construction period

In the second construction period (September 2015) the full-scale assemblage was built together with small-scale companion specimens and additional specimens for the tie test. During this period, the properties of fresh and hardened mortar were measured.

Both mortars show a consistently similar to the one observed in the first construction phase. The average cone diameter for the calcium silicate masonry mortar is 162 mm and for the clay masonry mortar is 183 mm.

Table 6 lists the results for the *calcium silicate masonry mortar*. The flexural strength test was performed on 6 specimens and the compressive strength test on 12 specimens. The mortar has a compressive strength of 7.24 MPa and flexural strength of 3.56 MPa. In both cases, the coefficient of variation is limited to less than 10%.

Table 7 lists the results for the *clay masonry mortar*. The flexural strength test was performed on 3 specimens and the compressive strength test on 6 specimens. The mortar has a compressive strength of 7.07 MPa and flexural strength of 2.93 MPa. In both cases, the coefficient of variation is limited to approximatively 10%.

Table 8 compares the results obtained in the two construction period. Both the flexural and compressive strength values resulted slightly higher in the second period. However, their values are within the standard deviation of the material.

Table 6 – Flexural and compressive strength of calcium silicate masonry mortar (second period).

Cast date	Cast	Flexural tests			Compression test		
		f_{mt} (MPa)	St. Dev.	C.o.V.	f_m (MPa)	St. Dev.	C.o.V.
04-09-2015	5	3.48	0.17	0.05	6.89	0.54	0.08
11-09-2015	3	3.64	0.18	0.05	7.59	0.45	0.06
Average all casts		**3.56**			**7.24**		
Standard deviation		**0.18**			**0.60**		
Coefficient of variation		**0.05**			**0.08**		

Table 7 – Flexural and compressive strength of clay masonry mortar (second period).

Cast date	Cast	Flexural tests			Compression test		
		f_{mt} (MPa)	St. Dev.	C.o.V.	f_m (MPa)	St. Dev.	C.o.V.
11-09-2015	2	**2.93**	0.32	0.11	**7.07**	0.64	0.09

Table 8 – Flexural and compressive strength of both mortar: comparison between first and second period.

Type of mortar	Period	Flexural tests			Compression test		
		f_{mt} (MPa)	St. Dev.	C.o.V.	f_m (MPa)	St. Dev.	C.o.V.
Calcium silicate masonry mortar	First period (MAT/COMP)	**2.79**	0.22	0.08	**6.59**	0.66	0.10
	Second period (BUILD/MAT-H and ties)	**3.56**	0.18	0.05	**7.24**	0.60	0.08
	$(P_{second}-P_{first}) / P_{first}$	**0.28**			**0.10**		
Clay masonry mortar	First period (MAT/COMP)	**2.43**	0.32	0.13	**6.11**	0.57	0.09
	Second period (BUILD/MAT-H and ties)	**2.93**	0.32	0.11	**7.07**	0.64	0.09
	$(P_{second}-P_{first}) / P_{first}$	**0.21**			**0.16**		

6 Compression strength of masonry

The compression strength and elastic modulus of the masonry were determined in agreement with EN 1052-1:1998 [7]. Additional test configurations were adopted to investigate the orthotropic behaviour of the masonry and the cyclic response of the material.

6.1 Testing procedure

The size of the specimens was determined on the basis of the masonry units [7]. The calcium silicate masonry specimens have dimensions of 434x476x102-mm (2x6x1-brick). The clay masonry specimens have dimensions of 430x470x100-mm (2x8x1-brick). A 10 mm thick layer of gypsum was applied to faces in contact with the loading plates, to ensure that the loaded faces of the specimens are levelled and parallel to one another. This is done to prevent additional stresses in the specimens.

The compression strength and elastic modulus of the masonry were determined in two orthogonal directions with respect to the bed joints. Two configurations were used (Figure 7): a *vertical configuration* in which the loading was perpendicular to the bed joints and a *horizontal configuration* in which the loading was parallel to the bed joint. The former is prescribed by the standard EN 1052-1:1998, while the latter is additionally used to investigate the orthotropic behaviour of the material.

The testing apparatus was provided with a 3500 kN hydraulic jack, positioned at the bottom. The hydraulic jack lifts a steel plate, the active side, and there is a passive load plate at the top. A hinge between the load cell and the top steel plate reduces possible eccentricities during loading. The hydraulic jack is operated in deformation control, using the displacement of the jack as control variable. A load cell that measures the applied force is attached to the top steel plate.

Four LVDTs (two for each side) are attached to the specimen to register vertical relative displacements over the height of the specimen (Figure 8). They are installed as closely as possible to the surface of the specimen to reduce possible errors caused by rotation of the contact points to which they are attached. Their measuring range is 2 mm with an accuracy of 0.5%. Additionally, two LVDTs (one for each side) are attached to the specimen to register the horizontal relative displacement over the length of the specimen (Figure 8). Their measuring range is 10 mm with an accuracy of 0.5%.

For the two configurations, three specimens were tested by applying a *monotonic loading* as prescribed by the EN 1052-1:1998 [7] (Figure 9). Half of the expected maximum compression force is applied in three equal steps and was kept constant for 2 ± 1 min. Afterwards, the maximum stress in reached monotonically. Subsequently, the test was continued to explore the post-peak behaviour. The load was applied with a rate of 0.002 mm/s to reach the peak stress in 15 to 30 min. The deformation and the force were registered, including the post-peak softening regime.
For the two configurations, three specimens were tested by applying a *cyclic loading* (Figure 9). This loading scheme gives additional information regarding the loading-unloading behaviour. Three set of three cycles were applied at approximatively 1/4, 1/2 and 3/4 of the expected maximum strength. The load was applied with a rate of 0.006 mm/s to reach the peak stress in approximatively 30 min. The deformation and the force were registered.

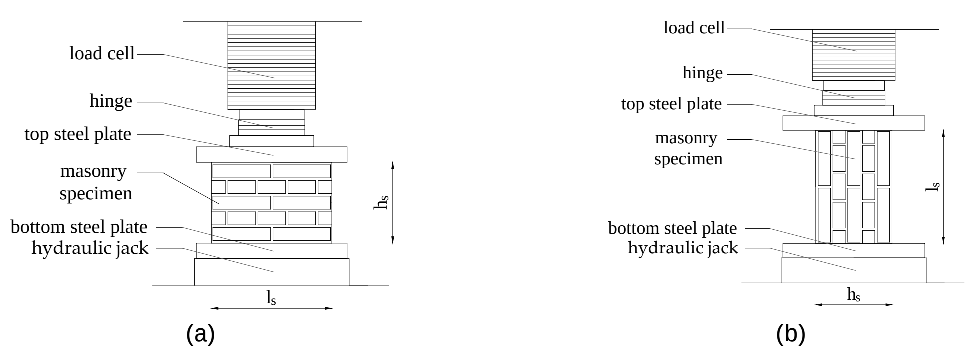

Figure 7 – Compression test on masonry: (a) vertical configuration; (b) horizontal configuration.

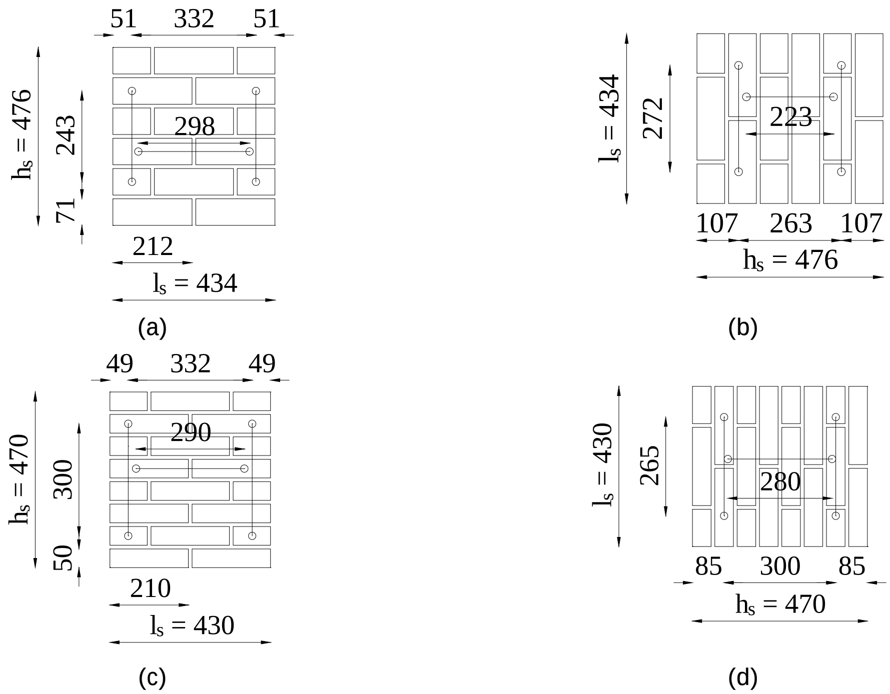

Figure 8 – Position of the LVDTs during the compression test on masonry: (a)-(b) calcium silicate masonry specimens; (c)-(d) clay masonry specimens.

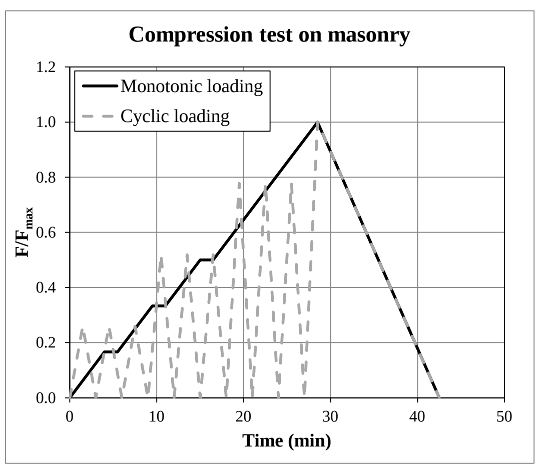

Figure 9 – Monotonic and cyclic loading scheme for compression test on masonry specimen.

6.2 Experimental results

Assuming that the stress is constant over the cross-section of the specimen, the compressive strength of masonry for the vertical, f'_m, and horizontal, $f'_{m,h}$, configuration can be determined as follows:

$$f'_m = \frac{F_{max}}{t_s l_s} \tag{5}$$

$$f'_{m,h} = \frac{F_{max}}{t_s h_s} \tag{6}$$

where F_{max} is the maximum load, l_s, h_s and t_s are the dimensions of the masonry specimen as built (Figure 7).

During the test the displacements and the force were measured continuously allowing the determination of the stress-strain relationship along the loading direction, which was defined as normal direction. Form this relation was possible to determine the elastic modulus of masonry. Three estimates of the elastic modulus were adopted (Figure 10a):

- E_1 ($E_{1,h}$) is the secant elastic modulus evaluated at 1/3 of the maximum stress;
- E_2 ($E_{2,h}$) is the secant elastic modulus evaluated at 1/10 of the maximum stress;
- E_3 ($E_{3,h}$) is the chord elastic modulus evaluated between 1/10 and 1/3 of the maximum stress.

The first estimate was consistent with the prescription of EN 1052-1:1998. The third estimate aimed to exclude the initial start-up of the stress-strain diagram, which would unrealistically affects the other two secant estimates with the initial lower slope.

The Poisson ratio ν is determined in the elastic phase as the ratio between the lateral strains, which are evaluated in the direction perpendicular to the loading one, and the normal strains (Figure 10b).

The displacement control procedure of the test allowed determining the post-peak behaviour of the material. The fracture energy in compression G_{c-f} was determined as the area underneath the normal stress versus normal strain diagram, taking the height of the specimen into account. This concept was introduced by van Mier [8] for concrete material and subsequently applied to masonry by Lourenco [9]. In the case of cyclic loading, the envelope curve was considered for the calculation of the fracture energy.

The strain obtained by LVDTs readings and by the jack's reading resulted similar. Consequently, the former were used to evaluate the pre-peak phase, while the latter were used to describe the post-peak phase, in which LVDTs may be detached from the specimen due to extensive cracking. The elastic modulus and the Poisson ratio were calculated on the basis of the LVDTs readings, while the fracture energy was calculated on the basis of the jack's reading.

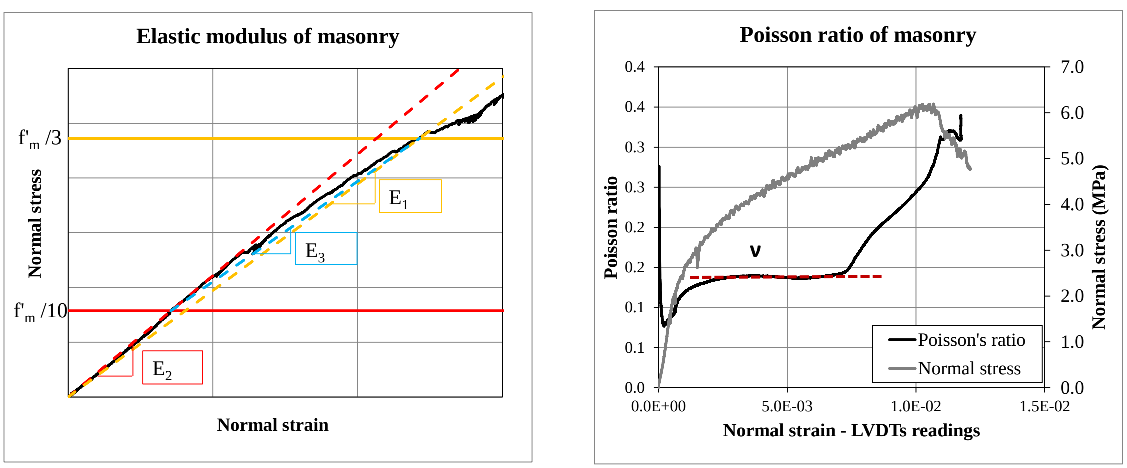

Figure 10 – Compression test on masonry: (a) three estimates of the elastic modulus; (b) evaluation of Poisson ratio.

6.2.1 Specimens casted during the first construction period

In the first construction period, small-scale specimens and large-scale walls were built during March and April 2015. The first were used to tests the material properties (MAT specimens), while the second to study the in-plane and out-of-plane behaviour of walls (COMP specimens). During this period, compressive behaviour of masonry was studied by performing tests both in the vertical and horizontal configuration.

Figure 11 and Figure 12 show the stress-strain diagram for the *calcium silicate masonry* under vertical and horizontal compression tests, respectively. The graphs refers to the normal direction that is defined as the one parallel to the loading direction.
For both configurations the stress-strain relationship in the normal direction showed a similar trend. The pre-peak stage was characterized by linear-elastic followed by an hardening behaviour until the peak. In this stage, the nonlinearity occurred at a stress level approximatively of 1/10 of the maximum stress. After the maximum stress was reached, a softening behaviour was observed. For the vertical configuration, the softening branch was approximatively linear, while for the horizontal configuration an exponential trend was observed. In the case of cyclic loading, the masonry showed an elastic unloading for both configurations.

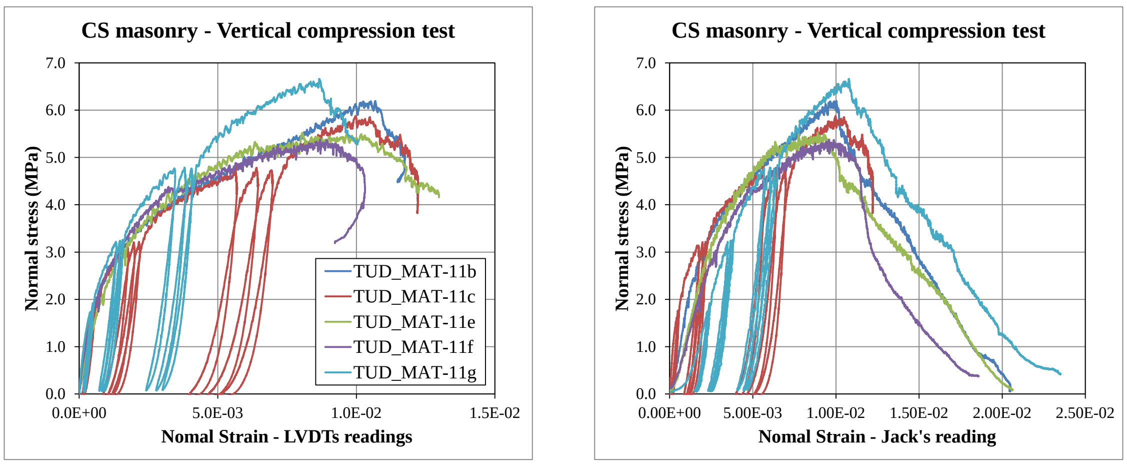

(a) (b)

Figure 11 – Vertical compression tests on calcium silicate masonry specimens (MAT/COMP): (a) normal strain obtained by LVDTs reading; (b) normal strain obtained by jack's reading.

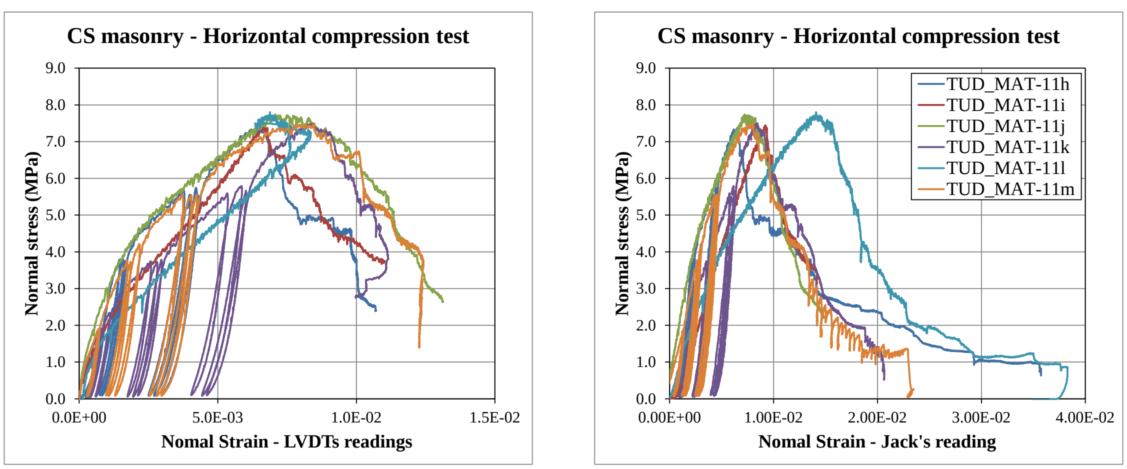

(a) (b)

Figure 12 – Horizontal compression tests on calcium silicate masonry specimens (MAT/COMP): (a) normal strain obtained by LVDTs reading; (b) normal strain obtained by jack's reading.

Figure 13 and Figure 14 analyse the development of cracks in two specimens tested under vertical and horizontal compression test, respectively. In both cases, cracks started at the mortar-brick interface for the joints orthogonal to the loading direction (Figure 13a, Figure 14a). When the maximum stress was reached, vertical cracks develop in the bricks. In the case of the vertical configuration, the cracks mainly occurred in the central part of the specimens (Figure 13b). On the contrary, for the horizontal configuration, the damage was concentrated in the bottom or upper part, where half bricks were located (Figure 14b).
In the post-peak phase, the specimens tested under the two configurations showed different behaviour. For the case of vertical configuration, the vertical cracks mainly occurred in the bricks and develops uniformly through the length of the specimen, by splitting it in two parts (Figure 13c, Figure 13d). For the horizontal configuration, the vertical cracks occurred in the bed joints and partially in the bricks. At failure, the cracks developed through the thickness of the specimen rather than through the length, creating a buckling mechanism eventually followed by cracking of the masonry unit (Figure 14c, Figure 14d). The cracking was observed to occur in a distributed manner over the height of the specimen; no localisation of the cracking at the boundary was observed.

σ_n = 5.3 MPa, ε_n = 7.4 ‰ (a) — σ_n = 6.2 MPa, ε_n = 11 ‰ (b) — σ_n = 2.0 MPa (c) — σ_n = 0.7 MPa (d)

Figure 13 – Crack pattern of specimen TUD_MAT-11b tested under vertical compression test: (a) first crack; (b) maximum stress; (c)-(d) post-peak phase.

σ_n = 5.4 MPa, ε_n = 3.2 ‰ (a) — σ_n = 7.7 MPa, ε_n = 7.1 ‰ (b) — σ_n = 2.5 MPa, ε_n = 15 ‰ (c) — σ_n = 1.3 MPa (d)

Figure 14 – Crack pattern of specimen TUD_MAT-11j tested under horizontal compression test: (a) first crack; (b) maximum stress; (c)-(d) post-peak phase.

Table 9, Table 10 and Table 11 list the main experimental results for the calcium silicate masonry specimens. Figure 15 and Figure 16 show the results with the histogram representation. The calcium silicate masonry showed an orthotropic behaviour, having a higher compressive strength in the direction parallel to the bed joints (f'_m / $f'_{m,h}$ = 0.8). A similar ratio was observed in terms of fracture energy ($G_{f\text{-}c}$ / $G_{f\text{-}c,h}$ = 0.6). On the contrary, the calcium silicate masonry resulted stiffer in the direction perpendicular to the bed joints (E / E_h = 1.4). By analysing the crack pattern, it was possible to note that when the masonry specimen was rotated and the direction of the bed joints coincided with the loading direction, the damage was mainly

located in the brick-mortar interfaces. Bricks and head joints form small columns that were subject to buckling rather than cracking in the bricks. This rigid movement induced a higher resistance. However, size effects, shape and boundary conditions can play an important role.
The secant elastic modulus E_1 and $E_{1,h}$ evaluated at 1/3 of the maximum stress and the chord modulus E_3 and $E_{3,h}$ provided a similar estimation, while the elastic modulus E_2 and $E_{2,h}$ evaluated at 1/10 of the maximum stress provided higher values. This confirms the start of the non-linearity for lower values of normal stress.
The average Poisson ratio ν was estimated equal to 0.14 for the vertical configuration, while it varied between 0.25 and 0.5 for the horizontal configuration.

Table 9 – Vertical compression test results on calcium silicate masonry specimens (first period).

Specimen name	**Test type**	f'_m	E_1	E_2	E_3	G_{f-c}	ν
		MPa	MPa	MPa	MPa	N/mm	
TUD_MAT-11b	monotonic	6.19	3081	3123	3063	34.4	0.14
TUD_MAT-11c	cyclic	5.88	3085	5304	2616	25.6	-
TUD_MAT-11e	monotonic	5.53	2518	3427	2338	32.1	0.13
TUD_MAT-11f	monotonic	5.38	3785	6632	2924	27.4	0.13
TUD_MAT-11g	cyclic	6.66	3400	6970	2788	38.2	0.15
Average		**5.93**	**3174**	**5091**	**2746**	**31.5**	**0.14**
Standard deviation		**0.52**	**467**	**1774**	**282**	**5.1**	**0.01**
Coefficient of variation		**0.09**	**0.15**	**0.35**	**0.10**	**0.16**	**0.07**

Table 10 – Horizontal compression test results on calcium silicate masonry specimens (first period).

Specimen name	**Test type**	$f'_{m,h}$	$E_{1,h}$	$E_{2,h}$	$E_{3,h}$	$G_{f-c,h}$	ν
		MPa	MPa	MPa	MPa	N/mm	
TUD_MAT-11h	cyclic	7.36	2482	1492	3469	47.5	0.25-0.3
TUD_MAT-11i	monotonic	7.44	1758	3187	1475	39.5	0.4-0.5
TUD_MAT-11j	cyclic	7.74	3167	6205	2618	39.0	0.25
TUD_MAT-11k	cyclic	7.50	1980	3838	1640	37.4	0.3-0.4
TUD_MAT-11l	monotonic	7.79	1313	2299	1109	56.2	-
TUD_MAT-11m	monotonic	7.49	2570	4477	2173	40.5	0.4-0.5
Average		**7.55**	**2212**	**3583**	**2081**	**43.4**	-
Standard deviation		**0.17**	**660**	**1668**	**864**	**7.2**	-
Coefficient of variation		**0.02**	**0.30**	**0.47**	**0.42**	**0.17**	-

Table 11 – Orthotropic behaviour of calcium silicate masonry (first period).

	f'_m $f'_{m,h}$	E_1 $E_{1,h}$	E_2 $E_{2,h}$	E_3 $E_{3,h}$	G_{f-c} $G_{f-c,h}$	ν
	MPa	MPa	MPa	MPa	N/mm	
Vertical configuration	5.93	3174	5091	2746	31.5	0.14
Horizontal configuration	7.55	2212	3583	2081	43.4	0.25-0.5
Ratio Vertical/Horizontal	**0.8**	**1.5**	**1.3**	**1.4**	**0.6**	

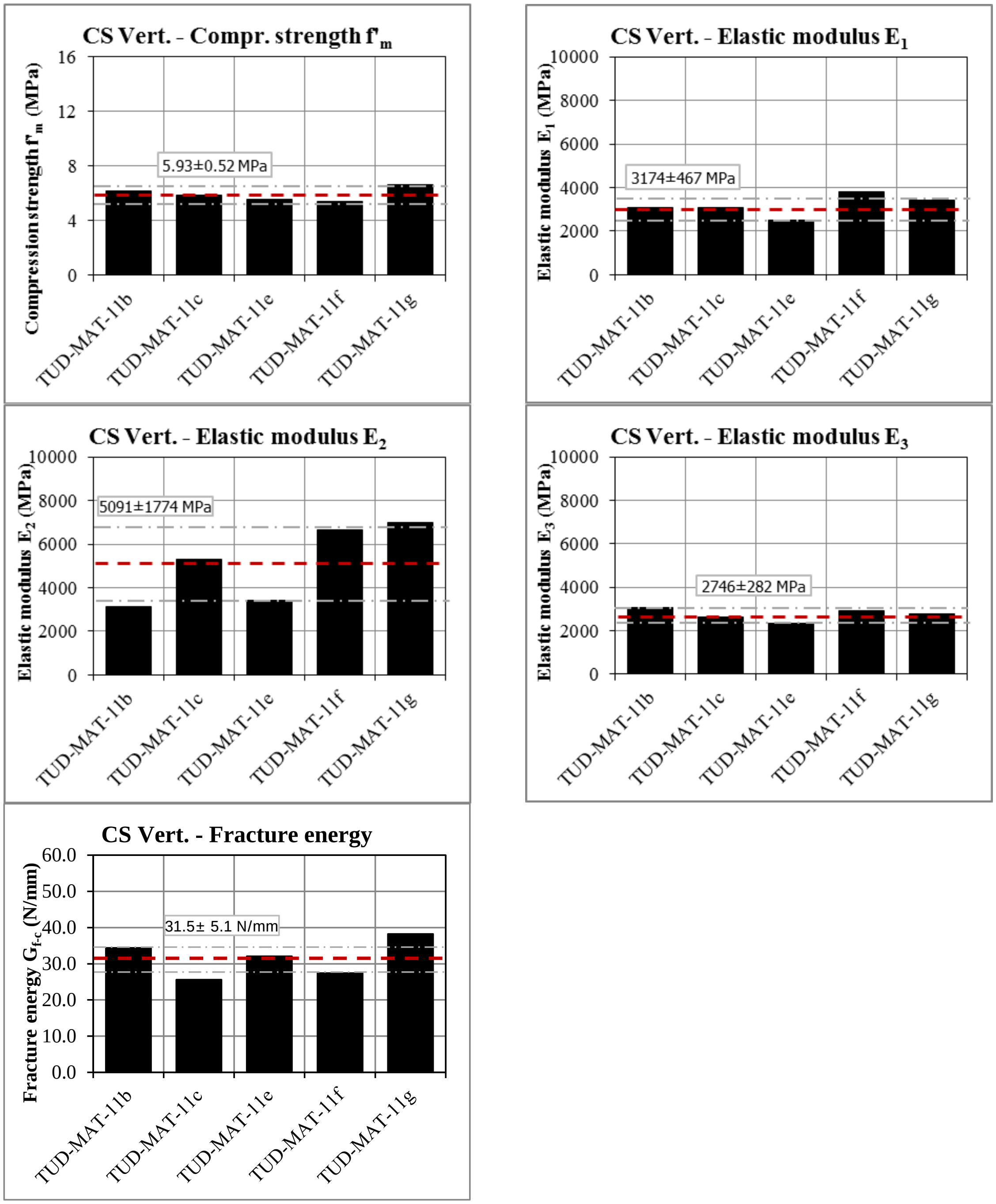

Figure 15 – Vertical compression tests on calcium silicate masonry specimens (first period): histogram representation.

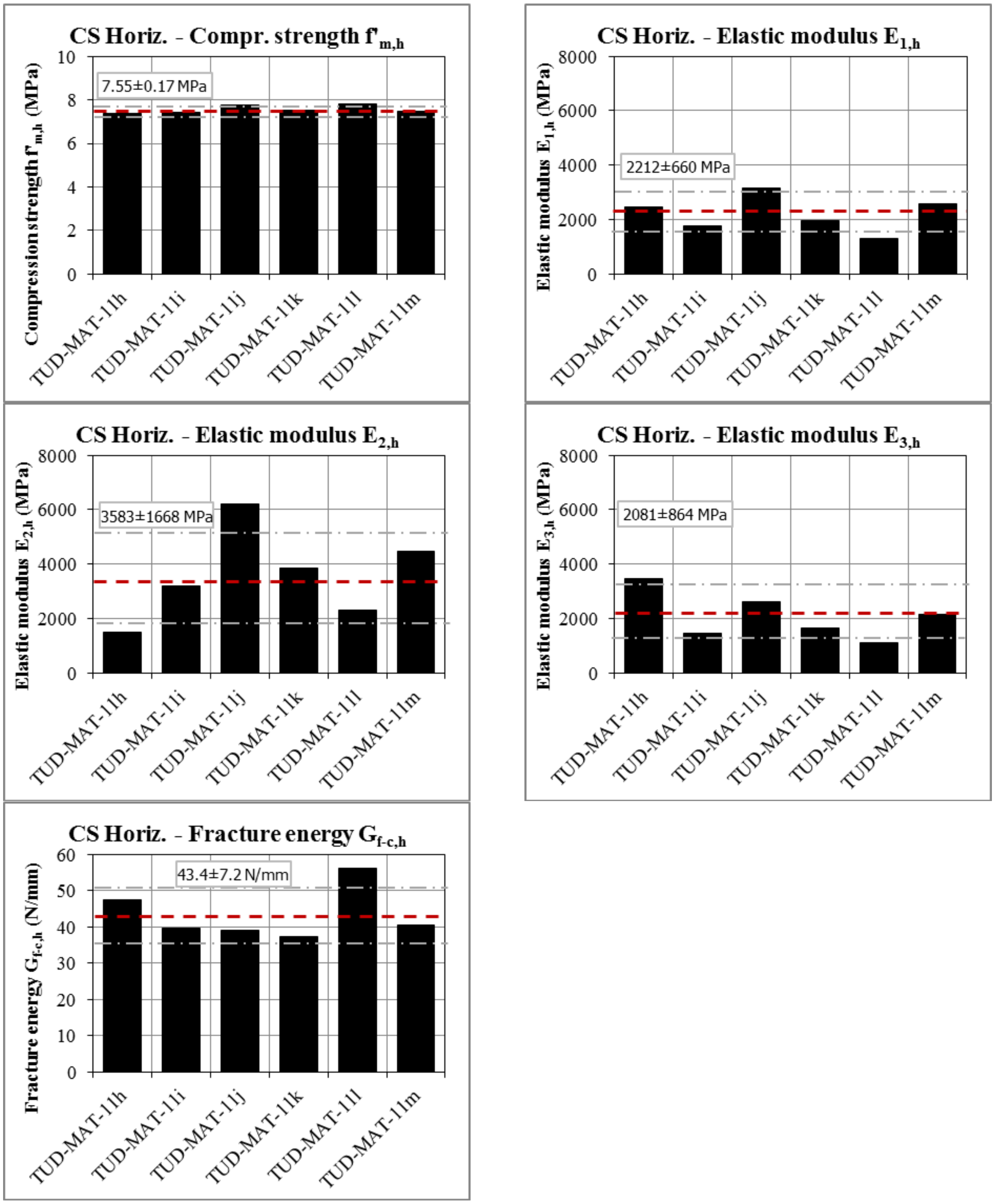

Figure 16 – Horizontal compression tests on calcium silicate masonry specimens (first period): histogram representation.

Figure 17 and Figure 18 show the stress-strain diagram for the *clay masonry* for the vertical and horizontal configurations, respectively. The graphs refer to the normal direction that is defined as the one parallel to the loading direction.
For both configurations the stress-strain relationship in the normal direction presents a similar trend. The pre-peak stage was characterized by linear-elastic followed by an hardening behaviour until the peak. In the case of the vertical configuration, the non-linearity started at approximatively 1/3 of peak stress, while in the case of the horizontal configuration the nonlinear behaviour occurred already at lower stress level between 1/10 and 1/3 of the maximum stress. After the peak stress was reached, an exponential softening behaviour was observed for both configurations. In the case of cyclic loading, the masonry showed an elastic unloading for both configurations.

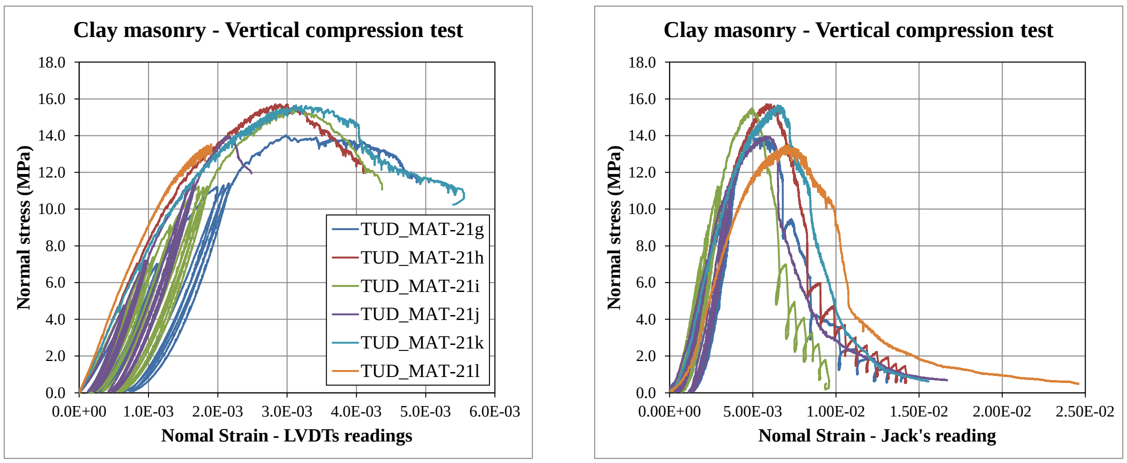

(a) (b)

Figure 17 – Vertical compression tests on clay masonry specimens (MAT/COMP): (a) normal strain obtained by LVDTs reading; (b) normal strain obtained by jack's reading.

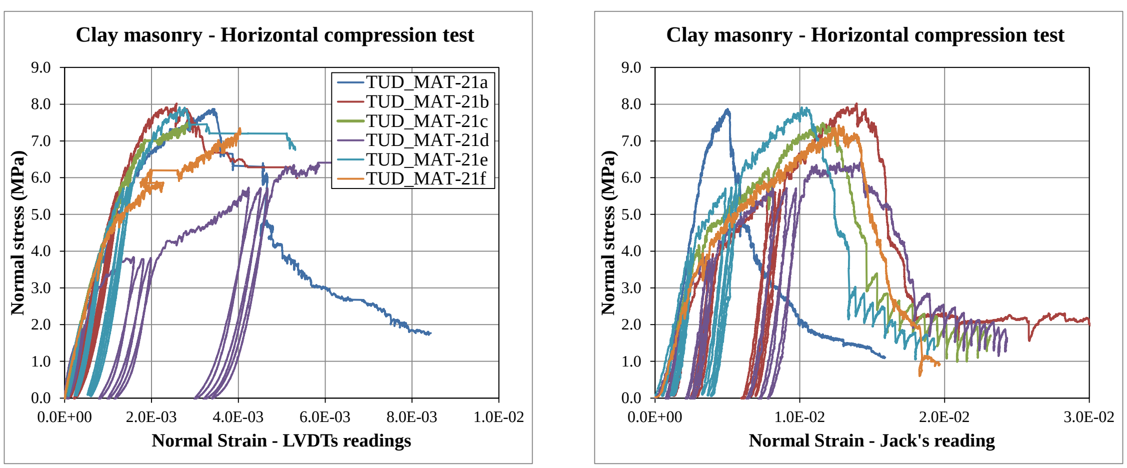

(a) (b)

Figure 18 – Horizontal compression tests on clay masonry specimens (first period): (a) normal strain obtained by LVDTs reading; (b) normal strain obtained by jack's reading.

Figure 19 and Figure 20 analyse the development of cracks in two specimens tested for the vertical and horizontal configurations, respectively. In both cases, cracks started in the bricks and were oriented parallel to the loading direction (Figure 19a, Figure 20a). Being the bricks were perforated, the vertical cracks occurred in the vicinity of the holes by spreading the damage in the normal plane (Figure 19b, Figure 20b). In the post-peak phase, the external surface of the bricks was spalled off (Figure 19c-d, Figure 20c-d). The cracking was observed to occur in a distributed manner over the height of the specimen; no localisation of the cracking at the boundary was observed.

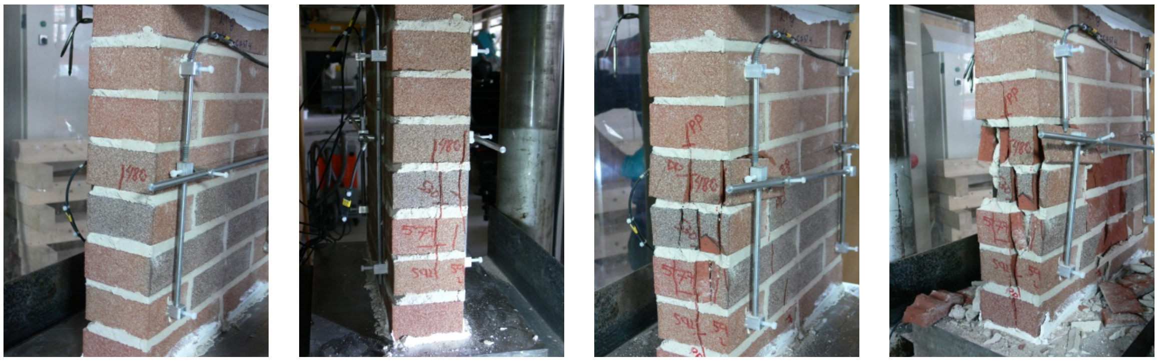

σ_n = 1.6 MPa, ε_n = 0.4 ‰ (a) | σ_n = 14 MPa, ε_n = 3.0 ‰ (b) | σ_n = 8.6 MPa, ε_n = 5.6 ‰ (c) | σ_n = 0.9 MPa, ε_n = 2.7 ‰ (d)

Figure 19 – Crack pattern of specimen TUD_MAT-21g tested under vertical compression test (first period): (a) first crack; (b) maximum stress; (c)-(d) post-peak phase.

σ_n = 7.3 MPa, ε_n = 2.6 ‰ (a) | σ_n = 7.8 MPa, ε_n = 3.4 ‰ (b) | σ_n = 4.8 MPa, ε_n = 4.6 ‰ (c) | σ_n = 3.2 MPa, ε_n = 5.7 ‰ (d)

Figure 20 – Crack pattern of specimen TUD_MAT-21a tested under horizontal compression test (first period): (a) first crack; (b) maximum stress; (c)-(d) post-peak phase.

Table 12, Table 13 and Table 14 list the main experimental results for the clay specimens. Figure 21 and Figure 22 show the results with the histogram representation. The clay masonry showed an orthotropic behaviour, having a higher compressive strength in the direction perpendicular to the bed joints (f_m / $f_{m,h}$ = 2.0). A similar ratio was observed in terms of fracture energy ($G_{f\text{-}c}$ / $G_{f\text{-}c,h}$ = 1.5). Considering the estimate of the elastic modulus at 1/3 of the peak stress (E_1 / $E_{1,h}$ = 1.5) and the chord elastic modulus (E_3 / $E_{3,h}$ = 1.7) a similar trend was observed. On the contrary, the estimate of the elastic modulus at 1/10 of the peak stress suggested an isotropic stiffness distribution (E_2 / $E_{2,h}$ = 1.1).

Table 12 – Vertical compression test results on clay masonry specimens (first period).

Specimen name	Test type	f'_m	E_1	E_2	E_3	G_{f-c}	v
		MPa	MPa	MPa	MPa	N/mm	
TUD_MAT-21g	cyclic	14.02	5806	5382	6009	44.73	-
TUD_MAT-21h	monotonic	15.71	8393	7596	8789	47.00	
TUD_MAT-21i	cyclic	15.50	7091	6410	7429	41.28	-
TUD_MAT-21j	cyclic	13.95	7353	5782	8322	44.40	-
TUD_MAT-21k	monotonic	15.65	8147	7566	8424	49.83	0.14
TUD_MAT-21l	monotonic	13.52	9579	8792	9961	54.94	-
Average		**14.73**	**7728**	**6921**	**8156**	**47.0**	-
Standard deviation		**1.00**	**1287**	**1288**	**1334**	**4.8**	-
Coefficient of variation		**0.07**	**0.17**	**0.19**	**0.16**	**0.10**	-

Table 13 – Horizontal compression test results on clay masonry specimens (first period).

Specimen name	Test type	$f'_{m,h}$	$E_{1,h}$	$E_{2,h}$	$E_{3,h}$	$G_{f-c,h}$	v
		MPa	MPa	MPa	MPa	N/mm	
TUD_MAT-21a	monotonic	7.87	4864	5541	4585	21.37	-
TUD_MAT-21b	cyclic	8.02	5262	5583	5119	35.70	-
TUD_MAT-21c	monotonic	7.49	5373	5473	5356	24.16	-
TUD_MAT-21d	cyclic	6.43	4113	9573	3213	41.94	-
TUD_MAT-21e	cyclic	7.92	5280	6917	4764	27.95	-
TUD_MAT-21f	monotonic	7.43	5287	6067	5017	37.42	-
Average		**7.53**	**5030**	**6526**	**4676**	**31.4**	**-**
Standard deviation		**0.59**	**483**	**1589**	**766**	**8.1**	**-**
Coefficient of variation		**0.08**	**0.10**	**0.24**	**0.16**	**0.26**	**-**

Table 14 – Orthotropic behaviour of clay masonry (first period).

	f'_m $f'_{m,h}$	E_1 $E_{1,h}$	E_2 $E_{2,h}$	E_3 $E_{3,h}$	G_{f-c} $G_{f-c,h}$	v
	MPa	MPa	MPa	MPa	N/mm	
Vertical configuration	14.73	7728	6921	8156	47.03	-
Horizontal configuration	7.53	5030	6526	4676	31.42	-
Ratio Vertical/Horizontal	**2.0**	**1.5**	**1.1**	**1.7**	**1.5**	

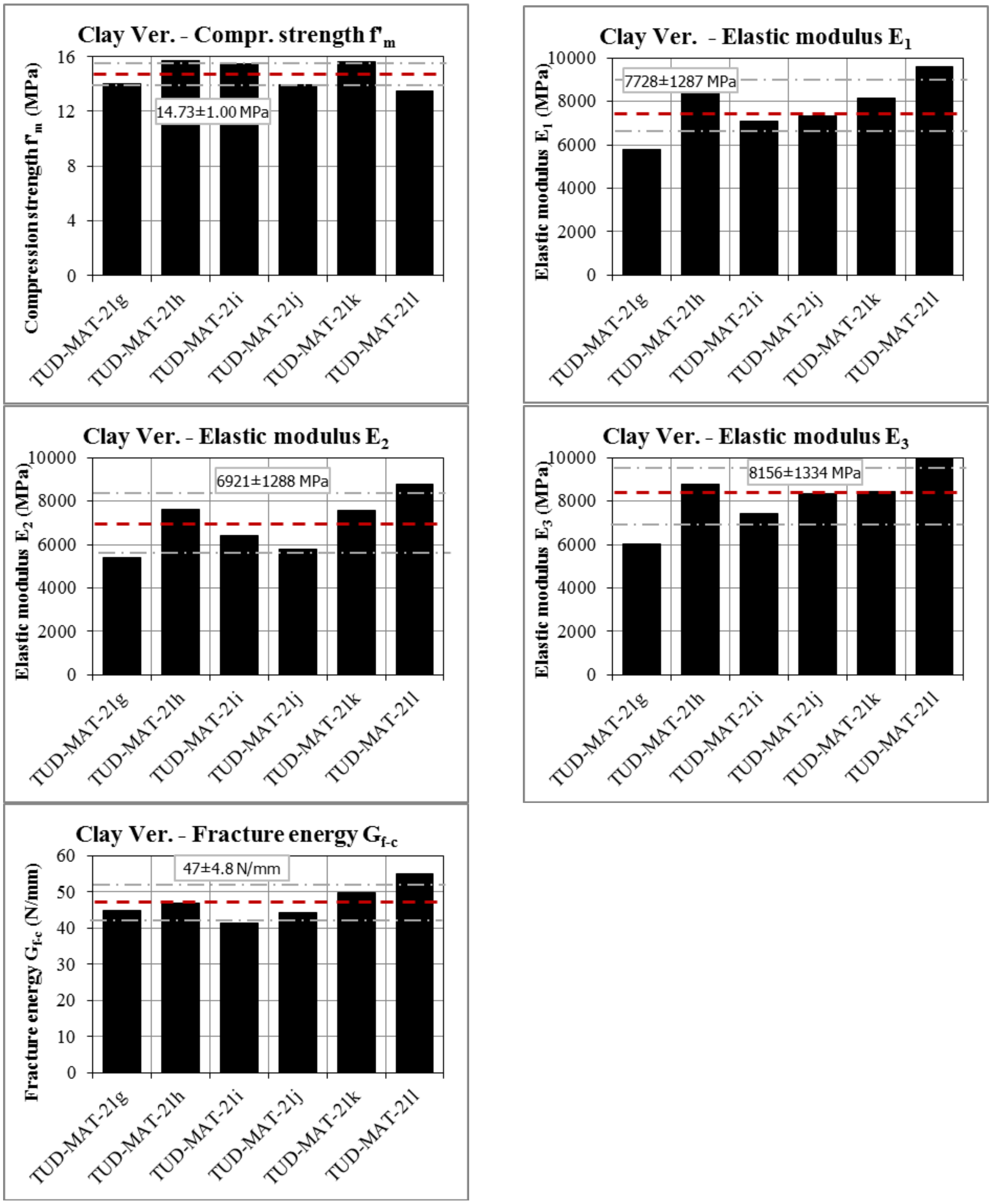

Figure 21 – Vertical compression tests on clay masonry specimens (first period): histogram representation.

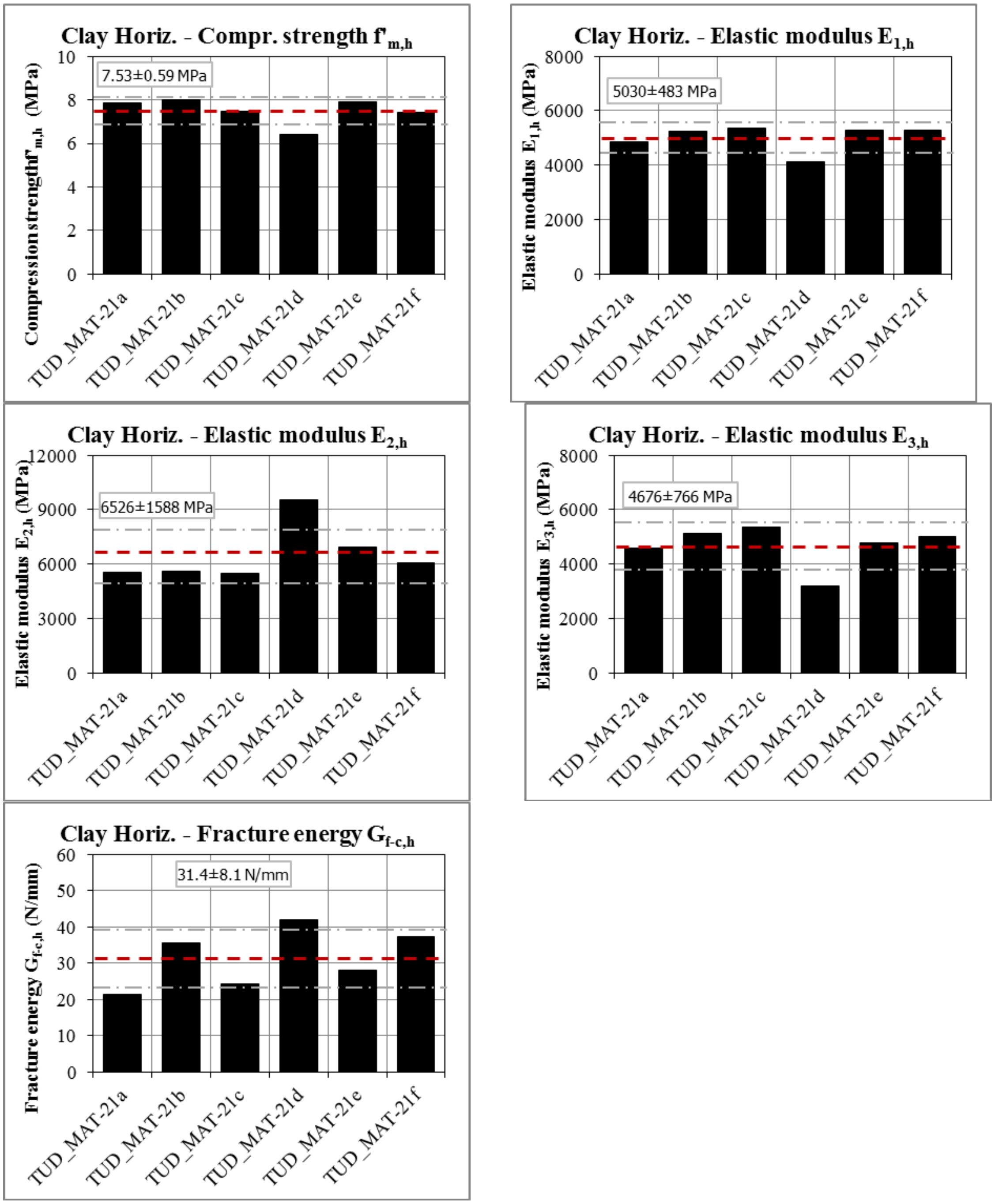

Figure 22 – Horizontal compression tests on clay masonry specimens (first period): histogram representation.

6.2.2 Specimens casted during the second construction period

In the second construction period (September 2015), the full-scale assemblage was built together with small-scale companion specimens. During this period, compressive tests were performed on calcium silicate specimens; only the vertical configuration was adopted.

Figure 23 shows the stress-strain diagram for the calcium silicate masonry under vertical compression tests. The graphs refer to the normal direction that was defined as the one parallel to the loading direction. The pre-peak stage was characterized by linear-elastic followed by an hardening behaviour until the peak. In this stage, the non-linearity occurred at a stress level approximatively of 1/5 of the maximum stress. After the maximum stress was reached a softening behaviour is observed. Mainly an exponential trend is observed for the softening branch; this differs from previous results where a linear softening was observed (Figure 11).

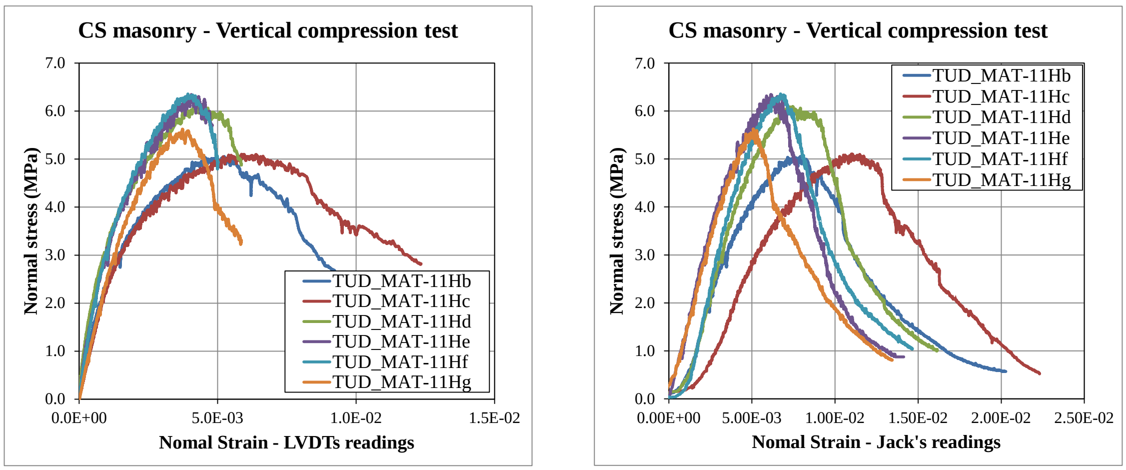

(a) (b)

Figure 23 – Vertical compression tests on calcium silicate masonry specimens (second period): (a) normal strain obtained by LVDTs reading; (b) normal strain obtained by jack's reading.

The crack pattern was mainly constituted by a vertical crack that develops uniformly through the length of the specimen, by splitting it in two parts (Figure 24). This failure mode was also observed in the previous tests (Figure 13).

Figure 24 – Crack pattern of specimen TUD_MAT-11Hb tested under vertical compression test (second period).

Table 15 lists the main experimental results for the calcium silicate masonry specimens. Among all specimens, TUD_MAT-11Hb and TUD_MAT-11Hc show some deviations. They had a maximum head joint thickness of 15 mm (prescribed head joint thickness = 9-12 mm) and showed cracking in some bed joints prior testing. The tests results related to these specimens deviate of approximatively 8-15% from the other tests. By excluding these data from the set, the coefficients of variation of the various properties slightly decrease (Table 9).

Table 15 – Results of vertical compression tests on calcium silicate masonry specimens (second period).

Specimen name	Test type	f'_m	E_1	E_2	E_3	G_{f-c}	v
		MPa	MPa	MPa	MPa	N/mm	
TUD_MAT-11Hb	monotonic	5.05	2994	4413	2589	22.6	0.13
TUD_MAT-11Hc	monotonic	5.10	2473	2630	2401	27.1	0.09
TUD_MAT-11Hd	monotonic	6.10	4607	7684	3841	24	0.29
TUD_MAT-11He	monotonic	6.35	3671	5480	3196	20.2	0.22
TUD_MAT-11Hf	monotonic	6.36	3665	4296	3414	20.1	0.14
TUD_MAT-11Hg	monotonic	5.63	2628	2716	2587	16.6	0.20
Average	All	**5.76**	**3340**	**4536**	**3005**	**21.8**	**0.18**
Standard deviation		0.59	800	1888	568	3.6	0.07
Coefficient of variation		0.10	0.24	0.42	0.19	0.17	0.41
Average	Excluding 11Hb,11Hc	**6.11**	**3643**	**5044**	**3260**	**20.2**	**0.21**
Standard deviation		0.34	808	2093	522	3.0	0.06
Coefficient of variation		0.06	0.22	0.41	0.16	0.15	0.29

Table 16 shows a comparison between the performed in the second period (BUILD, series TUD_MAT-11H) and the one performed in the first period (MAT/COMP, series TUD_MAT-11). The latest tests show slightly lower values for the compressive strength f'_m, the secant elastic modulus E_2 and the fracture energy G_{f-c}. On the contrary, the secant elastic moduli E_1, the elastic modulus E_3 and the Poisson ratio ν show slightly higher values. The results obtained in the second period are within the coefficients of variation of the material established in the first construction period (Table 9), with the exception of the fracture energy and the Poisson ratio.
Figure 15 and Figure 16 show the comparison in term of histogram diagrams.

Table 16 – Calcium silicate masonry subject to vertical compressive test: comparison between first and second period.

Series	Statistical parameter	f'_m	E_1	E_2	E_3	G_{f-c}	v
		MPa	MPa	MPa	MPa	N/mm	
First period (MAT/COMP) TUD_MAT-11	Average	**5.93**	**3174**	**5091**	**2746**	**31.5**	**0.14**
	Standard deviation	0.52	467	1774	282	5.1	0.01
	Coefficient of variation	0.09	0.15	0.35	0.10	0.16	0.07
Second period (BUILD/MAT-H and ties) TUD_MAT-11H	Average	**5.76**	**3340**	**4536**	**3005**	**21.8**	**0.18**
	Standard deviation	0.59	800	1888	568	3.6	0.07
	Coefficient of variation	0.10	0.24	0.42	0.19	0.17	0.41
$(P_{second}-P_{first}) / P_{first}$		**-0.03**	**0.05**	**-0.11**	**0.09**	**0.31**	**0.30**

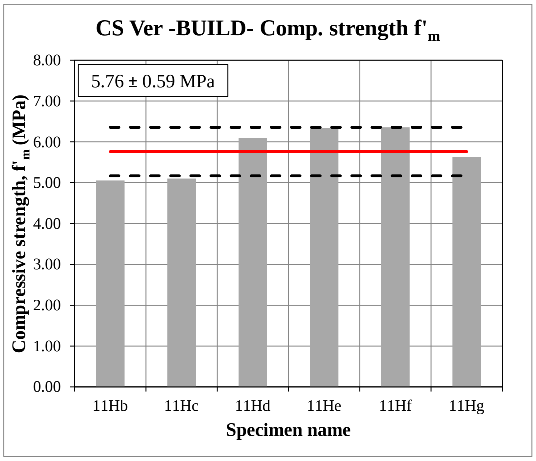

(a)

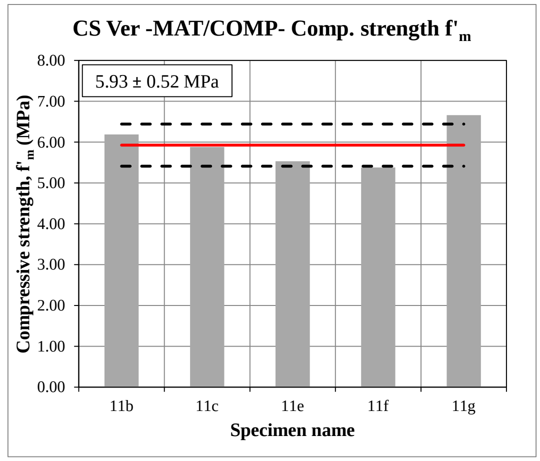

(b)

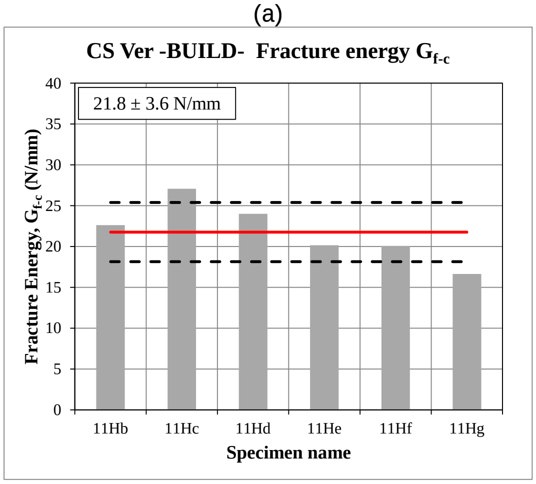

(c)

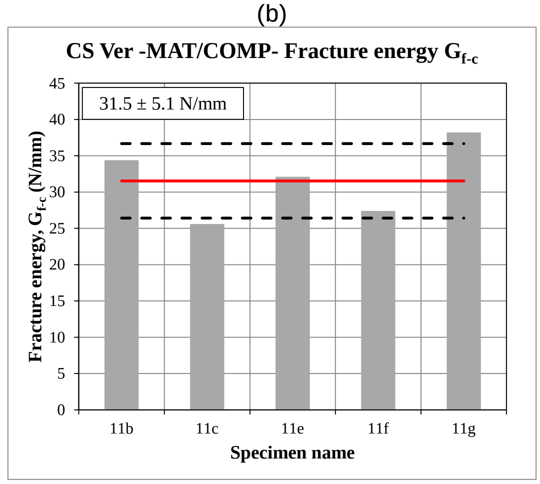

(d)

Figure 25 – Comparison between specimens tested under vertical compression loading in the second and first period in terms of: (a)-(b) compressive strength; (c)-(d) fracture energy.

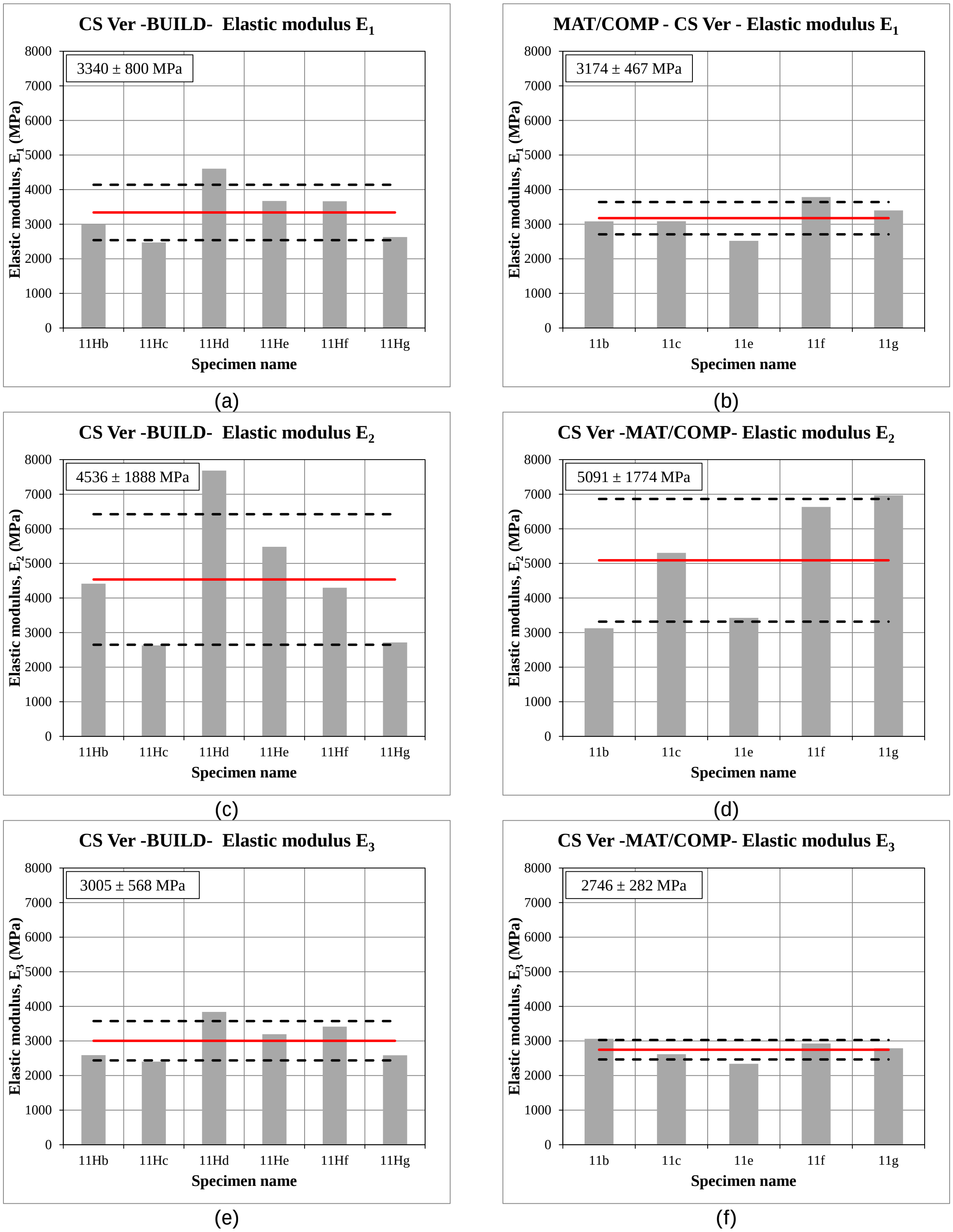

Figure 26 – Comparison between specimens tested under vertical compression loading in the second and first period in terms of elastic moduli.

7 Flexural strength of masonry

The flexural strength of masonry was determined for three configurations:

- Four-point bending test with the moment vector parallel to the bed joints and in the plane of the wall, which generates a plane of failure parallel to the bed joints (denoted as out-of-plane vertical bending test OOP1);
- Four-point bending with the moment vector orthogonal to the bed joints and in the plane of the wall, which generates a plane of failure perpendicular to the bed joints (denoted as out-of-plane horizontal bending test OOP2);
- Four-point bending with the moment vector orthogonal to plane of the wall (denoted as in-plane vertical bending test IP).

The first two tests were performed in agreement with EN 1052-2:1999 [10], while the third one was a no-standardized test.
The tests were performed only in the first period.

7.1 Testing procedure

The masonry specimens tested with the moment vector in the plane of the wallets were designed in agreement with EN 1052-2:1999 [10]. Table 17 provides an overview of the specimens tested. The masonry type, the dimensions and the distance between the bearing supports d_1 and loading supports d_2 are listed.

Table 17 – Overview of specimens for bending tests.

Test type	Specimen name	Masonry type	l_s (bricks)	h_s (bricks)	d_1 (mm)	d_2 (mm)
Bending test with moment vector parallel to the bed joints and in the plane of the wall (OOP1)	TUD_MAT-12a-f	Calcium silicate	2	10	720	360
	TUD_MAT-22a-f	Clay	2	10	440	220
Bending test with moment vector orthogonal to the bed joints and in the plane of the wall (OOP2)	TUD_MAT-13a-f	Calcium silicate	4	4	720	360
	TUD_MAT-23a-f	Clay	4	5	720	360
	TUD_MAT-23a4-f4	Clay	4	4	720	360
Bending test with moment vector orthogonal to the bed joints and in the plane of the wall (IP)	TUD_MAT-14a-f	Calcium silicate	4	4	720	360
	TUD_MAT-24a-f	Clay	4	5	720	360
	TUD_MAT-24a4-f4	Clay	4	4	720	360

Figure 27 shows the adopted test set-ups. The load was transfer to the specimen via steel profiles. To achieve a uniform distribution of the load along the depth of the specimen, rubber strips were placed between the masonry specimen and the loading frame. The distance between the loading, d_2, and bearing rollers, d_1, is chosen equal to 0.5 (Table 17).

The load was applied in displacement control by a spherical joint attached to a hydraulic jack with 100 kN capacity. The applied displacement rate was 0.002 mm/s. The applied load was recorded from the load cell attached to the hydraulic jack.

For each side a maximum of five LVDTs was attached to measure the vertical and horizontal displacements in the constant moment zone (Figure 28). The LVDTs had a measuring range of 10 mm with an accuracy of 0.5%.

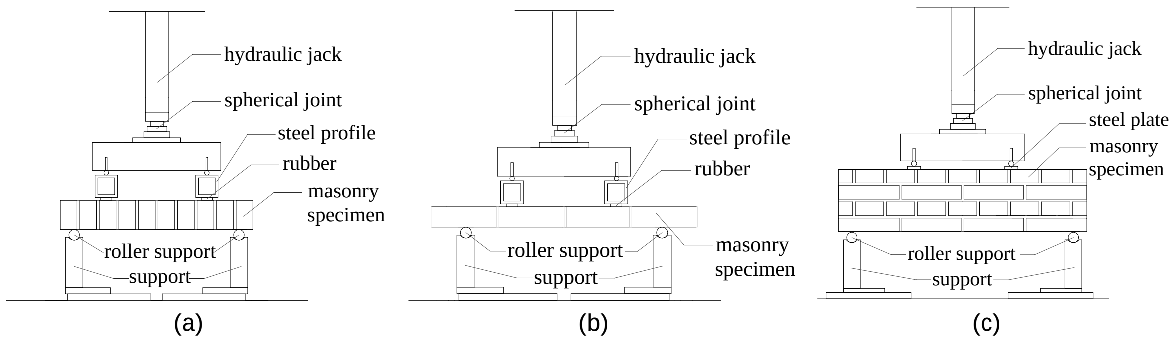

Figure 27 – Set-ups for the bending tests: (a) out-of-plane vertical bending test (OOP1); (b) out-of-plane horizontal bending test (OOP2); (c) in-plane vertical bending test (IP).

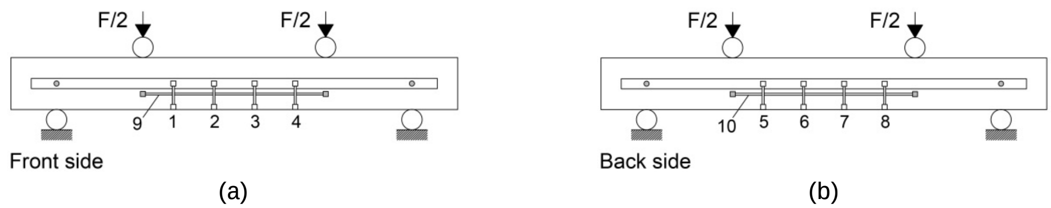

Figure 28 – Positions of the LVDTs during the bending tests: (a) front side; (b) back side (e.g. for out-of-plane bending test, similar for in-plane test).

7.2 Experimental results

The flexural strength f_x can be determined for every specimens as follows:

$$f_x = \frac{M_{\max}}{W} = \frac{F_{\max} d_3}{2W} \tag{7}$$

where M_{max} is the maximum bending moment, F_{max} is the maximum load at failure, d_3 (=180 mm) is the distance between the loading and the bearing support, W is the section modulus that is varying for the different configurations.

Figure 29 shows the force displacement curve for *calcium silicate masonry* specimens subject to bending tests. The mid-span displacement has been calculated from the readings of the vertical LVDTs, by applying a linear interpolation. In each bending test, the calcium silicate masonry showed a brittle failure mechanism. A stable post-peak softening path could only be found for two samples tested for out-of-plane vertical bending (TUD_MAT-13c, TUD_MAT-13e).

Figure 30 shows the crack pattern for each bending test. For the out-of-plane vertical test, the specimens crack in one bed joint located in the constant moment zone. In some cases, the simultaneous failure of two joints was observed. In the case of out-of-plane horizontal bending tests, the cracking occurred in both bed and head joints by a stepwise pattern. For the specimens TUD_MAT-13a, TUD_MAT-13c and TUD_MAT-13e the cracking occurred in both the constant moment zone and the shear zone (Figure 30b); these specimens showed a lower strength value with respect to the average value increasing the coefficient of variation. This variation in the failure mode could not be correlated neither to the test set-up or the initial status of the specimens. In the case of in-plane vertical bending tests, the cracking occurred in both bed and head joints in the constant moment zone, creating a stepwise pattern.

Table 18 lists the strength values for the three configurations. The calcium silicate masonry showed an orthotropic behaviour. The out-of-plane horizontal flexural strength resulted approximatively 4 times higher values than the out-of-plane vertical flexural strength (f_{x2} / f_{x1} = 3.6). The in-plane vertical strength resulted in the double of the out-of-plane vertical flexural strength (f_{x3} / f_{x1} = 1.9).

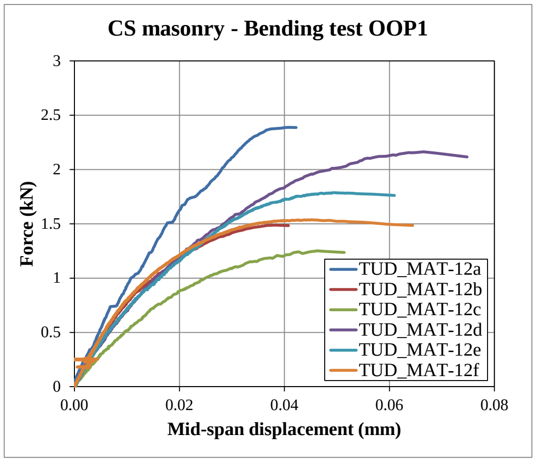

(a)

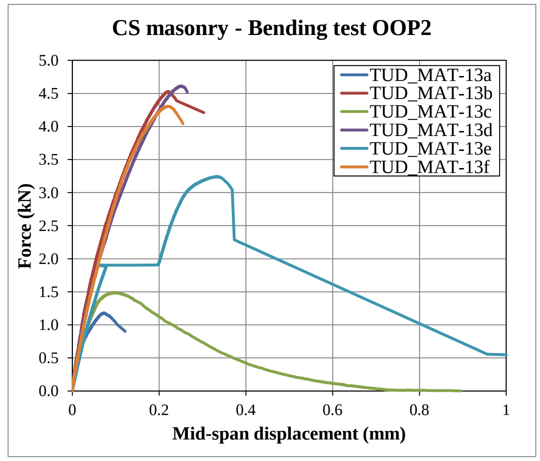

(b)

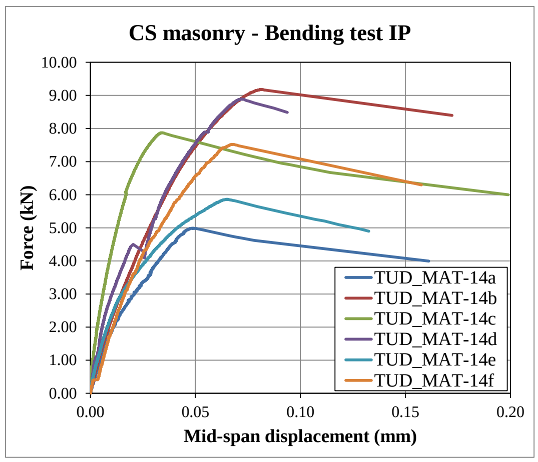

(c)

Figure 29 – Force-displacement curve for calcium silicate masonry specimens subject to: (a) out-of-plane vertical bending test; (b) out-of-plane horizontal bending test; (c) in-plane vertical bending test.

TUD_MAT-12f
(a)

TUD_MAT-13d and TUD_MAT-13e
(b)

TUD_MAT-14b
(c)

Figure 30 - Crack patterns of calcium silicate masonry specimens subject to: (a) out-of-plane vertical bending test; (b) out-of-plane horizontal bending test; (c) in-plane vertical bending test.

Table 18 – Flexural strength values of calcium silicate masonry.

Specimen name	f_{x1}	Specimen name	f_{x2}	Specimen name	f_{x3}
	MPa		MPa		MPa
TUD_MAT-12a	0.29	TUD_MAT-13a	0.28	TUD_MAT-14a	0.27
TUD_MAT-12b	0.18	TUD_MAT-13b	1.09	TUD_MAT-14b	0.49
TUD_MAT-12c	0.15	TUD_MAT-13c	0.36	TUD_MAT-14c	0.43
TUD_MAT-12d	0.26	TUD_MAT-13d	1.10	TUD_MAT-14d	0.47
TUD_MAT-12e	0.21	TUD_MAT-13e	0.77	TUD_MAT-14e	0.31
TUD_MAT-12f	0.18	TUD_MAT-13f	0.95	TUD_MAT-14f	0.41
Average	**0.21**		**0.76**		**0.40**
Standard deviation	**0.05**		**0.36**		**0.09**
Coefficient of variation	**0.25**		**0.47**		**0.23**
		f_{x2} / f_{x1}	**3.6**	f_{x3} / f_{x1}	**1.9**

Figure 31 shows the force displacement curve for *clay masonry* specimens subject to bending tests. In the out-of-plane vertical bending test, the clay masonry specimens showed a brittle failure mechanism; for the other bending tests the failure was more gradual probably due to the presence of the mortar dowels in the perforated bricks.
Figure 32 shows the crack pattern each bending test. For the out-of-plane vertical test, the specimens cracked in one bed joint located in the constant moment zone. For the out-of-plane horizontal test and in-plane test, the cracking occurred in both bed and head joints in the constant moment zone by creating a stepwise crack pattern. In the latter case, cracking of the bricks close to the support or loading points was observed.

Table 19 lists the strength values for the three configurations. The clay masonry, as the calcium silicate masonry, presented an orthotropic behaviour. The out-of-plane horizontal flexural strength resulted approximatively 3 times higher than the out-of-plane vertical flexural strength (f_{x2} / f_{x1} = 2.8). The in-plane vertical flexural strength resulted approximatively 50% higher than the out-of-plane vertical flexural strength (f_{x3} / f_{x1} = 1.5).
Out-of-plane horizontal bending tests and in-plane vertical bending tests were performed by using different specimen's dimensions. In both cases, the strength appeared not influenced by the size of the specimen. As a consequence, the average strength was determined by including all the specimens despite their size.

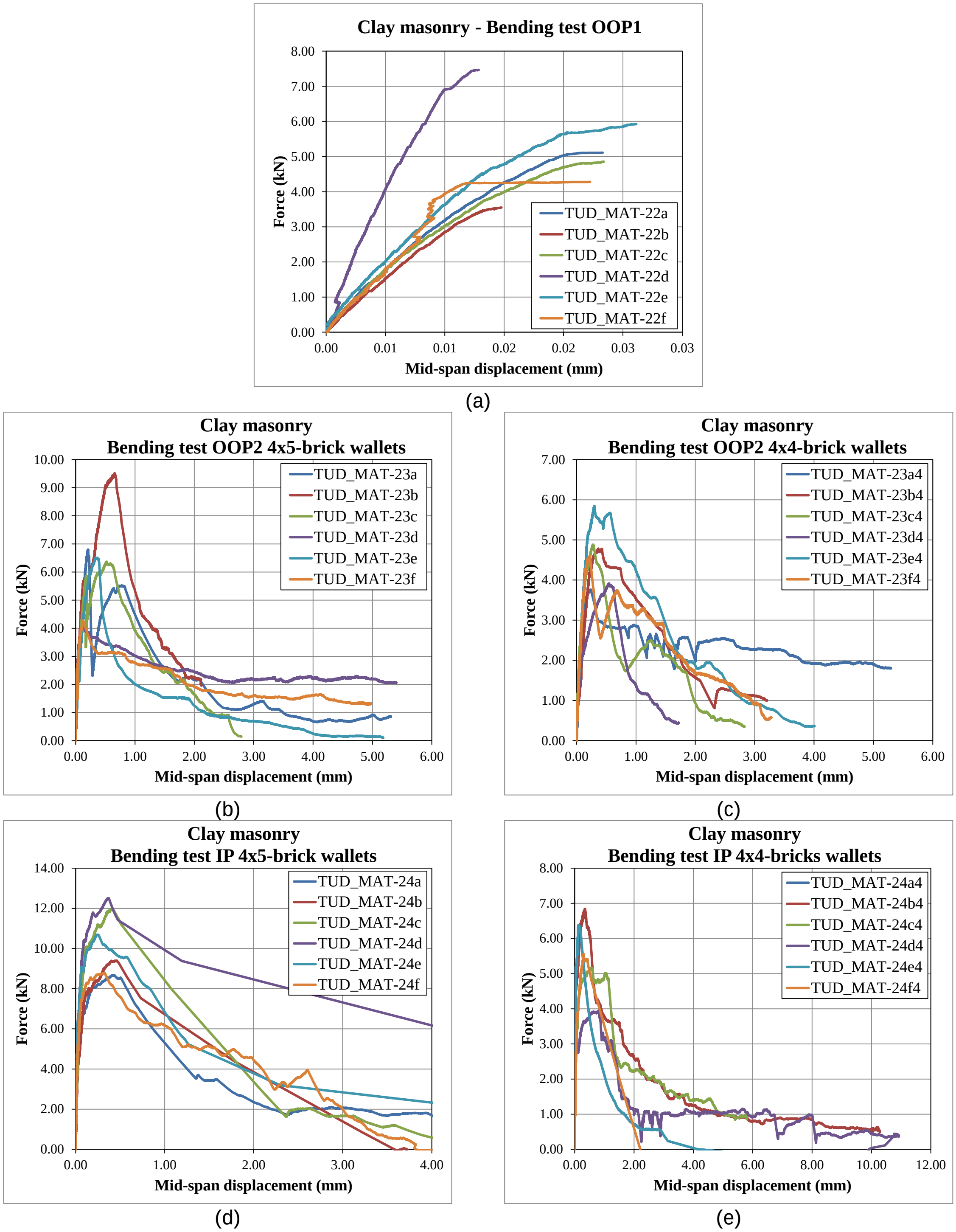

Figure 31 – Force-displacement curve for clay masonry specimens subject to: (a) out-of-plane vertical bending test; (b) out-of-plane horizontal bending test on 4x5-brick specimens; (c) out-of-plane horizontal bending test on 4x4-brick specimens; (d) in-plane vertical bending test on 4x5-brick specimens; (e) in-plane vertical bending test on 4x4-brick specimens.

(a) TUD_MAT-22a

(b) TUD_MAT-23f

(c) TUD_MAT-23f4

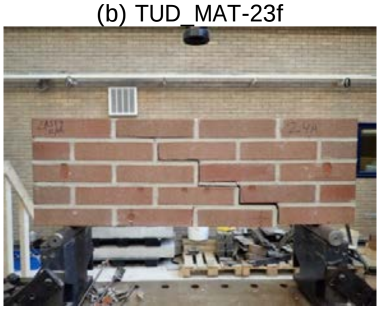

(d) TUD_MAT-24a

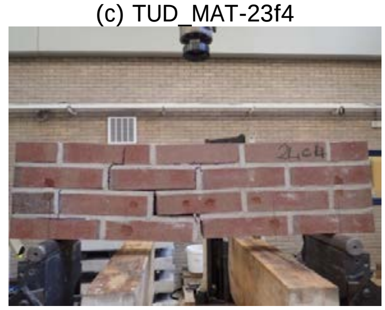

(e) TUD_MAT-24c4

Figure 32 - Crack patterns of clay masonry specimens subject to: (a) out-of-plane vertical bending test; (b)-(c) out-of-plane horizontal bending test; (d)-(e) in-plane vertical bending test.

Table 19 – Flexural strength values of clay masonry.

Specimen name	**f_{x1}**	**Specimen name**	**f_{x2}**	**Specimen name**	**f_{x3}**
	MPa		MPa		MPa
TUD_MAT-22a	0.39	TUD_MAT-23a	1.26	TUD_MAT-24a	0.55
TUD_MAT-22b	0.27	TUD_MAT-23b	1.76	TUD_MAT-24b	0.61
TUD_MAT-22c	0.37	TUD_MAT-23c	1.18	TUD_MAT-24c	0.75
TUD_MAT-22d	0.57	TUD_MAT-23d	0.75	TUD_MAT-24d	0.78
TUD_MAT-22e	0.45	TUD_MAT-23e	1.20	TUD_MAT-24e	0.68
TUD_MAT-22f	0.33	TUD_MAT-23f	0.79	TUD_MAT-24f	0.56
		TUD_MAT-23a4	0.89	TUD_MAT-24a4	0.64
		TUD_MAT-23b4	1.10	TUD_MAT-24b4	0.67
		TUD_MAT-23c4	1.14	TUD_MAT-24c4	0.51
		TUD_MAT-23d4	0.89	TUD_MAT-24d4	0.40
		TUD_MAT-23e4	1.37	TUD_MAT-24e4	0.65
		TUD_MAT-23f4	1.06	TUD_MAT-24f4	0.57
Average	**0.40**		**1.12**		**0.61**
Standard deviation	**0.11**		**0.28**		**0.11**
Coefficient of variation	**0.26**		**0.25**		**0.17**
		f_{x2} / f_{x1}	**2.8**	f_{x3} / f_{x1}	**1.5**

Figure 33 shows the flexural strength values of calcium silicate and clay masonry specimens by adopting histogram representation.

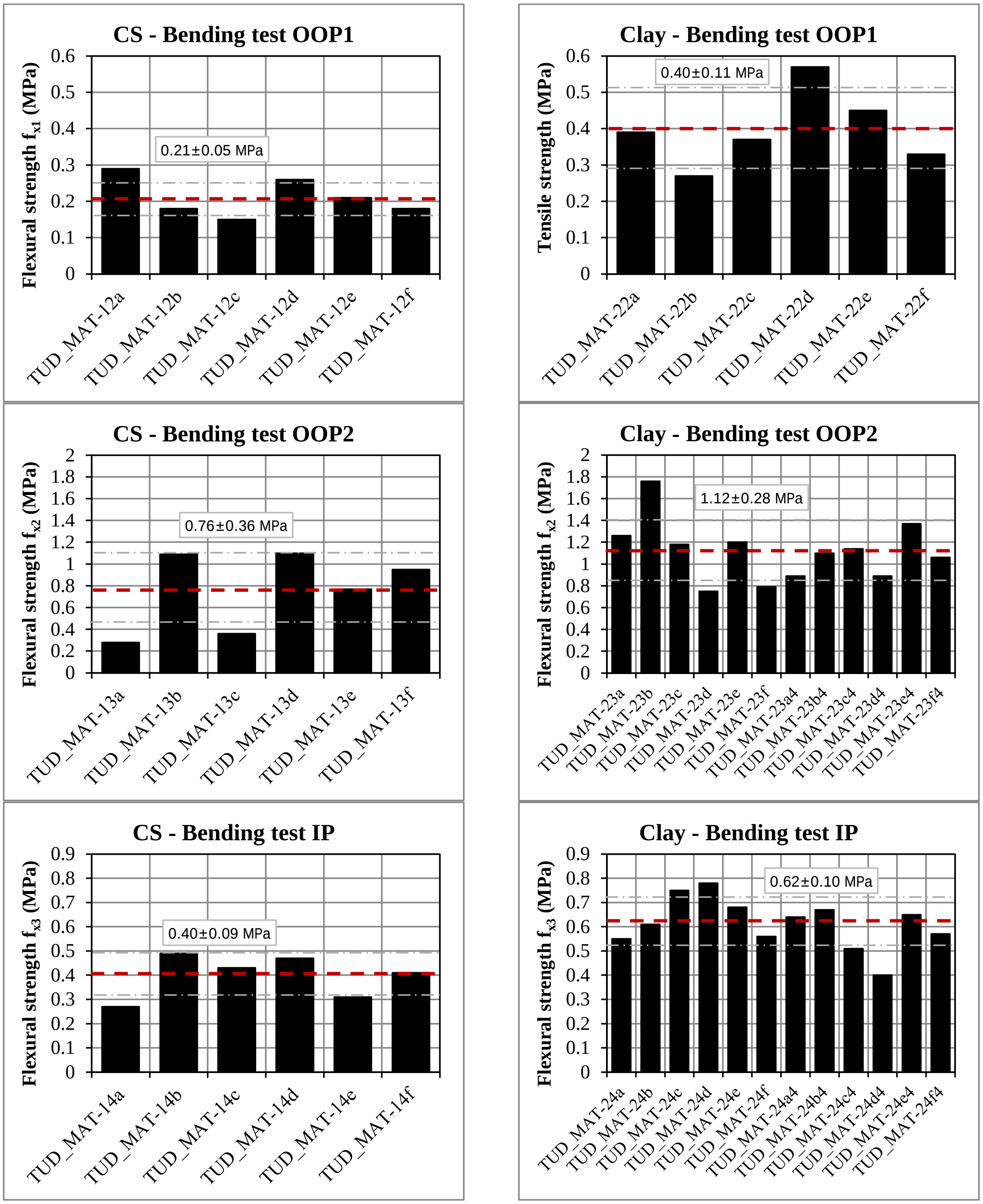

Figure 33 – Flexural strength values of calcium silicate and clay masonry: histogram representation.

8 Bond strength of masonry

The bond strength between masonry unit and mortar was determined in agreement with the bond wrench test proposed by EN 1052-5:2002 [11].

8.1 Testing procedure

The bond strength between masonry unit and mortar was determined by adopting stack bonded specimens. Additionally, specimens were sawn cut from remaining intact parts of specimens that were previously tested in bending. Figure 34 shows the various types of specimens used.

The test was performed for every bed joint in the specimens. The masonry unit below the tested joint was carefully clamped within the retaining frame. The retraining frame was primary composed by steel beams connected by rods; additionally wooden or rubber strips were added to ensure that the clamping does not influence other joints than the one tested (Figure 35).
A clamp provided with a lever was applied to the masonry unit above the tested. The lever was used to apply a bending moment to the brick-mortar interface. The applied moment was registered on an analogue scale. The apparatus was officially calibrated in the range 20–215 Nm, with a tolerance of 4%. Manual readings were accurate to 10 Nm.

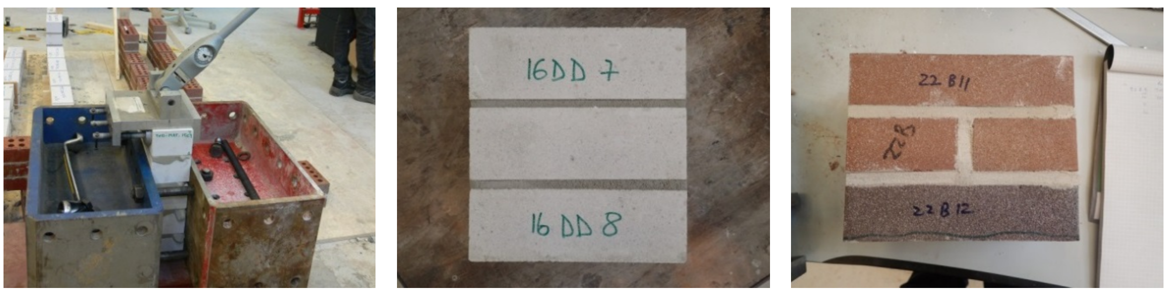

(a) (b) (c)

Figure 34 – Specimens for bond wrench test: (a) five stack bonded bricks specimen; (b) three stack bonded bricks specimen; (c) sawn cut specimen.

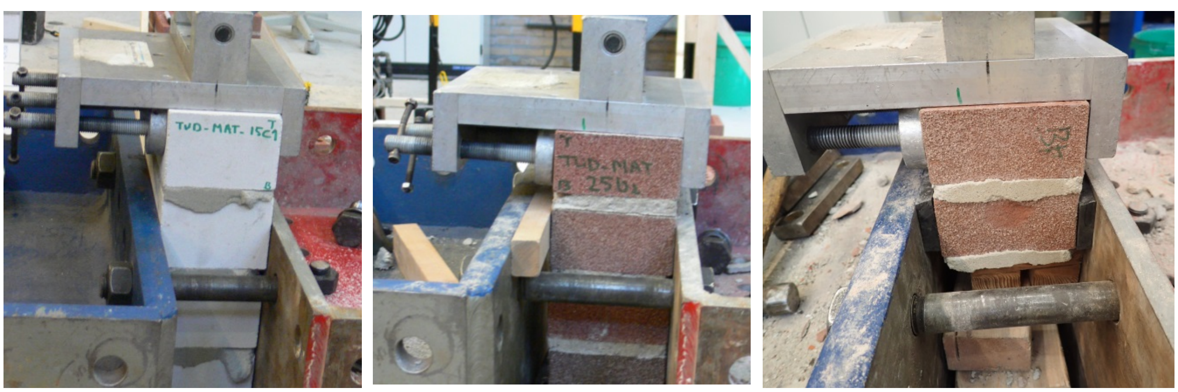

(a) (b) (c)

Figure 35 - Retraining frame: (a) steel beams; (b) steel beams with a wooden strip; (c) steel beams with rubber strips.

8.2 Elaboration of data

The bond wrench strength f_w was calculated on the assumption that the stress distribution is linear over the width of the top masonry unit [11]:

$$f_w = \frac{F_1 e_1 + F_2 e_2 - \frac{2}{3} t_u \left(F_1 + F_2 + \frac{F_3}{4} \right)}{l_j w_j^2 / 6} \tag{8}$$

where F_1 is the failure load, calculated from the lever arm length and the bending moment registered by the bond wrench scale. F_2 is the normal force as a result of the weight of the bond wrench apparatus (F_2 = 72.3 N). F_3 is the weight of the masonry unit pulled off from the specimen, including the weight of adherent mortar. Furthermore, e_1 is the distance from the applied load to the tension face of the specimen, e_2 is the distance from the centre of gravity of the clamp to the tension face of the specimen, l_j is the mean length of the bed joint, and w_j is the mean width of the bed joint. Figure 36 show the set-up and the definition of the various quantities.

Figure 37 reports the classification of the type of failures [11], while Figure 38 shows the observed failure mechanisms.

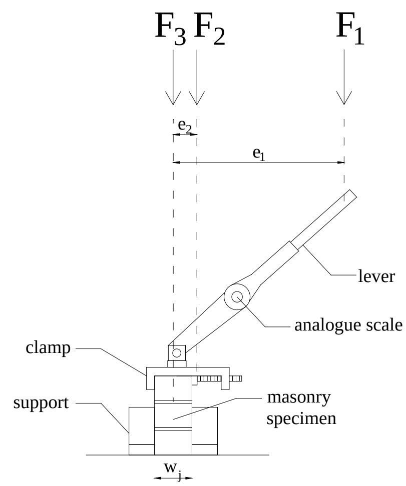

Figure 36 – Test set-up for the bond wrench test.

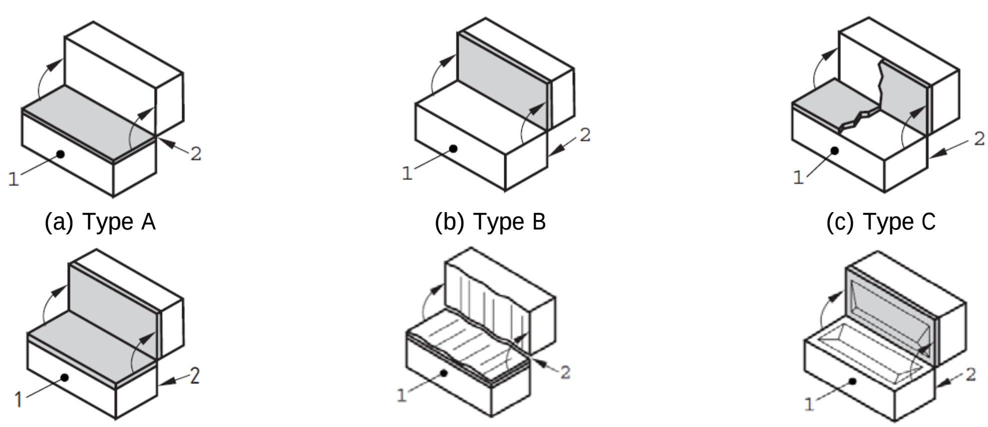

(a) Type A (b) Type B (c) Type C

(d) Type D (e) Type E (f) Type F

Figure 37 – Classification of failure modes (1 tension face, 2 compression face) [11].


(a) (b) (c) (d)

Figure 38 – Observed failure mechanisms: (a) type A in stack bonded specimens; (b) type B and mixed mode type B-C in stack bonded specimens; (c) type B sawn cut specimens; (d) type C in stack bonded specimens.

8.2.1 Specimens casted during the first construction period

In the first construction period, small-scale specimens and large-scale walls were built during March and April 2015. The first were used to tests the material properties (MAT specimens), while the second to study the in-plane and out-of-plane behaviour of walls (COMP specimens). During this period, bond-wrench test have been performed for both calcium silicate and clay masonry.

Table 20 and Table 21 list the results for the calcium silicate and clay masonry, respectively.

Table 20 – Bond strength of calcium silicate masonry specimens (first period).

Specimen type	Retraining frame	Specimen Name*	Maturation	l_j	w_j	F_3	F_1	e_1	e_2	f_w	Failure mode
			days	mm	mm	N	N	mm	mm	MPa	
Five stack bonded brick specimens	Only steel	15a1	40	211	101	27.4	674	323	23	0.47	A
		15a2	40	212	100	29.7	567	322	22	0.40	C
		15a3	40	212	100	28.5	585	322	22	0.41	A
		15b1	40	212	102	27.7	532	324	24	0.36	A
		15b2	40	212	102	32.7	585	324	24	0.40	C
		15b3	40	212	102	31.0	567	324	24	0.39	B-C
		15c1	41	213	102	28.4	532	324	24	0.36	C
		15c3	41	212	102	31.6	567	324	24	0.39	A
		15c4	41	212	103	31.8	567	325	25	0.38	C
		15d1	41	212	102	30.7	567	324	24	0.39	B-C
		15d2	41	212	102	30.0	532	324	24	0.36	C
		15d3	41	212	103	31.4	496	325	25	0.33	B-C
		15d4	41	212	102	29.9	479	324	24	0.32	B-C
		15e1	41	212	103	31.7	330	325	25	0.22	B
		15e2	41	212	103	30.8	426	325	25	0.28	C
Three stack bonded brick specimens	Steel and rubber	16aa1	57	212	102	27.6	292	522	42.4	0.35	A
		16aa2	57	213	101	28.9	188	521	41.4	0.23	C
		16bb3	57	212	102	30.1	250	522	42.4	0.30	B
		16bb4	57	212	102	27.6	250	522	42.4	0.30	A
		16cc5	57	212	101	30.2	240	521	41.4	0.29	B
		16cc6	57	212	102	27.4	313	522	42.4	0.38	A
		16dd7	57	212	102	31.1	219	522	42.4	0.26	B
		16dd8	57	212	102	28.6	281	522	42.4	0.34	A
		16ee9	57	212	101	30.2	167	521	41.4	0.20	C
		16ee10	57	212	102	28.3	198	522	42.4	0.24	A
Sawn cut specimens	Steel and rubber	12f1	58	211	101	27.8	94	521	41.4	0.11	A
		12f2	58	211	102	29.6	63	522	42.4	0.07	C
		12f3	58	211	102	28.6	94	522	42.4	0.11	A
		12f4	58	212	102	31.6	73	522	42.4	0.08	B
		12b1	58	211	102	28.6	63	522	42.4	0.07	A
		12b2	58	212	101	27.7	125	521	41.4	0.15	A
		12b3	58	211	103	28.6	167	523	43.4	0.20	A
		12b4	58	211	101	27.9	167	521	41.4	0.20	A
		12e1	58	211	101	27.6	104	521	41.4	0.13	A
		12e2	58	212	101	28.6	63	521	41.4	0.07	C

*Complete specimen name starting with TUD_MAT-.

Table 21 - Bond strength of clay masonry specimens (first period).

Specimen type	**Retraining frame**	**Specimen Name***	**Maturation**	**l_j**	**w_j**	**F_3**	**F_1**	**e_1**	**e_2**	**f_w**	**Failure mode**
			days	mm	mm	N	N	mm	mm	MPa	
Five stack bonded brick specimens	Steel and wood	25a1	28	210	101	17.6	284	323	23	0.19	A
		25a3	28	211	103	23.5	514	325	25	0.34	A
		25a4	28	210	102	22.2	284	324	24	0.19	B
		25b1	28	210	102	22.3	142	324	24	0.09	B
		25b2	28	211	101	23.4	124	323	23	0.08	B
		25b3	28	209	101	18.6	71	323	23	0.04	A
		25b4	28	210	100	23.0	213	322	22	0.14	A
		25c1	28	210	101	21.8	199	323	23	0.13	B
		25c2	28	209	98	18.8	71	320	20	0.04	A
		25c4	28	209	100	23.1	266	322	22	0.18	B
Sawn cut specimens	Steel only	22b1	82	205	102	18.5	313	522	42.4	0.39	A
		22b2	82	204	101	19.4	125	521	41.4	0.16	-
		22b3	82	208	99	19.8	313	519	39.4	0.41	-
		22b4	82	207	100	20.7	167	520	40.4	0.21	-
		22b5	82	209	101	20.8	417	521	41.4	0.53	C
		22b6	82	208	100	19.7	42	520	40.4	0.05	C
		22b7	82	206	100	20.6	344	520	40.4	0.45	C
		22b8	82	206	99	19.6	229	519	39.4	0.30	B
	Steel and rubber	22b9	82	210	100	23.5	167	520	40.4	0.21	B
		22b10	82	209	101	23.3	156	521	41.4	0.19	B
		22b11	82	209	101	23.2	208	521	41.4	0.26	B
		22b12	82	209	101	20.6	156	521	41.4	0.19	C
		22a1	82	209	101	19.6	298	521	41.4	0.37	A
		22a2	83	210	101	21.6	385	521	41.4	0.48	C
		22a3	83	205	101	19.7	281	521	41.4	0.36	C
		22a4	83	205	101	20.2	365	521	41.4	0.47	C
		22a5	83	210	100	19.4	379	520	40.4	0.48	A
		22a6	83	209	101	23.9	448	521	41.4	0.57	B
		22f1	84	207	100	23.0	229	520	40.4	0.29	B
		22f2	84	207	100	20.3	260	520	40.4	0.34	C
		22f3	84	211	101	21.7	83	521	41.4	0.10	C
		22f4	84	210	101	19.0	146	521	41.4	0.18	A
		22f5	84	212	101	19.1	260	521	41.4	0.32	A
		22f6	84	210	101	20.1	302	521	41.4	0.38	A
		22f7	84	207	99	23.5	333	519	39.4	0.44	B
		22f8	84	207	101	19.2	115	521	41.4	0.14	A
		22f9	84	210	101	19.0	302	521	41.4	0.38	A
		22f10	84	210	101	21.4	156	521	41.4	0.19	C

*Complete specimen name starting with TUD_MAT-.

Table 22 and Table 23 provide an overview of the bond wrench test results for the *calcium silicate and clay masonry* specimens, respectively. Figure 39 shows the results in terms of probability distribution function.
Both masonry types showed average bond strength of 0.27 MPa. However, in both cases, two data sets follow a similar distribution of the strength while one data set shows lower strength value. This variation could not be correlated to the type of specimen or to the type of retraining frame. By excluding the low strength data, the bond strength of the calcium silicate and clay masonry equals 0.33 MPa (C.o.V. = 20%) and 0.32 MPa (C.o.V. = 44%), respectively.

Table 22 - Average bond strength of calcium silicate masonry (first period).

Specimen type	**Retraining frame**	**No. data**	f_m **(MPa)**	f_w		
				Average (MPa)	**Standard deviation (MPa)**	**Coefficient of variations**
Five stack bonded brick specimen	Steel	15	7.13	0.36	0.06	0.16
Three stack bonded brick specimen	Steel & rubber	10	-	0.29	0.06	0.20
Sawn cut specimen	Steel & rubber	10	6.95	0.12	0.05	0.42
Total		35		**0.27**	**0.12**	**0.43**
Excluding sawn cut specimens		25		0.33	0.07	0.20

Table 23 - Average bond strength of clay masonry (first period).

Specimen type	**Retraining frame**	**No. data**	f_m **(MPa)**	f_w		
				Average (MPa)	**Standard deviation (MPa)**	**Coefficient of variations**
Five stack bonded brick specimen	Steel & wood	10	6.15	0.14	0.09	0.63
Sawn cut specimen	Steel	8	-	0.31	0.16	0.52
Sawn cut specimen	Steel & rubber	20	-	0.32	0.13	0.41
Total		38		**0.27**	**0.15**	**0.54**
Excluding stack bonded specimens		28		0.32	0.14	0.44

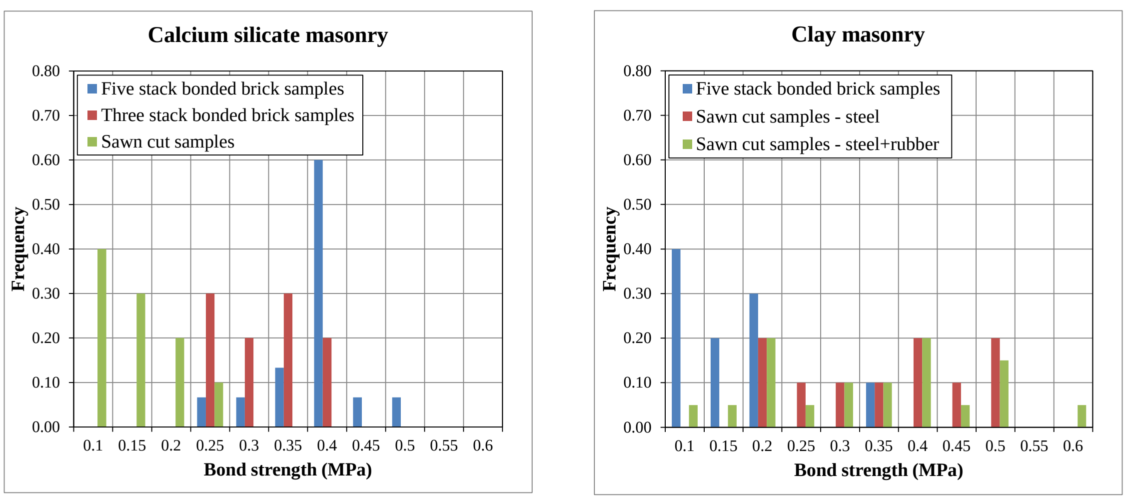

(a) (b)

Figure 39 – Probability distribution functions of bond strength (first period): (a) calcium silicate masonry specimens; (b) clay masonry specimens.

8.2.2 Specimens casted during the second construction period

In the second construction period (September 2015), the full-scale assemblage was built together with small-scale companion specimens. During this period, bond-wrench test were performed on calcium silicate specimens.

Table 24 lists the results for the bond wrench tests on calcium silicate masonry. Figure 40 shows the observed failure mechanisms.

Table 24 – Bond strength of calcium silicate masonry specimens (second period).

Specimen type	Retraining frame	Specimen name	Maturation	l_j	w_j	F_3	F_1	e_1	e_2	f_w	Failure mode
			days	mm	mm	N	N	mm	mm	MPa	
Five stack bonded brick specimens TUD_MAT_15H	Steel and rubber	15Ha1	45	212	100	28.5	167	458	38.4	0.18	A
		15Ha2	45	211	101	28.8	298	459	39.4	0.32	A
		15Ha3	45	212	101	28.6	321	459	39.4	0.34	A
		15Ha4	45	212	102	28.7	202	460	40.4	0.21	A
		15Hb1	45	212	101	28.4	238	459	39.4	0.25	A
		15Hb2	45	212	102	28.8	238	460	40.4	0.25	A
		15Hb3	45	211	102	28.4	190	460	40.4	0.20	A
		15Hb4	45	211	102	31.7	190	460	40.4	0.20	B
		15Hc1	45	212	102	28.4	119	460	40.4	0.12	A
		15Hc2	45	212	102	29.8	131	460	40.4	0.13	C
		15Hc3	45	211	102	28.4	167	460	40.4	0.17	A
		15Hc4	45	211	101	28.4	190	459	39.4	0.20	A
		15Hd1	45	212	102	27.4	155	460	40.4	0.16	A
		15Hd2	45	212	101	29.4	238	459	39.4	0.25	C
		15Hd3	45	211	101	28.5	238	459	39.4	0.25	A
		15Hd4	45	212	102	32.1	233	460	40.4	0.24	B
		15He1	39	212	101	28.9	345	459	39.4	0.37	C
		15He2	39	211	102	29.7	345	460	40.4	0.36	C
		15He3	39	212	102	29.0	369	460	40.4	0.39	C
		15He4	39	212	101	29.1	381	459	39.4	0.41	C
		15Hf1	39	211	102	28.4	345	460	40.4	0.36	A
		15Hf2	39	212	101	28.8	357	459	39.4	0.38	C
		15Hf3	39	212	102	28.5	310	460	40.4	0.32	A
		15Hf4	39	212	102	26.5	214	460	40.4	0.22	A
		15Hg1	39	212	101	28.4	190	459	39.4	0.20	A
		15Hg2	39	212	101	28.4	286	459	39.4	0.30	A
		15Hg3	39	212	102	30.3	310	460	40.4	0.32	C
		15Hg4	39	211	101	27.3	274	459	39.4	0.29	A
		15Hh1	39	212	103	28.4	274	461	41.4	0.28	A
		15Hh2	39	211	102	27.9	357	460	40.4	0.38	C
		15Hh3	39	212	102	29.8	357	460	40.4	0.37	C
		15Hh4	39	212	102	28.4	345	460	40.4	0.36	A
		15Hi1	39	211	100	29.9	262	458	38.4	0.28	B
		15Hi2	39	212	101	28.4	310	459	39.4	0.33	A
		15Hi3	39	212	102	30.4	286	460	40.4	0.30	B-C
		15Hi4	39	212	101	26.2	357	459	39.4	0.38	A

(a) (b) (c)

Figure 40 – Observed failure mechanisms: (a) type A; (b) type B; (c) type C.

Table 25 compares the bond wrench results for *calcium silicate masonry* obtained in the first and second period. Both series showed an average bond strength value of approximatively 0.27 MPa. In the second period, the coefficient of variation was approximatively 30%, thus slightly lower than in the first period. Figure 39 shows the comparison in terms of probability distribution function between the two periods.

Table 25 – Comparison between bond wrench test results obtained in the first and second period for calcium silicate masonry.

Period	**No. Specimens**	f_w		
		Average (MPa)	**St. dev. (MPa)**	**C.o.V.**
First period (MAT/COMP)	35	**0.27**	0.12	0.43
Second period (BUILD/MAT-H and ties)	36	**0.28**	0.08	0.29
$(P_{second}-P_{first}) / P_{first}$		**0.04**		

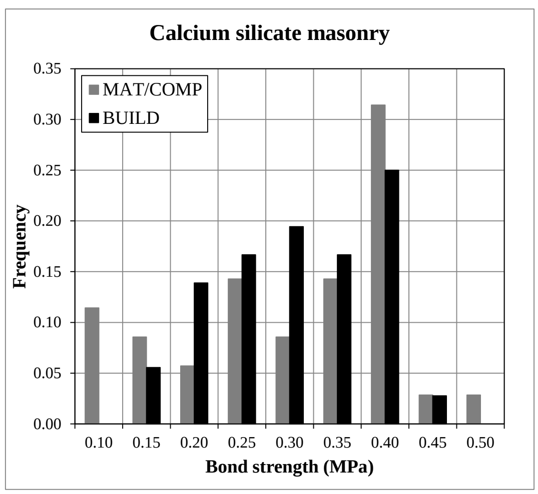

Figure 41 – Probability distribution functions of bond strength value obtained in the first (MAT/COMP) and second (BUILD) period.

9 Shear strength of masonry

The initial shear properties of masonry were determined in agreement with EN 1052-3:2002 [12]. However, a displacement control procedure was used, instead of the prescribed force control procedure, to evaluate the residual strength properties.
The tests were performed only in the first period.

9.1 Testing procedure

Fifteen specimens for each type of masonry were prepared. The masonry specimens were composed by one brick in length ($l_s = l_u$) and three bricks in height. The thickness of the masonry specimen was the same of the masonry unit ($t_s = t_u$). A layer of gypsum was applied to the external faces of the specimens

Figure 42a shows the test set-up used. During the test, the specimen was rotated of 90 degree with respect to the casting position (Figure 42b). The specimen was kept under constant lateral pre-compression, while a shear load was applied at the mid masonry unit. Three different levels of pre-compression were investigated. Being the compressive strength of the masonry unit greater than 10 N/mm^2 [15], the pre-compression stresses applied were 0.2, 0.6 and 1.0 N/mm^2. For each pre-compression level, three specimens were tested.

Two independently operated jacks were required to apply the shear and pre-compressive load. The shear load acts in a vertical direction using a displacement controlled apparatus. The apparatus has a 100 kN jack and a spherical joint. The displacement increased at a rate of 0.005 mm/s. During unloading, the displacement was decreased with a rate of 0.05 mm/s. The pre-compressive load was applied perpendicular to the bed joint plane by a manually operated hydraulic jack. The horizontal hydraulic jack was load controlled and applied a transverse compressive load to the specimen. The jack was kept in position by means of four steel rods positioned on opposite sides of the specimen, which were in turn kept in position by steel plates (Figure 42a).

Both on the front and the back side of the specimens, three LVDTs are attached (Figure 42c). Two vertical LVDTs measured the relative vertical displacement of the middle masonry unit with respect to the later ones. LVDTs measured the horizontal displacement between the two external masonry units. Their measuring range was 10 mm with an accuracy of 0.5%.

(a) (b) (c)

Figure 42 – Test set-up for shear-compression test on masonry specimen.

9.2 Experimental results

The shear strength f_v was calculated for each specimen as follows [12]:

$$f_v = \frac{F_{\max}}{2A_s} \tag{9}$$

where F_{max} is the maximum load, A_s is the cross sectional area of the specimen parallel to the bed joints. In the case of perforated bricks, the net area is considered.
The pre-compression stress f_p can be calculated for each specimen as follows [12]:

$$f_p = \frac{F_p}{A_s} \tag{10}$$

where F_p is the pre-compression force.
The test was carried out in displacement control allowing for the determination of the post-peak behaviour. As a consequence, the residual shear strength $f_{v,res}$ was also determined. The residual strength occurred at an almost constant load where a plateau of large sliding displacement was observed. The resistance in the post-peak phase can be associated to friction only since large relative displacement occurs.

The results of all the tests were plotted in a pre-compressive stress versus shear strength diagram. Considering a linear regression of the date, the initial shear strength f_{v0} and the coefficient of friction μ can be found such as the intercept with the horizontal axis and the gradient of the line, respectively. The angle of internal friction α was determined as the angle between the regression line and the horizontal axis.
Similar consideration can be applied to determine the residual initial shear strength $f_{v0,res}$ and the residual coefficient of friction μ_{res}. In the Coulomb friction formulation, the result is:

$$f_v = f_{v0} + \mu f_p \tag{11}$$

$$f_{v,res} = f_{v0,res} + \mu_{res} f_p \tag{12}$$

Table 26 lists the shear properties for both the calcium silicate and clay masonry.
Table 27 and Figure 43 show the results for *calcium silicate masonry*. The calcium silicate masonry showed an initial shear strength equal to 0.14 MPa and a coefficient of friction equal to 0.43 MPa. In the residual phase the coefficient of friction increased to 0.54 indicating a friction/hardening behaviour. All the specimens presented a shear failure in the unit/mortar bond area. Figure 44 shows a typical crack pattern.

Table 28 and Figure 45 show the results for the *clay masonry*. The clay masonry showed an initial shear strength equal to 0.15 MPa and a coefficient of friction equal to 0.87 MPa. As the bricks were perforated, mortar dowels were present. Their detachment from the mortar joint, induced by the shear off of the central masonry unit, was observed both in the pre-peak and post-peak phase. As a consequence, the shear stress versus displacement curve presents small irregularity around the peak (Figure 45a). All the specimens presented a shear failure in the unit-mortar bond area. Figure 46 shows a typical crack pattern.

Table 26 - Shear properties of calcium silicate and clay masonry.

Property	Symbol	Unit	Calcium silicate masonry	Clay masonry
Initial shear strength	f_{v0}	MPa	0.14	0.15
Coefficient of friction	μ		0.43	0.87
Angle of internal friction	α		23°	41°
Residual initial shear strength	f^*_{v0}	MPa	0.03	0.01
Residual coefficient of friction	μ^*		0.54	0.74
Residual angle of internal friction	α^*		28°	37°

Table 27 - Maximum and residual shear strength of calcium silicate masonry specimens.

f_p = 0.2 MPa			f_p = 0.6 MPa			f_p = 1.0 MPa		
Specimen name*	**f_v**	**$f_{v,res}$**	**Specimen name***	**f_v**	**$f_{v,res}$**	**Specimen name***	**f_v**	**$f_{v,res}$**
	MPa	MPa		MPa	MPa		MPa	MPa
16a	0.23	0.13	16b	0.41	0.36	16c	0.57	0.56
16k	0.24	0.13	16h	0.36	0.35	16f	0.56	0.56
16n	0.20	0.13	16l	0.43	0.38	16g	0.58	0.56
Average	**0.22**	**0.13**	Average	**0.40**	**0.36**	Average	**0.57**	**0.56**
St. dev.	**0.02**	**0.00**	St. dev.	**0.04**	**0.02**	St. dev.	**0.01**	**0.00**
C.o.V.	**0.09**	**0.00**	C.o.V.	**0.09**	**0.04**	C.o.V.	**0.02**	**0.00**

*Complete specimen name starting with TUD_MAT-.

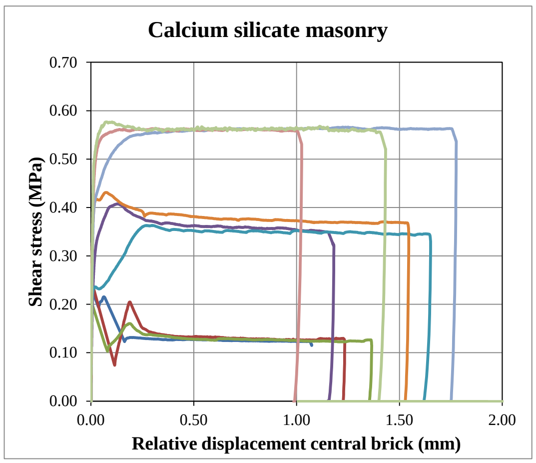

(a)

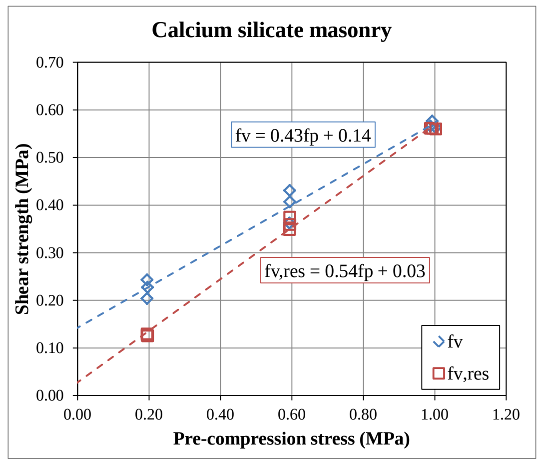

(b)

Figure 43 – Shear test results for calcium silicate masonry: (a) shear stress versus relative displacement of the central brick (LVDTs readings); (b) shear strength versus pre-compression stress.

(a)

(b)

Figure 44 – Crack pattern of calcium silicate masonry specimen under shear test: (a) front-left joint; (b) front-right joint.

Table 28 - Maximum and residual shear strength of clay masonry specimens.

f_p = 0.2 MPa			f_p = 0.6 MPa			f_p = 1.0 MPa		
Specimen name*	**f_v**	**$f_{v,res}$**	**Specimen name***	**f_v**	**$f_{v,res}$**	**Specimen name***	**f_v**	**$f_{v,res}$**
	MPa	MPa		MPa	MPa		MPa	MPa
26c	0.37	0.16	26b	0.57	0.46	26a	0.97	0.78
26d	0.28	0.16	26l	0.70	0.47	26m	1.12	0.74
26e	0.34	0.15	26j	0.71	0.46	26n	1.05	0.76
Average	**0.33**	**0.16**	Average	**0.66**	**0.46**	Average	**1.05**	**0.76**
St. dev.	**0.05**	**0.01**	St. dev.	**0.08**	**0.01**	St. dev.	**0.08**	**0.02**
C.o.V.	**0.14**	**0.04**	C.o.V.	**0.12**	**0.01**	C.o.V.	**0.07**	**0.03**

*Complete specimen name starting with TUD_MAT-.

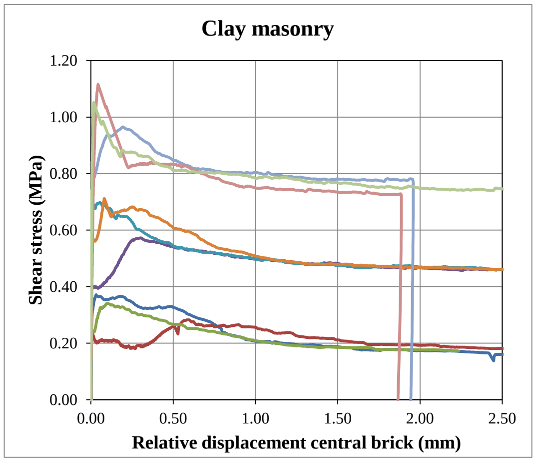

(a)

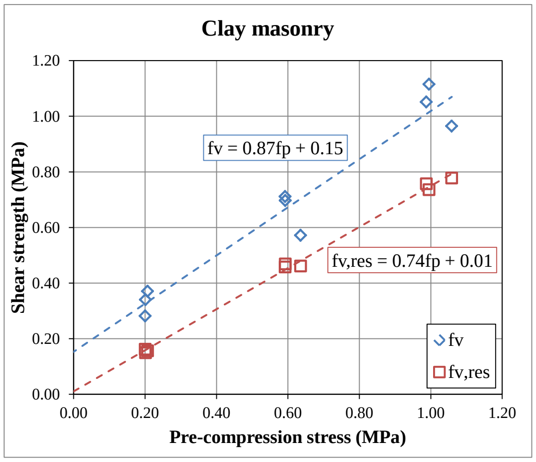

(c)

Figure 45 – Shear test results for clay masonry: (a) shear stress versus relative displacement of the central brick (LVDTs readings); (b) shear strength versus pre-compression stress.

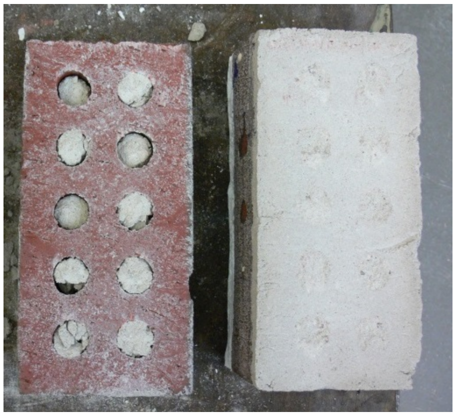

(a)

(b)

Figure 46 – Crack pattern of clay masonry specimen under shear test: (a) front-left joint; (b) front-right joint.

10 Friction behaviour between concrete and masonry

In the full-scale building, the concrete floor was bearing on the masonry walls perpendicular to the façades. The connection between the concrete floor and the masonry walls was provided by a layer of general purpose mortar, the same adopted in the construction of the calcium silicate masonry.
In order to determine the behaviour of the floor-to-wall connection, a friction has been performed similarly to the shear-compression test for masonry.
This test has been performed only in the second period.

10.1 Testing procedure

The specimens were composed of a concrete unit place between two calcium silicate bricks (Figure 47). During testing, the specimen was rotated of 90 degree with respect to the casting position. A layer of gypsum was applied to the external faces of the specimens.

The specimen was positioned in the testing apparatus between the two steel plates and it was supported by roller bearings (Figure 47). A constant lateral pre-compression was applied, while the middle masonry unit was subject to a vertical displacement. Three levels of pre-compression stresses were applied 0.2, 0.6 and 1.0 N/mm^2. For each pre-compression level, three specimens were tested.

Two independently operated jacks were required to apply the shear and pre-compressive load. The shear load acted in a vertical direction using displacement controlled apparatus. The apparatus had a 10 tons jack and a spherical joint. The displacement increased at a rate of 0.005 mm/s, which was prescribed by the piston of the jack. During unloading, the displacement was decreased with a rate of 0.05 mm/s.
The pre-compressive load was applied by a manually operated hydraulic jack, in a horizontal direction, perpendicular to the bed joint plane. The horizontal hydraulic jack was load controlled and applied a transverse compressive load to the specimen. The jack was kept in position by means of four steel rods positioned on opposite sides of the specimen, which were in turn kept in position by steel plates.

Both on the front and the back side of the specimens, three LVDTs were attached (Figure 47c). Two vertical LVDTs measured the relative vertical displacement of the middle masonry unit with respect to the later ones. LVDTs measured the horizontal displacement between the two external masonry units. Their measuring range was 10 mm with an accuracy of 0.5%.

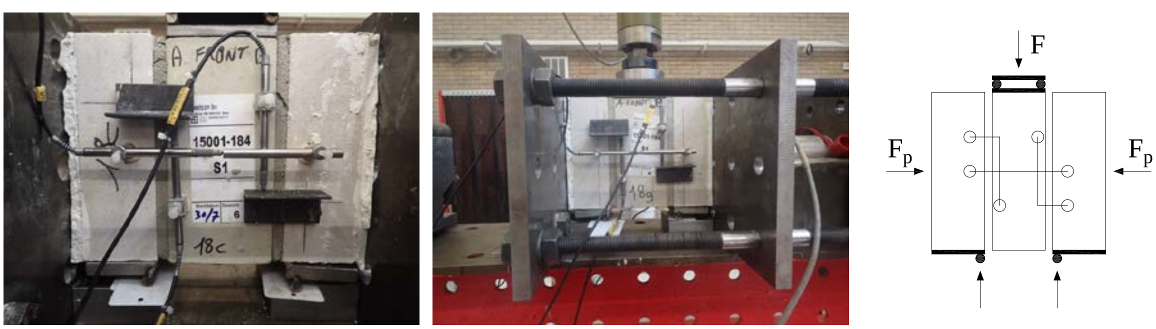

(a) (b) (c)

Figure 47 – Test set-up for the shear-compression test.

10.2 Experimental results

The shear strength f^*_v was calculated for each specimen as follows [12]:

$$f_v^* = \frac{F_{\max}}{2A_s} \tag{13}$$

where F_{max} is the maximum load, A_s is the cross sectional area of the specimen parallel to the bed joints.

The pre-compression stress f_p was calculated for each specimen as follows [12]:

$$f_p = \frac{F_p}{A_s} \tag{14}$$

where F_p is the pre-compression force.
The test was carried out in displacement control allowing for the determination of the post-peak behaviour. As a consequence, the residual shear strength $f_{v,res}$ was also determined. The residual strength occurred at an almost constant load where a plateau of large sliding displacement was observed. The resistance in the post-peak phase can be associated to friction only since large relative displacement occurs.

The results of all the tests are plotted in a pre-compressive stress versus shear strength diagram. Considering a linear regression of the date, the initial shear strength f^*_{v0} and the coefficient of friction μ were found such as the intercept with the horizontal axis and the gradient of the line, respectively. The angle of internal friction α was determined as the angle between the line and the horizontal axis.
Similar consideration were applied to determine the residual initial shear strength $f^*_{v0,res}$ and the residual coefficient of friction μ_{res}. In the Coulomb friction formulation, the result is:

$$f_v^* = f_{v0}^* + \mu^* f_p \tag{15}$$

$$f_{v,res}^* = f_{v0,res}^* + \mu_{res}^* f_p \tag{16}$$

Table 29 compare the frictional/shear properties obtained by testing a mortar joint between concrete and masonry unit and one between two calcium silicate masonry units. The behaviour resulted similar for both interfaces, making that the floor-to-wall dry connection was not a critical elements among any other mortar joint. The masonry showed a slightly higher initial strength and coefficient of friction with respect to the floor-to-wall interfaces. In both cases, an increase of the coefficient of friction in the residual phase was observed, showing a frictional/hardening behaviour.

Table 29 – Properties of floor-to-wall interface and masonry interface.

	Floor-to-wall interface	**Masonry interface**
Initial shear strength f^*_{v0} , f_{v0} (MPa)	0.09	0.14
Coefficient of friction μ^*, μ	0.52	0.43
Angle of internal friction α^*, α	27°	23°
Residual initial shear strength $f^*_{v0,res}$, $f_{v0,res}$ (MPa)	0.00	0.03
Residual coefficient of friction μ^*_{res} , μ_{res}	0.59	0.54
Residual angle of internal friction α^*_{res} , α_{res}	31°	28°

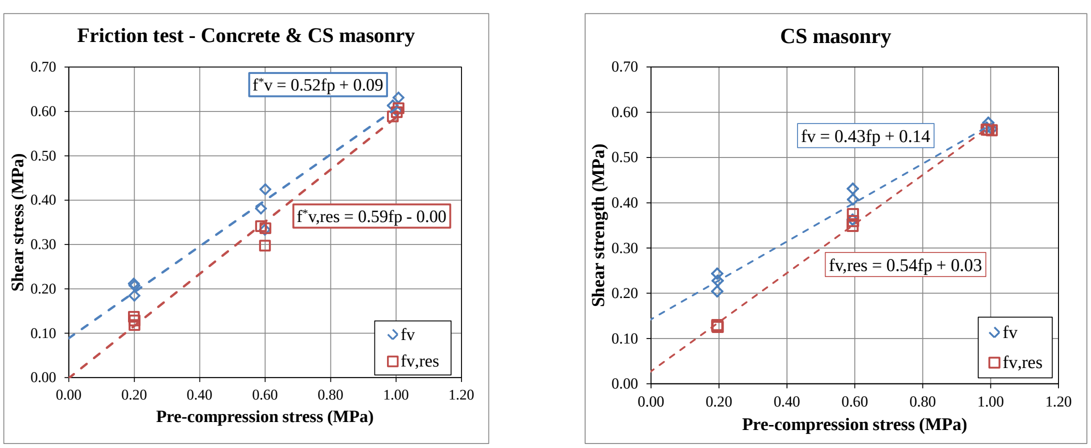

(a) (b)

Figure 48 – Comparison in terms of Coulomb friction law between: (a) friction test on floor-to-wall interface; (b) shear test on calcium silicate masonry.

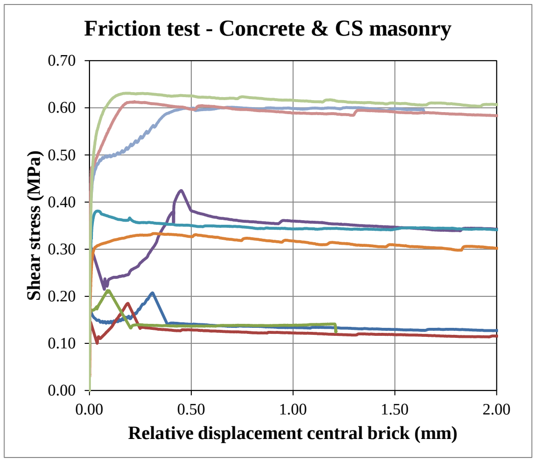

(a)

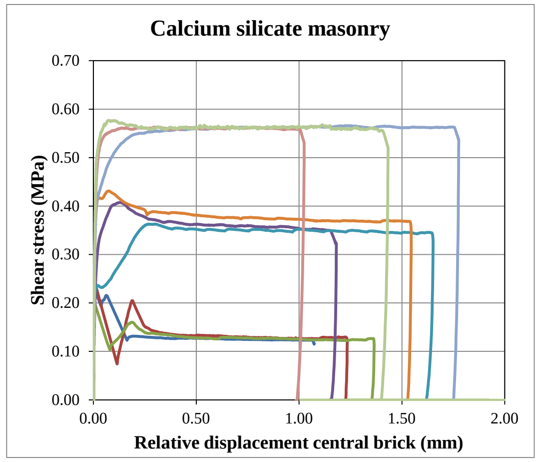

(b)

Figure 49 – Comparison in terms of shear stress versus relative displacement of the central unit: (a) friction test floor-to-wall interface; (b) shear test on calcium silicate masonry.

Figure 48 shows the comparison in terms of Coulomb friction law, while Figure 49 compares the behaviour in terms of force-displacement curves.

Table 27 lists the maximum and residual shear strength values for all the performed tests, making a distinction on the basis of the pre-compression stress applied. For the various pre-compression levels, a limited variation of the strength value was obtained (C.o.V. ~ 10%).
Figure 50 shows a typical crack pattern observed during the test on floor-to-wall interface. In the majority of the cases, a net separation between the mortar joint and one of the unit surface was observed with a limited separation of the mortar joints in two parts. A similar crack pattern was observed during the shear test on calcium silicate masonry (Figure 44).

Table 30 - Maximum and residual shear strength of the floor-to-wall interface.

f_p = 0.2 MPa			f_p = 0.6 MPa			f_p = 1.0 MPa		
Specimen name*	f^*_v	$f^*_{v,res}$	**Specimen name***	f^*_v	$f^*_{v,res}$	**Specimen name***	f^*_v	$f^*_{v,res}$
	MPa	MPa		MPa	MPa		MPa	MPa
18b	0.21	0.13	18h	0.42	0.34	18g	0.60	0.60
18d	0.18	0.12	18j	0.38	0.34	18k	0.61	0.59
18f	0.21	0.14	18l	0.33	0.30	18m	0.63	0.61
Average	**0.20**	**0.13**	Average	**0.38**	**0.33**	Average	**0.62**	**0.60**
St. dev.	**0.01**	**0.01**	St. dev.	**0.05**	**0.02**	St. dev.	**0.01**	**0.01**
C.o.V.	**0.07**	**0.07**	C.o.V.	**0.12**	**0.07**	C.o.V.	**0.02**	**0.02**

*Complete specimen name starting with TUD_MAT-.

(a)

(b)

Figure 50 – Crack pattern of concrete-masonry specimens subject to friction test: (a) front-left joint; (b) front-right joint.

11 Cubic compressive strength of concrete

The floors used in the full-scale assemblage are made by pre-cast concrete slabs. During the construction of these slabs, the factory cast concrete cubes to be tested under uniaxial compression loading. The specimens were tested by the factory after 28 days from the construction.

Table 31 lists the cubic compressive strength values for the samples taken during the various construction days. The average cubic compressive strength was equal to 74.7 MPa.

Table 31 – 28-day cubic compressive strength of the concrete floor used in the full-scale assemblage.

Cast date	f_{cc} MPa
27-07-2015	76.2
28-07-2015	73.6
29-07-2015	76.8
30-07-2015	73.6
31-07-2015	72.5
03-08-2015	75.3
Average	**74.7**
Standard deviation	**1.7**
Coefficient of variation	**0.02**

12 Load capacity of wall ties

The tensile load capacity of masonry wall ties was determined in agreement with EN 846-5:2012 [13]. In the first period, monotonic pull-out tests have been carried out. In the second period, monotonic tests in tension and compression, cyclic test in tension and fully cyclic tests have been performed.

12.1 Testing procedure

The wall ties used in the testing campaign were L-shaped ties with a diameter of 3.6 mm and a length of 200 mm. The specification of the product are given in the Appendix.
The tests referred to cavity walls composed by two masonry walls having a thickness of 100 mm approximatively and a cavity space of 80 mm. In cavity walls, the L-shaped part of the ties is embedded in the inner leaf, which is usually made of calcium silicate masonry or clay masonry, while the zigzag part lies in outer leaf made of clay masonry.
The specimens used for these tests were composed by a single tie embedded in the mortar joint of a masonry specimen (Figure 51, Table 32). The following type of specimens are tested:

- TUD_MAT-17: tie embedded in calcium silicate masonry representing the inner leaf of a cavity wall (hook part of the tie embedded, anchoring length 70 mm),
- TUD_MAT-27: tie embedded in clay masonry representing the outer leaf of a cavity wall (zigzag part of the tie embedded, anchoring length 50 mm),
- TUD_MAT-28: tie embedded in clay masonry representing the inner leaf of a cavity wall (hook part of the tie embedded, anchoring length 70 mm).

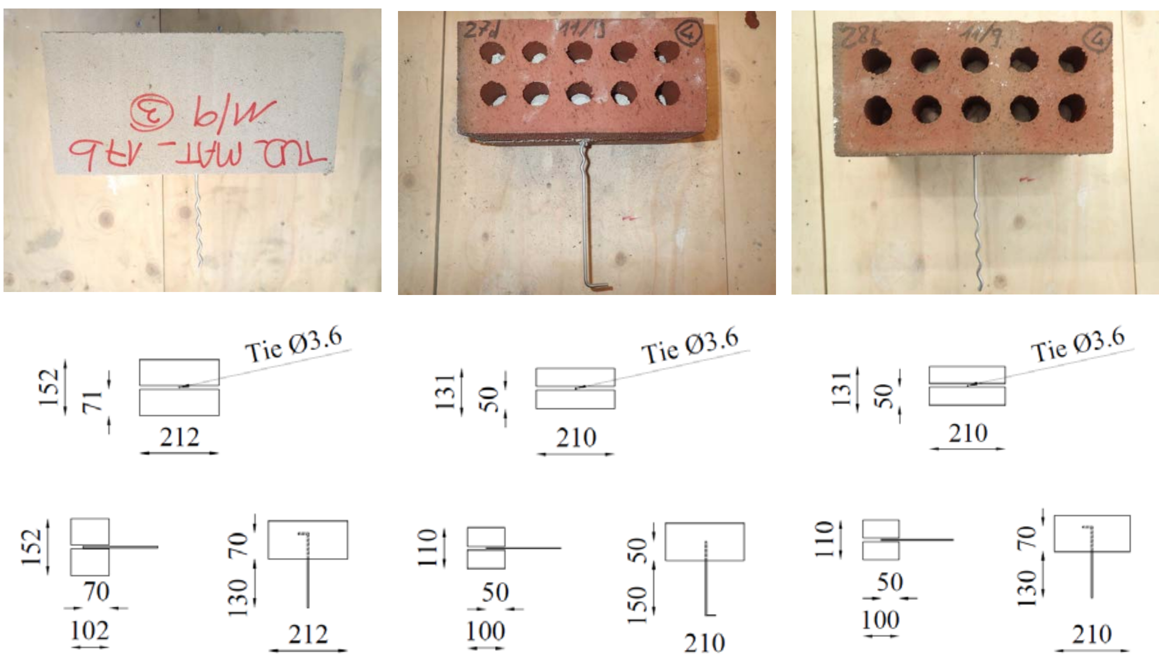

(a) TUD_COMP-17 (b) TUD_COMP-27 (c) TUD_COMP-28

Figure 51 – Tie specimens: (a) ties embedded calcium silicate masonry – inner leaf configuration; (b) tie embedded in clay masonry – outer leaf configuration; (c) tie embedded in clay masonry – inner leaf configuration.

Table 32 - Dimensions of the specimens adopted to test the capacity of ties.

Dimensions	**Calcium silicate TUD_COMP-17**	**Clay TUD_COMP-27**	**Clay TUD_COMP-28**
l_s **(mm)**	212	210	210
h_s **(mm)**	152	110	110
t_s **(mm)**	102	100	100
h_t **(mm)**	130	150	130

The specimen was kept under a constant lateral pre-compression, while a pull-out load was applied to the tie via a displacement controlled apparatus. First, the pre-compression load was applied. Second, an initial displacement is applied on the ties and the measurements were reset to zero. The initial displacement was limited to not exceed a tensile load of 200 N or a maximum take-up of slack of 1 mm. Eventually, the displacement was increased monotonically.
The specimens were placed in the test machine such that the tie body is axial and aligned at the centre of the test machine. The tie was clamped for a minimum length of 50 mm.

Two independently operated jacks were required to apply the pull-out and pre-compressive loads (Figure 52). The pull-out load acted in a vertical direction using displacement controlled apparatus. The apparatus had a 45 kN jack. In the first period, the apparatus consisted also of a spherical joint, which allowed reducing the eccentricities of the load due to the possible not centred position of the ties. This apparatus was modified with a fixed clamping system in the second period, in order to allow compression displacements. The displacement increases at a rate of 0.5 mm/min to respect the maximum load rate of 200 N/mm for low resistant ties prescribed by EN 846-5:2012 [13]. The pre-compressive load is applied in the direction perpendicular to the bed joint plane, by a manually operated hydraulic jack.
Two LVDTs (installed symmetrically on the two opposite sides of the clamp) measure the displacement of the couplet in relation to the clamp. Their measuring range is 10 mm with an accuracy of 0.5%.

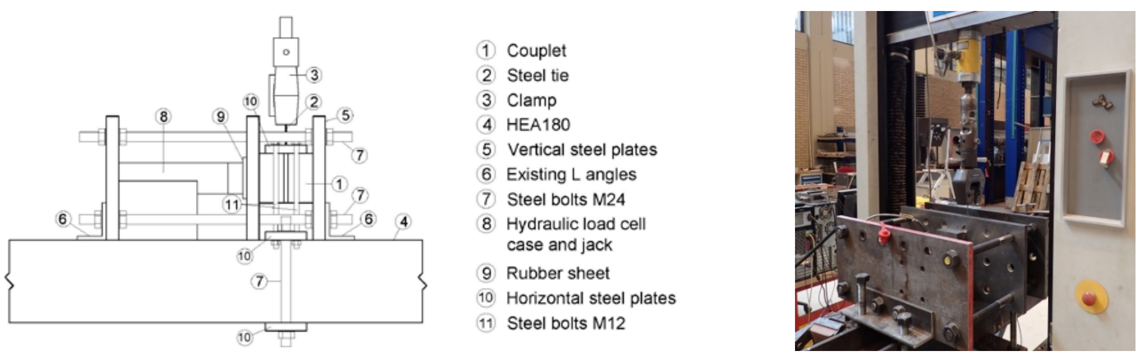

(a) (b)

Figure 52 – Test set-up for masonry wall ties.

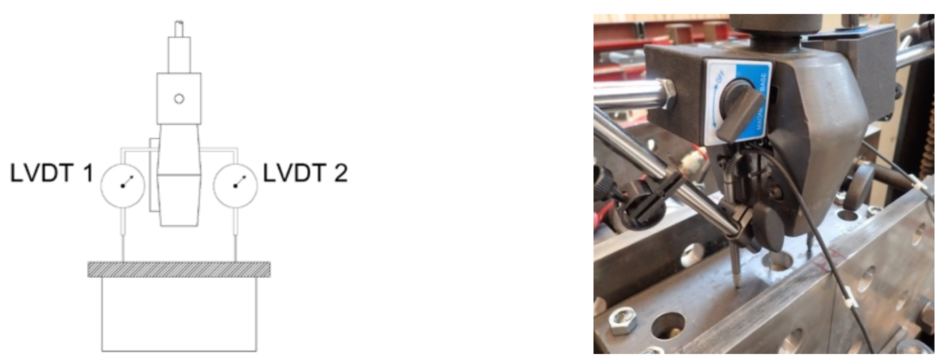

(a) (b)

Figure 53 – Measuring system for masonry wall ties.

The pull-out capacity of wall ties has been investigated during the first construction phase. The monotonic pull-out test was carried out accordingly to the following protocol:

- **Protocol 0T***: the pull-out behaviour of the ties (tensile loading) is determined by monotonically increasing the displacement with a rate a rate of 0.1 mm/s. During the test the specimens were kept under a constant pre-compression stress equal to 0.1 ± 0.01 MPa.

In the second period, both the monotonic and the cyclic behaviour of the wall ties have been investigated accordingly to four different loading schemes:

- **Protocol 0T**: the pull-out behaviour of the ties (tensile loading) was determined by monotonically increasing the displacement with a rate of 0.1 mm/s. During the test the specimens were kept under a constant pre-compression stress equal to 0.3 ± 0.01 MPa.
- **Protocol 0C**: the push-out behaviour of the ties (compressive loading) was determined by monotonically increasing the displacement with a rate of 0.1 mm/s. During the test the specimens were kept under a constant pre-compression stress equal to 0.3 ± 0.01 MPa.
- **Protocol 1** (Figure 54)**:** the displacement was cyclically varied applying a tensile loading on the tie. Each cycle consists of three runs with the same amplitude. The amplitude of the cycles was proportional to the nominal displacement corresponding at the peak Δ_{peak}, which was determined by the monotonic test performed according to the loading protocol 0T. First, two initial cycles of reduced amplitude (0.25 mm and 1 mm) were imposed. Second, the amplitude of each cycle was increased of $0.25\Delta_{peak}$ in the pre-peak stage. Eventually, in the post-peak phase an increment of $0.50\Delta_{peak}$ was adopted for the ties embedded in calcium silicate masonry and an increment of $0.25\Delta_{peak}$ for the ties embedded in the clay masonry. These different amplitude in the post-peak stage have been determined considering the test performed in the first period (protocol 0T*). In each unloading run, the displacement was imposed to reach a zero force. A constant duration for every cycle was assumed and the testing velocity was varied accordingly. During the test the specimens were kept under a constant pre-compression stress equal to 0.3 ± 0.01 MPa.
- **Protocol 2** (Figure 54): the displacement was cyclically varied applying both tensile and compression loading on the tie. The amplitude of the cycles was proportional to the nominal displacement corresponding at the peak Δ_{peak}, which was determined by previous monotonic pull-out test on ties (protocol T0). First, three cycles, composed by three runs, of amplitude equal to 0.1, 0.25 and 0.5 mm were applied. Subsequently, cycled composed by two runs of increased displacements and two runs of reduced displacement were applied. The reduced displacement was calculated as the 60% of the displacements of the two previous runs. The loading rate was chosen to maintain a constant duration of every cycle until reaching the post-peak phase with a reduction of 50% of the peak force. Afterwards, the rate was kept constant at 0.8 mm/s. During the test the specimens were kept under a constant pre-compression stress equal to 0.3 ± 0.01 MPa.

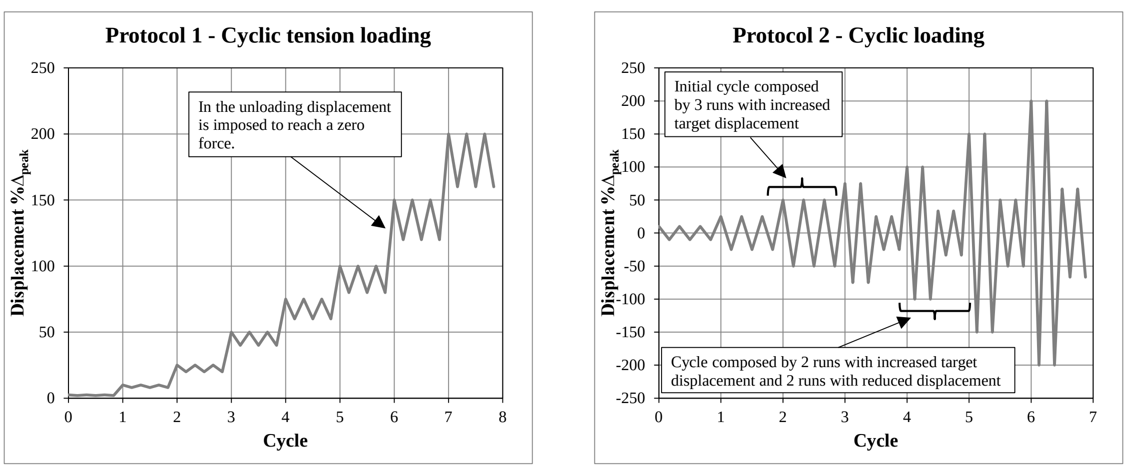

Figure 54 – Cyclic loading protocol for testing masonry wall ties: a) cyclic tension loading protocol 1; b) fully cyclic loading protocol 2.

12.2 Experimental results

This test allowed determining the load capacity and load displacement characteristics of wall ties embedded in mortar joints. The load capacity was evaluated in terms of maximum force, which is defined as tensile load capacity F_{po} and compressive load capacity F_c. The corresponding slip value were respectively named as s_{Fpo} and s_{Fc}.

The slip of the ties was computed from both the clam and the LVDTs measurements. Considering the good agreement between the two measurements (Figure 55a), the clamp measurements is adopted to define the slip of the ties. This choice has been made, because the LVDTs could be only used within a range of displacement of 10 mm.

In the second period, a fixed clamp system has been adopted in order to apply compression stresses. This system resulted in an initial offset of the force for zero imposed displacement (Figure 55b).

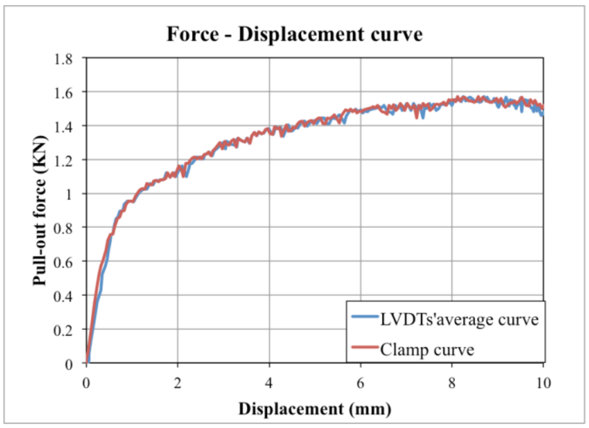

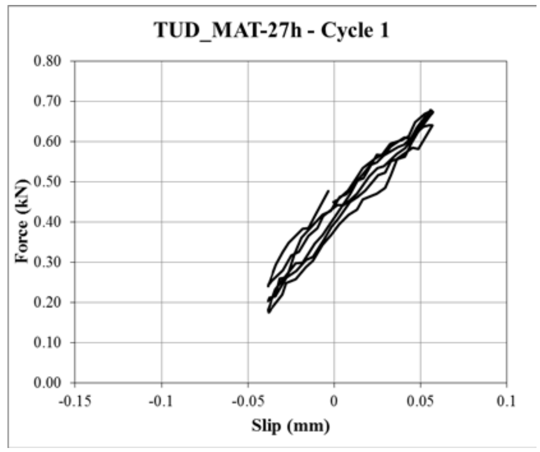

(a) (b)

Figure 55 – Test on ties: (a) comparison between clamp and LVDTs measurements, (b) initial offset due to fixed clamping system.

12.2.1 Specimens casted during the first construction period

In the first construction period small-scale specimens and large-scale walls were built during March and April 2015. The first were used to tests the material properties (MAT specimens), while the second to study the in-plane and out-of-plane behaviour of walls (COMP specimens). During this period specimens for determining the pull-out behaviour of masonry wall ties were built. This first phase includes only monotonic pull-out test according to the loading protocol 0T* on specimens TUD_MAT-17 and TUD_MAT-27.

Figure 56a shows the force displacement curves related to the pull-out of the ties from *calcium silicate masonry* specimens (TUD_MAT-17). The tie slip is evaluated by reading the vertical displacement of the clamp. The two LDVTs were employed to verify that the contrast steel plate did not translate or rotate.
The failure mechanism was similar for all specimens and it consisted of straightening of the embedded hook combined with crushing of the adjacent mortar (Figure 57a). The average load capacity of the tie embedded in calcium silicate masonry specimens (Figure 58a, Table 33) results equal to 1.25 kN with a limited coefficient of variation (7%). The corresponding slip value is equal to 10.3 mm.

Figure 56b shows the force displacement curves related to the pull-out of the ties from clay masonry specimens (TUD_MAT-27). Two failure mechanisms were observed: a cone failure (Figure 57b) and a bond failure (Figure 57c). The high variation of the results and the observed difference in failure mechanism, could be input to the preparation of the specimens. During construction the specimens were placed on the floor and the free part of ties was not supported. In the second period, more attention was taken in the preparation of the specimens. On average, the load capacity of the tie embedded in the clay masonry specimens (Figure 58b, Table 34) results equal to 1.28 kN. The corresponding slip value is equal to approximatively 5 mm.

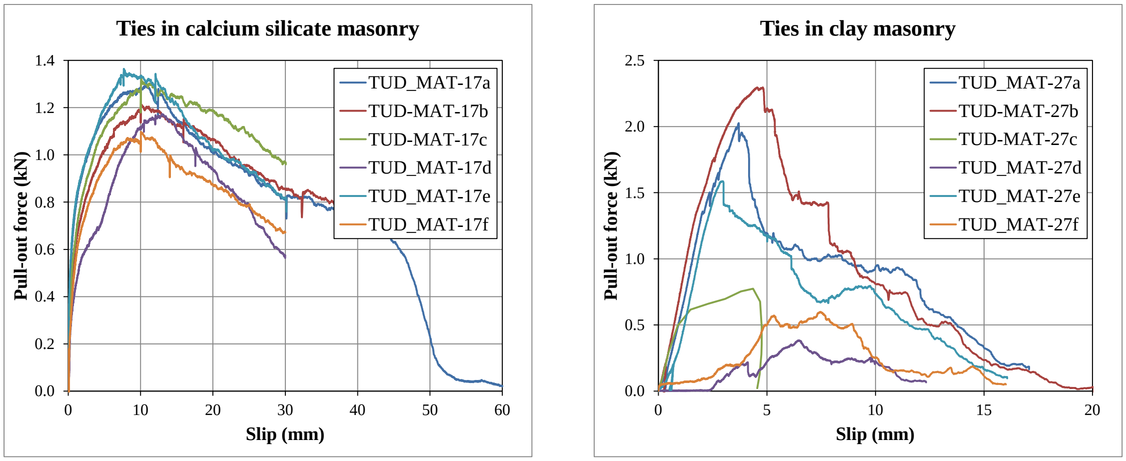

(a) (b)

Figure 56 - Pull-out force versus slip curves of ties in: (a) calcium silicate masonry; (b) clay masonry.

(a) (b) (c)

Figure 57 – Crack patterns for masonry wall ties: (a) straightening of the hook combined with mortar crushing; (b) cone failure; (c) bond failure.

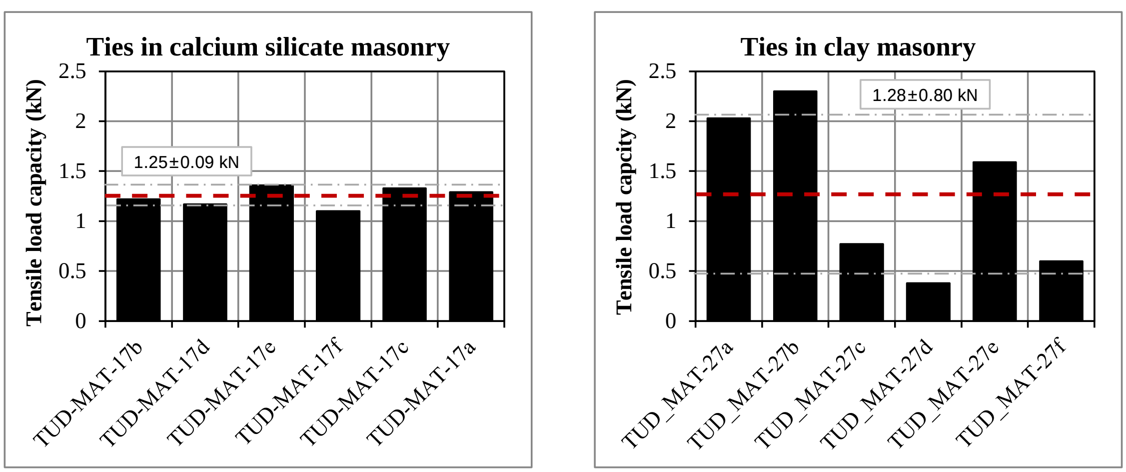

(a) (b)

Figure 58 – Tensile load capacity of ties embedded in: (a) calcium silicate masonry; (b) clay masonry (first period).

Table 33 – Capacity of ties in calcium silicate masonry under monotonic tensile loading (first period).

Specimen name	$F_{po,0}$	$s_{Fpo,0}$
	kN	mm
TUD_MAT-17b	1.29	10.72
TUD_MAT-17d	1.22	10.07
TUD_MAT-17e	1.33	10.09
TUD_MAT-17f	1.17	12.94
TUD_MAT-17c	1.36	7.69
TUD_MAT-17a	1.10	10.06
Average	**1.25**	**10.26**
Standard deviation	**0.10**	**1.68**
Coefficient of Variation	**0.08**	**0.16**

Table 34 – Capacity of ties in clay masonry under monotonic tensile loading (first period).

Specimen name	$F_{po,0}$	s_F	**Failure mechanism**
	kN	mm	
TUD_MAT-27a	2.03	3.70	Cone failure
TUD_MAT-27b	2.30	4.81	Cone failure
TUD_MAT-27c	0.77	4.37	Bond failure
TUD_MAT-27d	0.38	6.23	Bond failure
TUD_MAT-27e	1.59	2.96	Cone failure
TUD_MAT-27f	0.60	7.47	Bond failure
Average	**1.28**	**4.92**	
Standard deviation	**0.80**	**1.67**	
Coefficient of Variation	**0.63**	**0.34**	

12.2.2 Specimens casted during the second construction period

In the second construction period (September 2015) the full-scale assemblage was built together with small-scale companion specimens. During this period specimens for determining the behaviour of masonry wall ties were built. In this second period, the behaviour of wall ties under both monotonic (protocol 0T, 0C) and cyclic (protocol 1 and 2) loading has been studied for all three type of specimens.

Ties embedded in calcium silicate masonry specimens (TUD_MAT-17)

Figure 59 shows the behaviour of *ties embedded in calcium silicate masonry* specimens subject to *monotonic tensile test* in terms of force versus tie's slip curve. The behaviour of the ties in tension was characterised by an hardening/softening behaviour. In the pre-peak stage an initial linear-elastic behaviour was observed up to 40% of the maximum force, followed by an hardening behaviour. Subsequently, a softening behaviour was observed up to 50 mm slip, which corresponds to 75% of the anchoring length.

Figure 60 shows the failure mechanism stages during the monotonic test for specimen TUD_MAT-17b. The crack first concentrate around the tie within the mortar joint. In the post-peak stage, a cone of mortar surrounding the tie slipped out from the bed joint. The failure consisted of strengthening of the L-shaped part of the tie inside the mortar joint.

Table 35 lists the main experimental results for the monotonic tensile tests on ties in calcium silicate masonry specimens. The specimens presented an average tensile load capacity of 1.40 kN, which occurred at a slip of 8.4 mm.

Comparing the results with the one of the first period, a variation of 10% in tensile load capacity was observed for an increase of 3 times of the lateral pre-compression (Table 36). Being this increment, within the coefficient of variation of the results, a direct correlation between lateral pre-compression and tensile load capacity could not be established. The failure mechanism was the same as already observed in the test performed in the first period (Figure 60, Figure 57a)

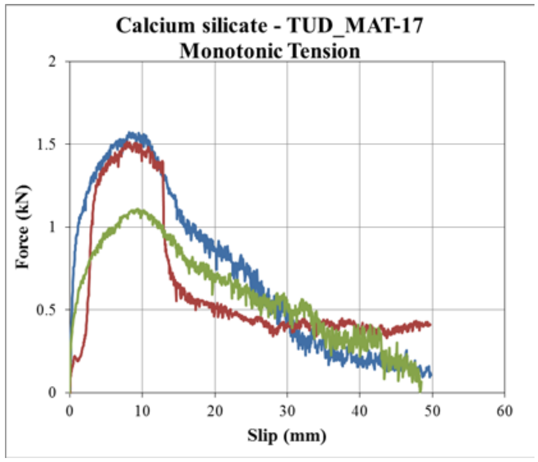

Figure 59 – Force-slip curves for ties embedded in calcium silicate masonry specimens subject to monotonic tensile test (second period).

Table 35 – Capacity of ties in calcium silicate masonry under monotonic tensile loading (second period).

Specimen	Loading protocol	$F_{po,0}$	$s_{Fpo,0}$
		kN	mm
TUD_MAT-17b	P0T	1.57	8.12
TUD_MAT-17c	P0T	1.51	7.86
TUD_MAT-17d	P0T	1.11	9.27
Average		**1.40**	**8.42**
Standard deviation		**0.25**	**0.75**
Coefficient of variation		**0.18**	**0.09**

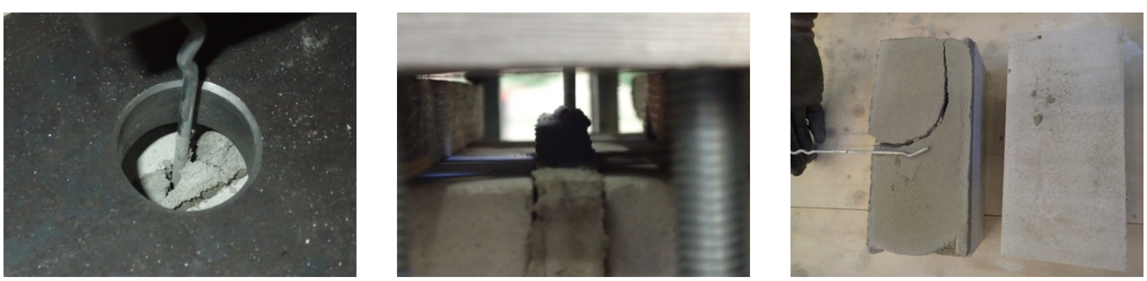

(a) (b) (c)

Figure 60 – Crack pattern of specimen TUD_MAT-17b tested under monotonic tensile loading: (a) maximum force; (b) post-peak stage; (c) failure.

Table 36 – Capacity of ties in calcium silicate masonry under monotonic tensile loading: comparison between first and second period.

	No. specimens	**f_p**	$F_{po,0}$	$s_{Fpo,0}$
		MPa	kN	mm
First period	6	0.1	1.25	8.42
Second period	3	0.3	1.40	10.26
$(P_{second}-P_{first}) / P_{first}$		**0.6**	**0.1**	**0.2**

Figure 61 shows the behaviour of *ties embedded in calcium silicate masonry* specimens subject to *monotonic compressive test* in terms of force versus tie's slip curve. The behaviour of the ties in compression was characterised by an linear behaviour up to the peak and a mixed softening/hardening behaviour in the post peak phase. The maximum force was reached at a slip of approximately 1 mm. In the post-peak phase, a softening behaviour was observed up to 20 mm slip, followed by an hardening behaviour up to 50 mm. The hardening behaviour was caused by the piercing of the zigzag part of the ties against the bed joint, which generates additional friction.

Figure 62 shows the failure mechanism stages during the monotonic test for specimen TUD_MAT-17ac. In correspondence of the peak force, the mortar failed in the bottom part of the specimen and it was pulled out downward by the tie. The increasing downward movements of the tie determined the complete detachment and the expulsion of a mortar cone. At failure, the tie appeared nearly undeformed (Figure 62c) or showed buckling deformation (Figure 62d). This difference can be caused by the strength of the mortar and of the bond.

Table 38 lists the main experimental results for the monotonic compressive tests on ties in calcium silicate masonry specimens. The specimens presented an average compressive load capacity of -1.09 kN, which occurred at a slip of -0.94 mm.

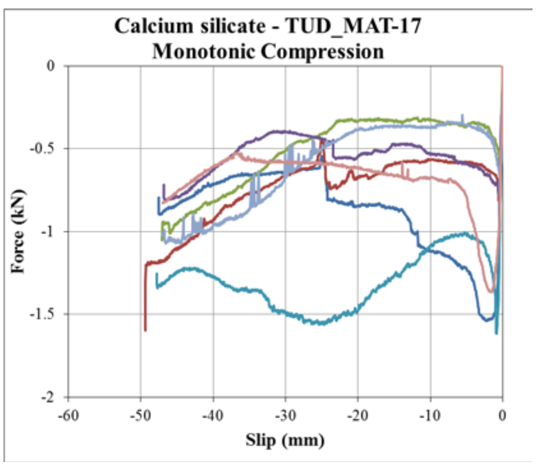

Figure 61 – Force-slip curves for ties embedded in calcium silicate masonry specimens subject to monotonic compressive test.

Table 37 – Capacity of ties embedded in calcium silicate masonry specimens under compressive monotonic loading.

Specimen	**Loading protocol**	$F_{c,0}$	$s_{Fc,0}$
		kN	mm
TUD_MAT-17o	P0C	-1.54	-2.24
TUD_MAT-17p	P0C	-0.81	-0.52
TUD_MAT-17q	P0C	-0.68	-0.38
TUD_MAT-17r	P0C	-0.77	-0.57
TUD_MAT-17s	P0C	-1.62	-0.85
TUD_MAT-17ac	P0C	-0.85	-0.35
TUD_MAT-17ad	P0C	-1.37	-1.66
Average		**-1.09**	**-0.94**
Standard deviation		**0.40**	**0.73**
Coefficient of variation		**0.37**	**0.78**

(a) (b)

(c) (d)

Figure 62 – Crack pattern of specimen TUD_MAT-17ac: (a) cracks formation at the peak force level; (b) slipping of a mortar cone of the bed joint in the post-peak stage; (c)-(d) rupture mechanism for tie and mortar joint and final deformed configuration for the tie.

Figure 63 shows the behaviour of *ties embedded in calcium silicate masonry* specimens subject to *cyclic tensile test* in terms of force versus tie's slip curve. The behaviour of the ties under cyclic tensile loading was similar to the one observed for the monotonic tension tests. The pre-peak stage was characterized by a highly nonlinear behaviour since the onset of the tests, followed after the peak by a softening branch until failure (Figure 63a). The unloading was elastic (Figure 63b).

Figure 64 shows the failure mechanism stages during the cyclic tension test for specimen TUD_MAT-17f. The mechanism was similar to the one observed in the monotonic test. The cracks were concentrated in a cone of mortar surrounding the ties. The failure was characterized by the straightening of the L-shaped part of the tie.

Table 38 lists the main experimental results for the cyclic tension tests on ties in calcium silicate masonry specimens. The specimens presented an average tensile load capacity of 1.46 kN, which occurred at a slip of 9.5 mm. The results in terms of peak values were similar to the one for the monotonic test.

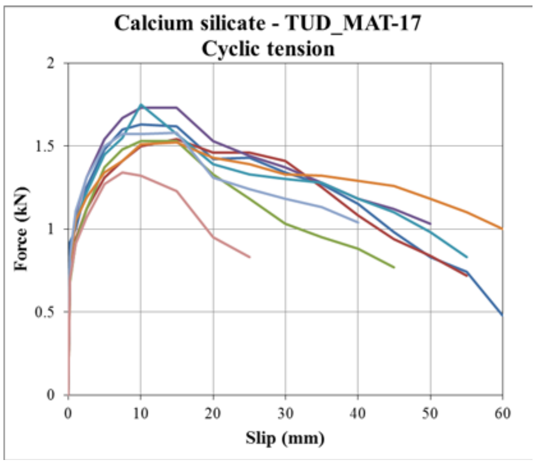

(a)

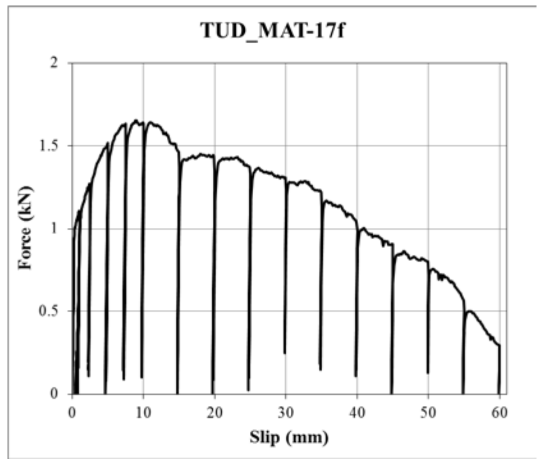

(b)

Figure 63 – Force-slip curves for ties embedded in calcium silicate masonry specimens subject to cyclic tension test.

(a)

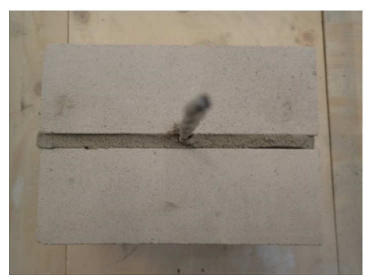

(b)

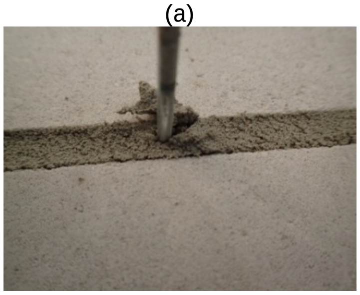

(c)

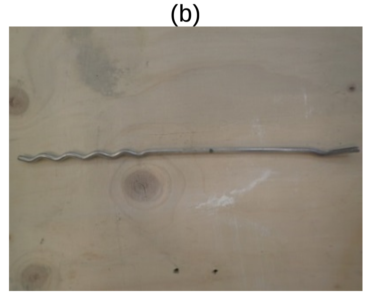

(d)

Figure 64 – Crack pattern of specimen TUD_MAT-17f: (a) cracks formation at the peak force level; (b)-(c) rupture mechanism for the mortar joint; (d) final deformed configuration for the tie.

Table 38 – Capacity of ties embedded in calcium silicate masonry specimens under cyclic tension loading.

Specimen name	Loading protocol	$F_{po,1}$	$s_{Fpo,1}$
		kN	mm
TUD_MAT-17f	P1	1.65	8.81
TUD_MAT-17g	P1	1.10	12.41
TUD_MAT-17h	P1	1.10	9.60
TUD_MAT-17i	P1	1.76	9.59
TUD_MAT-17j	P1	1.60	9.20
TUD_MAT-17k	P1	1.54	12.57
TUD_MAT-17l	P1	1.59	6.97
TUD_MAT-17m	P1	1.35	7.12
Average		**1.46**	**9.53**
Standard deviation		**0.25**	**2.09**
Coefficient of variation		**0.17**	**0.22**

To investigate the influence of the number of runs on the load capacity, Figure 65 shows the variation of the maximum force in each cycle. For every cycle, the maximum force was achieved during the first run, while it reduced in the second and third run (Figure 65a). Figure 65b shows the normalised maximum force for the second and third run of every cycle. The normalised value has been calculated as the ratio to the maximum force reached in the first run. It is possible to note that for every cycle, a similar reduction in terms of maximum force was observed for both the second and third run. An exception to this behaviour was only observed for cycle 6, which corresponds to the cycle in which the tensile load capacity of the tiles was reached.

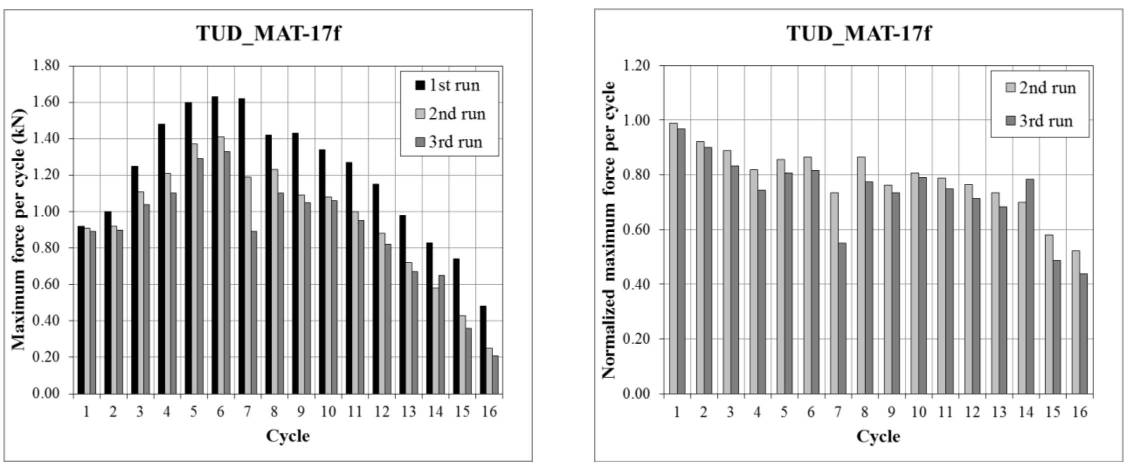

(a) (b)

Figure 65 – Cyclic behaviour in tension of ties embedded in calcium silicate masonry specimens: (a) maximum force per cycle; (b) normalised maximum force per cycle.

Figure 66 shows the behaviour of *ties embedded in calcium silicate masonry* specimens subject to *fully cyclic test* in terms of force versus tie's slip curve.

In tension, an hardening/softening behaviour was observed. The peak forced was reached for slip of 5 to 10 mm. Between 10 and 40 mm slip, the force remained nearly constant; for some specimens a fluctuation of force could be observed. For some specimens a more the pre-peak stage was characterized by a highly nonlinear behaviour since the onset of the tests. For larger slip values, a softening behaviour was observed till the failure of the specimen.

In compression, the behaviour of the ties was characterised by an linear behaviour up to the peak and a mixed softening/hardening behaviour in the post peak phase. The maximum force in compression was reached at 1 mm displacement approximatively. Afterwards, a softening branch is observed. In some cases, for slip larger than 30 mm, an hardening behaviour was observed, which was caused by the piercing of the zigzag part of the tie against the bed joint.

Figure 67 shows the failure mechanism stages during the cyclic test for specimen TUD_MAT-17w. The mechanisms in tension and compression were similar to the ones observed in the monotonic test. In the case of tensile loading, the cracks were concentrated in a cone of mortar surrounding the ties. In the case of compression loading, expulsion of the mortar from the bottom of the specimen was observed. The failure of the specimen was characterised by a deboning of the tie in the bed joint and by the straightening of the L-shaped part of the tie.

Table 39 lists the main experimental results for the fully cyclic tests on ties in calcium silicate masonry specimens. The specimens showed an average tensile load capacity of 1 kN, which occurred at a slip of 12.87 mm. The specimens showed an average compression load capacity of -0.36 kN, which occurred at a slip of -0.83 mm. Comparing the results with the ones of monotonic test, a reduction in capacity is observed for both tensile and compressive forces.

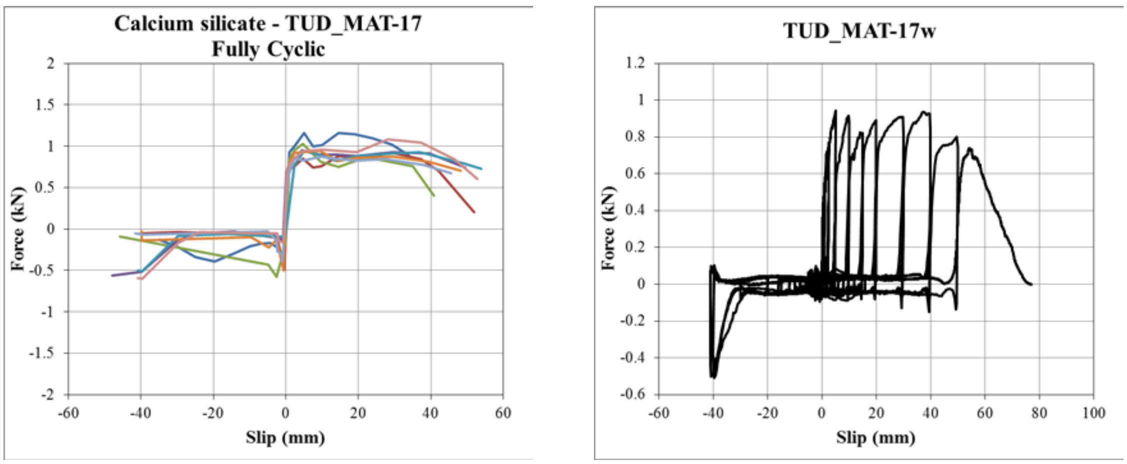

(a) (b)

Figure 66 – Force-slip curves for ties embedded in calcium silicate masonry specimens subject to cyclic test.

(a) (b) (c) (d)

Figure 67 – Crack pattern of the specimen TUD_MAT-17w: (a) cracks formation at the maximum tensile force;(b) expulsion of the mortar for compressive forces; (c)-(d) failure mechanism.

Table 39 – Capacity of ties embedded in calcium silicate masonry specimens under fully cyclic loading.

Specimen name	Loading protocol	$F_{PO,2}$	$s_{Fpo,2}$	$F_{C,2}$	$s_{Fc,2}$
		kN	mm	kN	mm
TUD_MAT-17n	P2	1.17	14.86	-0.40	-0.39
TUD_MAT-17t	P2	0.92	29.75	-0.49	-0.48
TUD_MAT-17v	P2	1.29	0.00	-0.65	-1.73
TUD_MAT-17z	P2	0.97	4.96	-0.14	-0.87
TUD_MAT-17w	P2	0.94	4.98	-0.09	-0.79
TUD_MAT-17x	P2	0.93	9.88	-0.50	-0.69
TUD_MAT-17y	P2	0.87	9.87	-0.39	-0.98
TUD_MAT-17aa	P2	1.08	28.64	-0.18	-0.67
Average		**1.02**	**12.87**	**-0.36**	**-0.83**
Standard deviation		**0.15**	**10.99**	**0.20**	**0.41**
Coefficient of variation		**0.14**	**0.85**	**0.55**	**0.50**

To analyse the cyclic response, Figure 68 the force-slip curve for every cycle. The tie behaved linearly in the first two cycle (maximum slip 0.25 mm); however, a different stiffness is observed for tensile and compressive forces. The figure compare also the response for the two runs imposing 100% of the target slip and the followed runs imposing only 40% of the target slip. During the runs imposing only 40% of the target slip, no further degradation in capacity was observed for both the tensile and compressive forces.

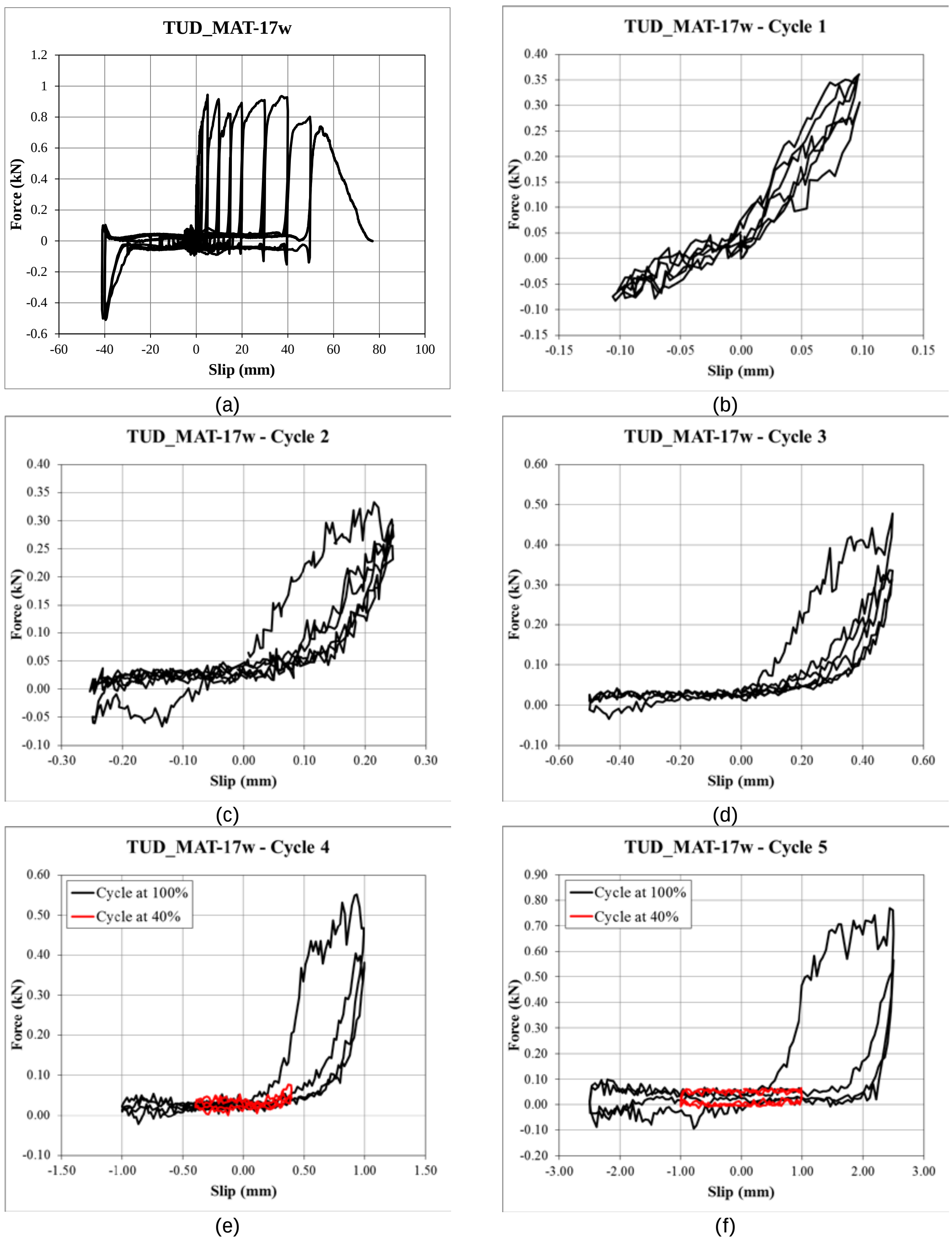

Figure 68 – Cyclic behaviour of tie embedded in calcium silicate specimen (TUD_MAT-17w) subject to fully cyclic test: (a) force-slip curve; (b)-(n) Comparison between cycle at 100% and 40% of the target displacement.

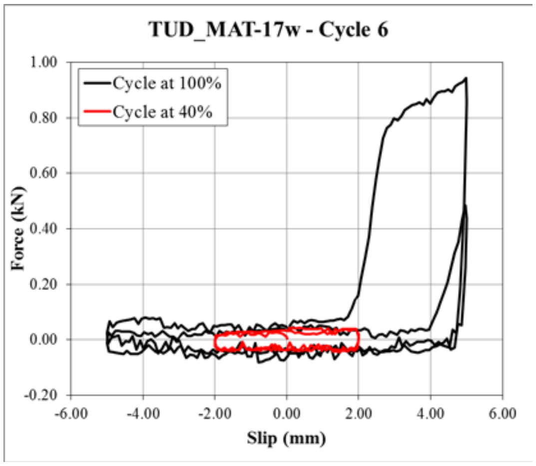

(g)

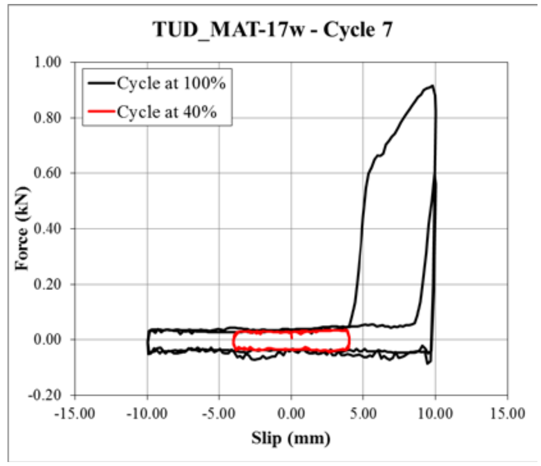

(h)

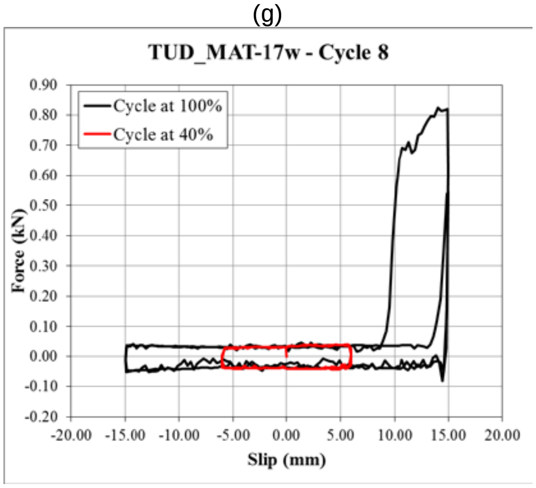

(i)

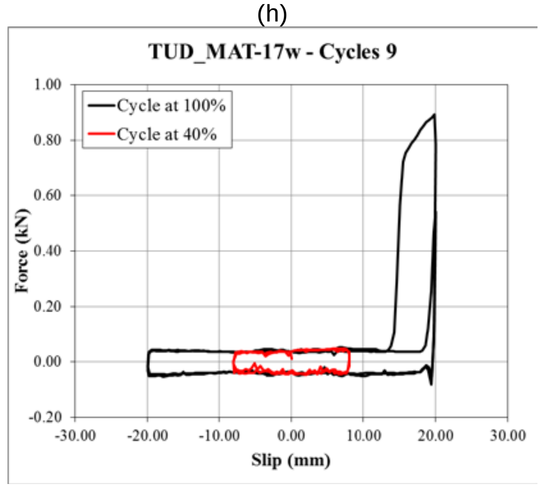

(l)

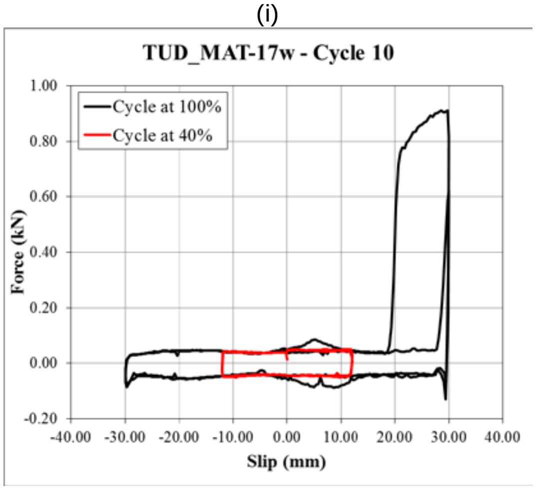

(m)

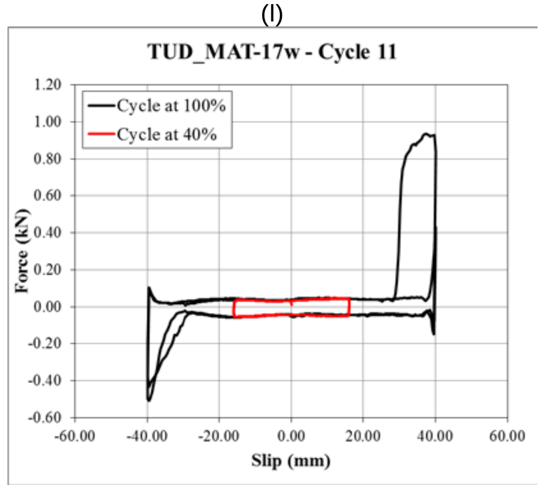

(n)

Figure 68 – Cyclic behaviour of tie embedded in calcium silicate specimen (TUD_MAT-17w) subject to fully cyclic test: (a) force-slip curve; (b)-(n) Comparison between cycle at 100% and 40% of the target displacement. (Cont.)

Figure 69 and Table 40 show a comparison between the monotonic and the cyclic tests performed on ties embedded in calcium silicate masonry specimens.
Considering the behaviour in tension, a similar tensile load capacity was observed for the monotonic and cyclic tension test, while a decrease of approximately 30% was observed in the case of fully cyclic test. The corresponding peak slip increase of 13% in the case of cyclic tension load and of 50% in the case of fully cyclic load. The force-slip curve was characterised by an initial elastic branch followed by hardening branch up to the peak and a softening branch in the post-peak stage. The application of cyclic loading highly influenced the post-peak behaviour by increasing its ductility, especially in the case of fully cyclic tests.
Considering the behaviour in compression, a reduction of 67% of the compressive load capacity was observed in the case of cyclic tests. The corresponding peak slip was subject to nearly any variation. The force-slip curve present similar characteristics in the two type of tests. First, a linear elastic behaviour was observed till the peak. Second, a softening branch up to approximatively 30 mm slip was observed. Eventually, an hardening behaviour was observed caused by the piercing of the zigzag part of the tie against the mortar joint.

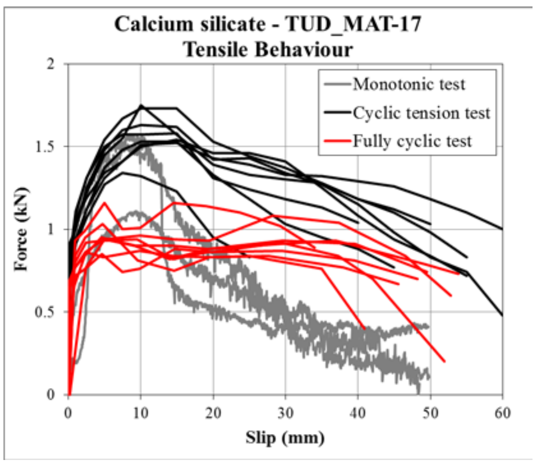

(a)

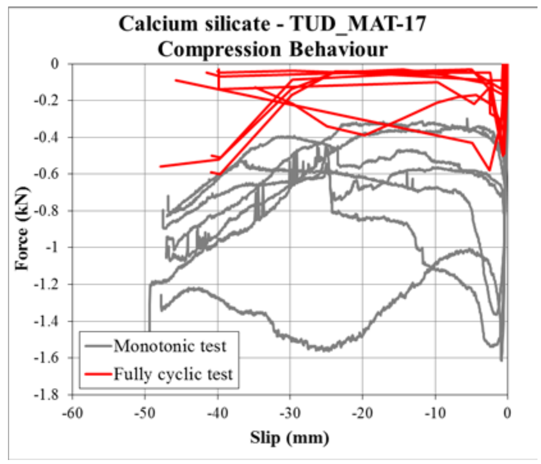

(b)

Figure 69 – Comparison between monotonic, cyclic tension and fully cyclic test on ties embedded in calcium silicate specimens: (a) tensile behaviour; (b) compressive behaviour.

Table 40 – Capacity of ties embedded in calcium silicate specimens (TUD_MAT-17, second period): maximum force and corresponding slip value for tensile and compressive stresses.

Specimens	Loading protocol	F_{po}		s_{Fpo}		F_c		s_{Fc}	
			Average (C.o.V.)		**Average (C.o.V.)**		**Average (C.o.V.)**		**Average (C.o.V.)**
		kN	kN	mm	mm	kN	kN	mm	mm
TUD_MAT-17b	P0T	1.57	**1.40 (0.18)**	8.12	**8.42 (0.09)**				
TUD_MAT-17c	P0T	1.51		7.86					
TUD_MAT-17d	P0T	1.11		9.27					
TUD_MAT-17o	P0C					-1.54	**-1.09 (0.37)**	-2.24	**-0.94 (0.78)**
TUD_MAT-17p	P0C					-0.81		-0.52	
TUD_MAT-17q	P0C					-0.68		-0.38	
TUD_MAT-17r	P0C					-0.77		-0.57	
TUD_MAT-17s	P0C					-1.62		-0.85	
TUD_MAT-17ac	P0C					-0.85		-0.35	
TUD_MAT-17ad	P0C					-1.37		-1.66	
TUD_MAT-17f	P1	1.65	**1.46 (0.17)**	8.81	**9.53 (0.22)**				
TUD_MAT-17g	P1	1.10		12.41					
TUD_MAT-17h	P1	1.10		9.60					
TUD_MAT-17i	P1	1.76		9.59					
TUD_MAT-17j	P1	1.60		9.20					
TUD_MAT-17k	P1	1.54		12.57					
TUD_MAT-17l	P1	1.59		6.97					
TUD_MAT-17m	P1	1.35		7.12					
TUD_MAT-17n	P2	1.17	**1.02 (0.14)**	14.86	**12.87 (0.85)**	-0.40	**-0.36 (0.55)**	-0.39	**-0.83 (0.50)**
TUD_MAT-17t	P2	0.92		29.75		-0.49		-0.48	
TUD_MAT-17v	P2	1.29		0.00		-0.65		-1.73	
TUD_MAT-17z	P2	0.97		4.96		-0.14		-0.87	
TUD_MAT-17w	P2	0.94		4.98		-0.09		-0.79	
TUD_MAT-17x	P2	0.93		9.88		-0.50		-0.69	
TUD_MAT-17y	P2	0.87		9.87		-0.39		-0.98	
TUD_MAT-17aa	P2	1.08		28.64		-0.18		-0.67	
$(P_{P1}-P_{P0})$ / P_{P0}			**-0.04**		**0.13**				
$(P_{P2}-P_{P0})$ / P_{P0}			**-0.27**		**0.53**		**-0.67**		**0.12**

Ties embedded in clay masonry specimens – outer leaf configuration (TUD_MAT-27)
The behaviour of ties embedded in clay masonry was investigated by performing monotonic tensile and compression test as well as fully cyclic tests. In this section the results related to the specimens resembling the outer leaf of a cavity walls are presented. This configuration is composed by a tie embedded with the zigzag part within the mortar joint.

Figure 70 shows the behaviour of *ties embedded in clay masonry* specimens (outer leaf configuration) subject to *monotonic tensile test* in terms of force versus tie's slip curve. The behaviour of the ties in tension was characterised by an hardening/softening behaviour. In the pre-peak stage an initial linear-elastic behaviour was observed up to 40% of the maximum force. Subsequently, a softening behaviour was observed up to 20 mm slip, which corresponded to 40% of the anchoring length.

Figure 71 shows the failure mechanism stages during the monotonic test for specimen TUD_MAT-27b. The crack first concentrated around the tie within the mortar joint. The failure consisted of a cone of mortar surrounding the tie slips out from the bed joint.

Table 41 lists the main experimental results for the monotonic tensile tests on ties in clay masonry specimens. The specimens showed an average tensile load capacity of 2.76 kN, which occurred at a slip of 5.43 mm.

Comparing the results obtained in the first and second period, a large variation in terms of tensile load capacity was observed (Table 42). In this variation could be addresses to the construction process. In the first period, the specimens were built on the floor and the ties was not supported after construction. This resulted in a tensile capacity of 1.28 kN and the observation of two failure mechanism: a cone failure and a bond failure. In the second period, the specimens were built on a table and the ties were supported immediately after construction. In this case, a higher tensile load capacity of 2.76 kN was observed; all the specimens presented a cone failure.

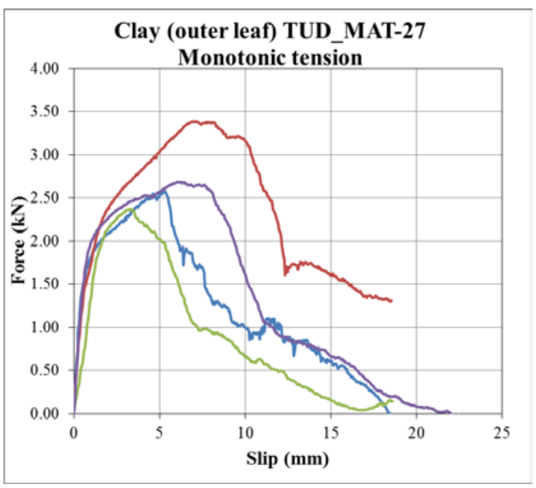

Figure 70 – Force-slip curves for ties embedded in clay masonry specimens (outer leaf configuration) subject to monotonic tensile test.

(a) (b) (c)

Figure 71 – Crack pattern for specimens TUD_MAT-27b: (a) cracks formation at the peak force; (b) failure cone mode for the mortar around the embedded tie; (c) final deformed configuration.

Table 41 – Capacity of ties embedded in clay masonry specimens (outer leaf configuration) subject to monotonic tensile test.

Specimen	**Loading protocol**	$F_{po,0}$	$s_{Fpo,0}$
		kN	mm
TUD_MAT-27a	P0T	2.58	5.34
TUD_MAT-27b	P0T	3.39	7.08
TUD_MAT-27c	P0T	2.38	3.28
TUD_MAT-27m	P0T	2.68	6.01
Average		**2.76**	**5.43**
Standard deviation		**0.44**	**1.60**
Coefficient of variation		**0.16**	**0.29**

Table 42 – Capacity of ties embedded clay masonry specimens (outer leaf configuration) under monotonic tensile loading: comparison between first and second period.

	No. specimens	f_p	$F_{po,0}$	$s_{Fpo,0}$	**Note**
		MPa	kN	mm	
First period	6	0.1	1.28	4.92	Specimens built on the floor, tie not supported after construction
Second period	4	0.3	2.76	5.43	Specimens built on a table, tie supported immediately after construction
$(P_{second}-P_{first}) / P_{first}$		**0.6**	**1.2**	**0.1**	

Figure 72 shows the behaviour of *ties embedded in clay masonry* specimens (outer leaf configuration) subject to *monotonic compressive test* in terms of force versus tie's slip curve. The behaviour of the ties in compression was characterised by an linear behaviour up to the peak and a softening behaviour in the post peak phase. The maximum force was reached at a slip of approximately 1.2 mm. In the post-peak phase, a softening behaviour was observed up to 15 mm slip.

Figure 73 shows the failure mechanism stages during the monotonic test for specimen TUD_MAT-27d. In correspondence of the peak force, the buckling of the ties occurred. Afterwards, only deformation in the ties were observed till the buckling failure of the tie.

Table 43 lists the main experimental results for the monotonic compressive tests on ties in clay masonry specimens. The specimens showed an average compressive load capacity of -1.83 kN, which occurred at a slip of -1.21 mm.

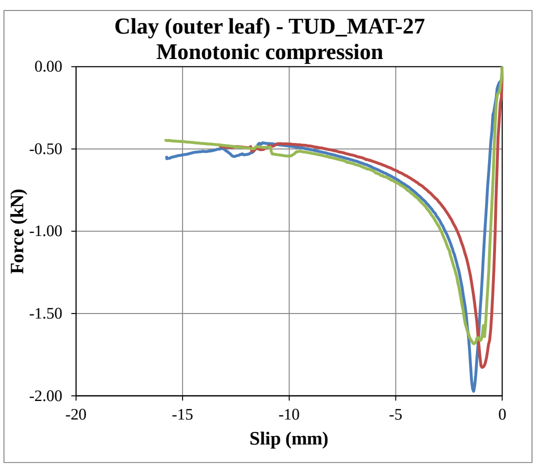

Figure 72 – Force-slip curves for ties embedded in clay masonry specimens (outer leaf configuration) subject to monotonic compressive test.

(a)

(b)

Figure 73 – Crack pattern of specimens TUD_MAT-27: (a) buckling of the tie at the peak force level; (b) final deformed configuration for TUD_MAT-27d.

Table 43 – Capacity of ties embedded in clay masonry specimens (outer leaf configuration) subject to monotonic compressive test.

Specimen	**Loading protocol**	$F_{c,0}$	$s_{Fc,0}$
		kN	mm
TUD_MAT-27d	P0C	-1.97	-1.34
TUD_MAT-27e	P0C	-1.83	-0.95
TUD_MAT-27f	P0C	-1.68	-1.34
Average		**-1.83**	**-1.21**
Standard deviation		**0.14**	**0.23**
Coefficient of variation		**0.08**	**0.19**

Figure 74 shows the behaviour of *ties embedded in clay masonry* specimens (outer leaf configuration) subject to *fully cyclic test* in terms of force versus tie's slip curve.
In tension, a softening behaviour was observed. The pre-peak stage was characterized by a highly nonlinear behaviour. The peak force was reached for slip of 5 to 10 mm. Afterwards a linear softening branch was observed up to 20-30 mm.
In compression, the behaviour of the ties was characterised by an linear behaviour up to the peak and a softening behaviour in the post-peak phase. The maximum force in compression was reached at -0.6 mm slip approximatively. Afterwards, an exponential softening branch was observed. For slip in compression larger than 10 mm an asymptotic residual force value was reached.

Figure 75 shows the crack pattern evolution during the fully cyclic test for specimen TUD_MAT-27g. The mechanisms in tension and compression were similar to the ones observed in the monotonic test. In the case of tensile loading, the cracks were concentrated in a cone of mortar surrounding the ties. In the case of compression loading, buckling of the tie was observed. The failure of the specimen was reached for tensile forces and it was characterised by a deboning of the tie in the bed joint and its extraction in buckled configuration.

Table 44 lists the main experimental results for the fully cyclic tests on ties in clay masonry specimens. The specimens showed an average tensile load capacity of 3.03 kN, which occurred at a slip of 5.87 mm. The specimens showed an average compression load capacity of -1.42 kN, which occurred at a slip of -0.62 mm. Comparing the results with the ones of monotonic test, a reduction in capacity was observed for both tensile and compressive loading.

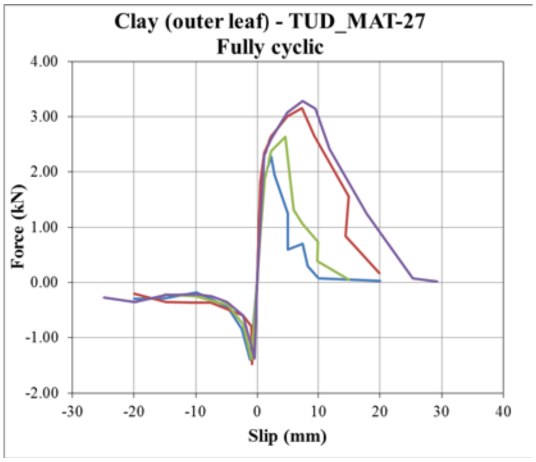

(a)

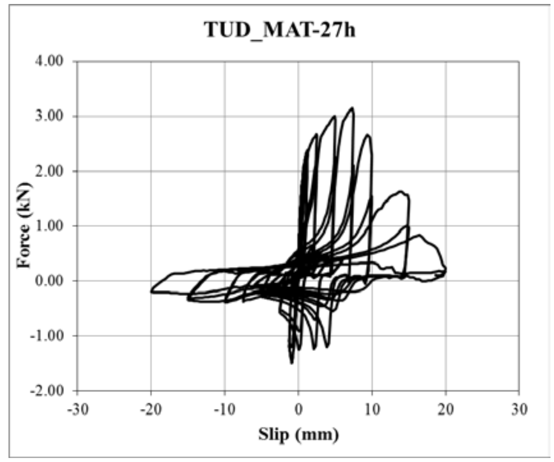

(b)

Figure 74 – Force-slip curves for ties embedded in clay masonry specimens (outer leaf configuration subject to fully cyclic test: (a) backbone curve; (b) cyclic test.

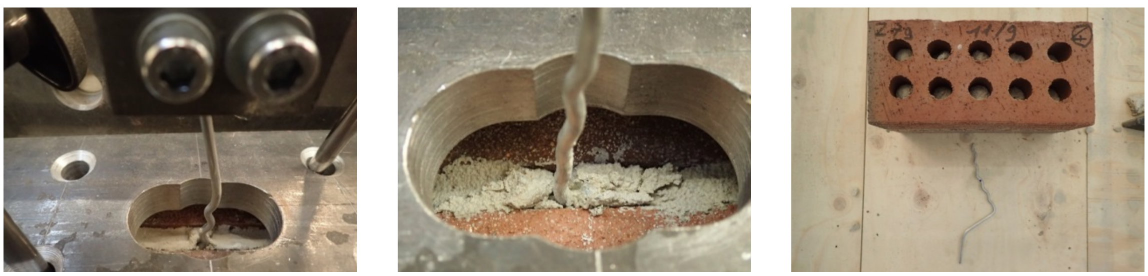

(a) (b) (c)

Figure 75 – Crack pattern of specimen TUD_MAT-27g: (a) initial buckling of the tie in under the maximum compressive force; (b) cracks formation at the peak tensile force; (c) final deformed configuration.

Table 44 – Capacity of ties embedded in clay masonry specimens (outer leaf configuration) subject to fully cyclic test.

Specimen name	Loading protocol	$F_{po,2}$	$s_{Fpo,2}$	$F_{c,2}$	$s_{Fc,2}$
		kN	mm	kN	mm
TUD_MAT-27g	P2	2.30	2.42	-1.40	-1.30
TUD_MAT-27h	P2	3.15	7.31	-1.49	-0.91
TUD_MAT-27i	P2	2.64	4.62	-1.39	-0.96
TUD_MAT-27l	P2	3.28	7.48	-1.38	-0.55
TUD_MAT-27n	P2	3.04	4.89	-1.39	-0.45
TUD_MAT-27o	P2	2.54	1.24	-1.33	-0.44
TUD_MAT-27p	P2	3.69	9.73	-1.55	-0.13
TUD_MAT-27q	P2	3.57	9.30	-1.43	-0.24
Average		**3.03**	**5.87**	**-1.42**	**-0.62**
Standard deviation		**0.50**	**3.10**	**0.07**	**0.40**
Coefficient of variation		**0.16**	**0.53**	**0.05**	**0.64**

To analyse the cyclic response, Figure 76 show the force-slip curve for every cycle. Under pull-out displacements the specimen behaved linearly within the first three cycles (max slip 0.15 mm).
The figure compare also the response for the two runs imposing 100% of the target slip and the followed runs imposing only 40% of the target slip. During the runs imposing only 40% of the target slip, a slight degradation of the capacity was observed. In both type of runs, the unloading was elastic.

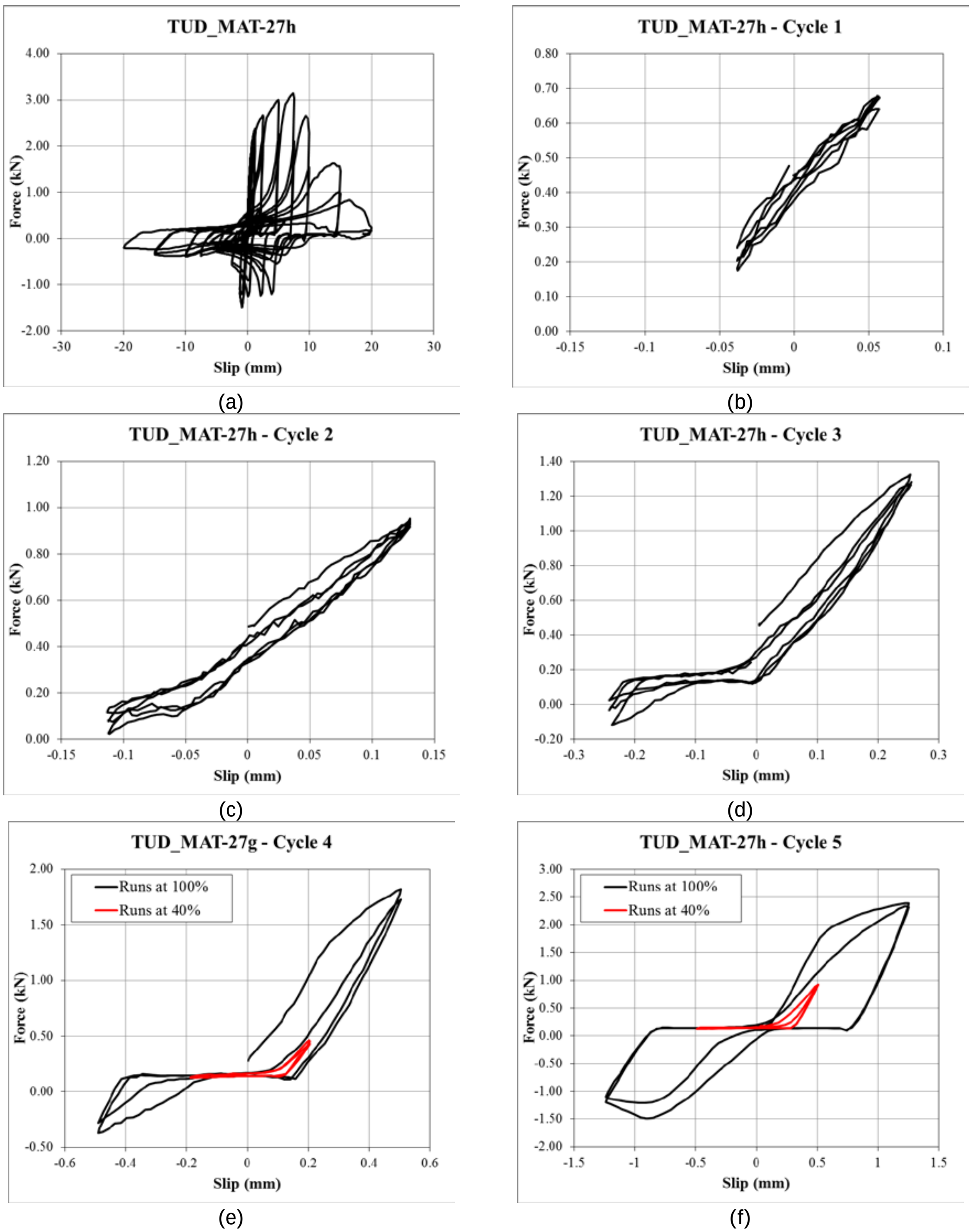

Figure 76 – Cyclic behaviour of tie embedded in clay masonry specimen (outer leaf configuration) subject to fully cyclic test: (a) force-slip curve; (b)-(m) Comparison between cycle at 100% and 40% of the target displacement.

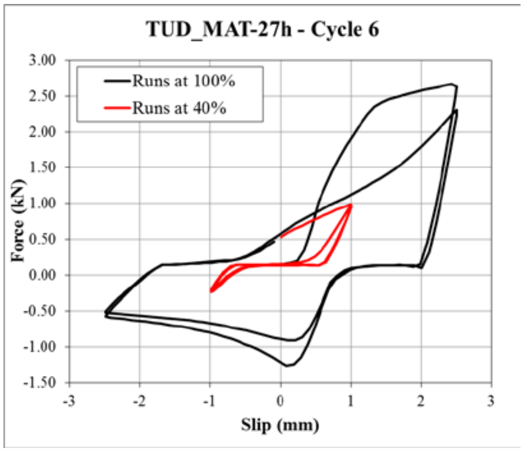

(g)

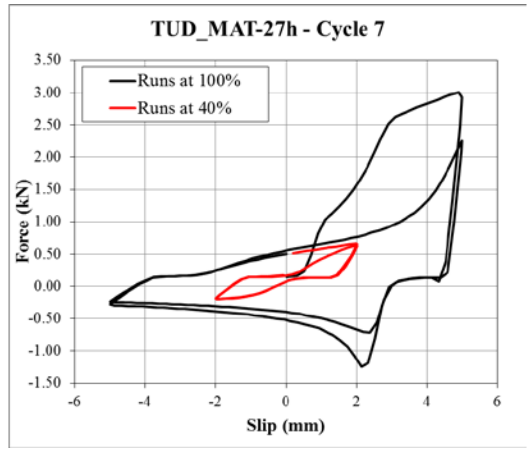

(h)

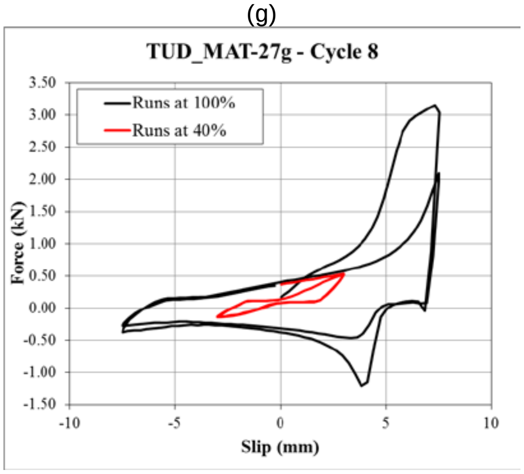

(i)

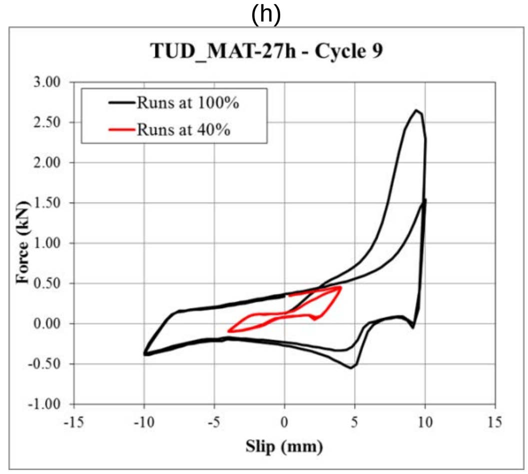

(l)

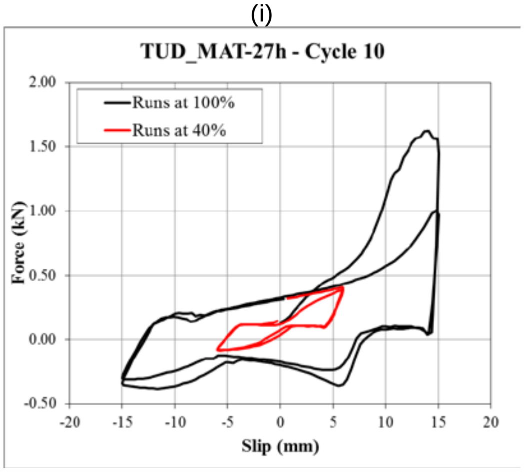

(m)

Figure 76 – Cyclic behaviour of tie embedded in clay masonry specimen (outer leaf configuration) subject to fully cyclic test: (a) force-slip curve; (b)-(m) Comparison between cycle at 100% and 40% of the target displacement. (Cont.)

Figure 77 and Table 45 show a comparison between the monotonic and the cyclic tests performed on ties embedded in clay masonry specimens.
Considering the behaviour in tension, a limited variation was observed comparing the results of monotonic and fully cyclic test. The tensile load capacity and the corresponding peak slip only varied of 10%. In both cases, the force-slip curve was characterised by an initial elastic branch followed by hardening branch up to the peak and a linear softening branch in the post-peak stage.
Considering the behaviour in compression, a reduction of 20% of the compressive load capacity was observed in the case of cyclic tests. The force-slip curve showed similar characteristics in the two type of tests. First, a linear elastic behaviour was observed till the peak. Second, a softening branch up to approximatively -10 mm slip was observed. Eventually, a plateau of constant residual force was reached.

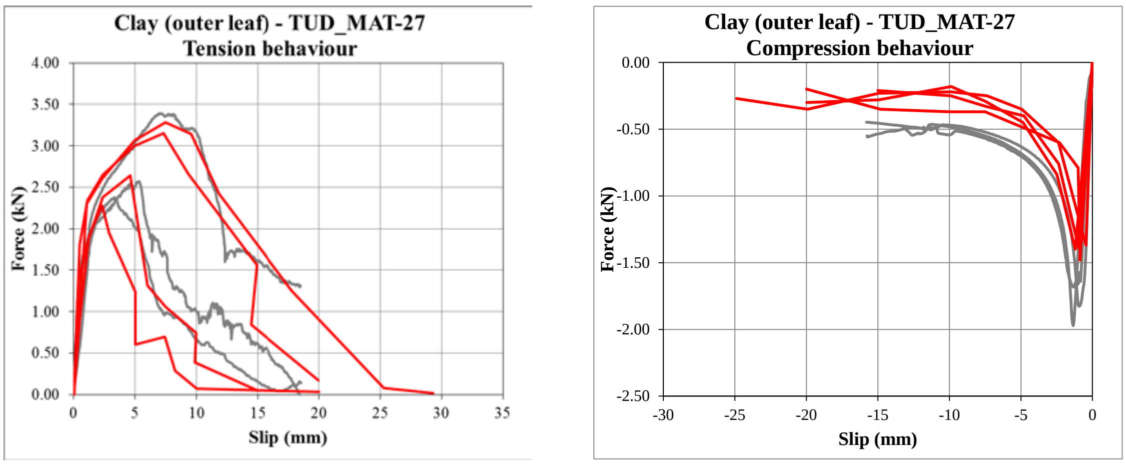

(a) (b)

Figure 77 – Comparison between monotonic and fully cyclic test on ties embedded in clay masonry specimens (outer leaf configuration): (a) tensile behaviour; (b) compressive behaviour.

Table 45 – Capacity of ties embedded in clay masonry specimens (outer leaf configuration).

Specimens	Loading protocol	F_{po}		s_{Fpo}		F_c		s_{Fc}	
			Average (C.o.V.)		**Average (C.o.V.)**		**Average (C.o.V.)**		**Average (C.o.V.)**
		kN	kN	mm	mm	kN	kN	mm	mm
TUD_MAT-27a	P0T	2.58		5.34					
TUD_MAT-27b	P0T	3.39	**2.76 (0.16)**	7.08	**5.43 (0.29)**				
TUD_MAT-27c	P0T	2.38		3.28					
TUD_MAT-27m	P0T	2.68		6.01					
TUD_MAT-27d	P0C					-1.97		-1.34	
TUD_MAT-27e	P0C					-1.83	**-1.83 (0.08)**	-0.95	**-1.21 (0.19)**
TUD_MAT-27f	P0C					-1.68		-1.34	
TUD_MAT-27g	P2	2.30		2.42		-1.40		-1.30	
TUD_MAT-27h	P2	3.15		7.31		-1.49		-0.91	
TUD_MAT-27i	P2	2.64		4.62		-1.39		-0.96	
TUD_MAT-27l	P2	3.28	**3.03 (0.16)**	7.48	**5.87 (0.53)**	-1.38	**-1.42 (0.05**	-0.55	**-0.62 (0.64)**
TUD_MAT-27n	P2	3.04		4.89		-1.39		-0.45	
TUD_MAT-27o	P2	2.54		1.24		-1.33		-0.44	
TUD_MAT-27p	P2	3.69		9.73		-1.55		-0.13	
TUD_MAT-27q	P2	3.57		9.30		-1.43		-0.24	
$(P_{P2}-P_{P0}) / P_{P0}$			**-0.10**		**0.09**		**-0.22**		**-0.49**

Ties embedded in clay masonry specimens – inner leaf configuration (TUD_MAT-28)
The behaviour of ties embedded in clay masonry was investigated by performing monotonic tensile and compression test as well as fully cyclic tests. In this section, the results related to the specimens resembling the inner leaf of a cavity walls are presented. This configuration is composed by a tie embedded with its L-shaped part within the mortar joint.

Figure 78 shows the behaviour of *ties embedded in clay masonry* specimens (inner leaf configuration) subject to *monotonic tensile test* in terms of force versus tie's slip curve. The specimens had a liner elastic behaviour up to 25% of the maximum force. Subsequently, an hardening behaviour up to the peak was observed. After the peak, a brittle failure occurred due to the rapture of the tie at the level of the clamp. Only in one case the brittle rupture of the tie did not occur and a softening behaviour was observed up to 50 mm slip, which corresponds to the 70% of the anchoring length.

Figure 79 shows the failure mechanism stages during the monotonic test for specimen TUD_MAT-27b and TUD_MAT-27c. The crack first concentrated around the tie within the mortar joint. The failure of the specimen was reached for tensile forces, which induced a brittle failure of the tie at the level of the clamp rather than in the connection with the mortar joint. This mechanisms could be caused by the presence of mortar dowels, which were present due to the perforation of the bricks, reducing the slip of the tie within the bed joint and thus generating tensile stresses in the tie itself.

Table 46 lists the main experimental results for the monotonic tensile tests on ties in clay masonry specimens. The specimens showed an average tensile load capacity of 3.51 kN, which occurred at a slip of 19.73 mm.

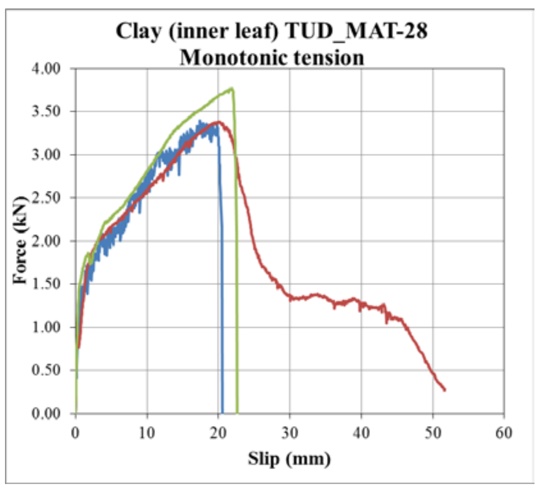

Figure 78 – Force-slip curves for ties embedded in clay masonry specimens (inner leaf configuration) subject to monotonic tensile test.

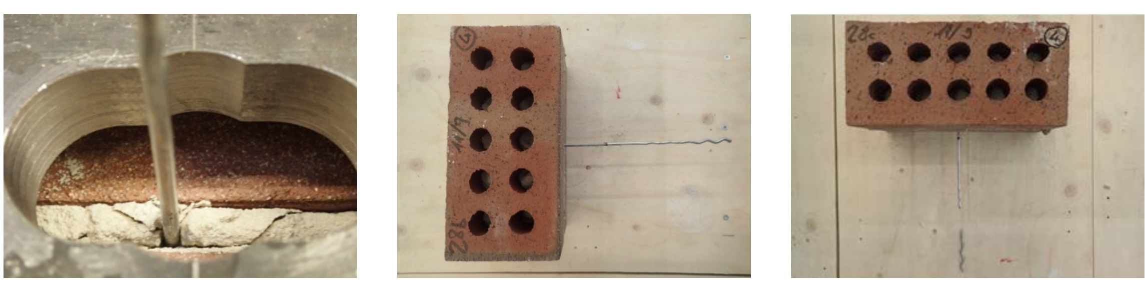

(a) (b) (c)

Figure 79 – Crack pattern of specimens TUD_MAT-27b and c: (a) cracks formation at the peak force; (b)-(c) failure mechanism without and with rupture of the tie.

Table 46 – Capacity of ties embedded in clay masonry specimens (inner leaf configuration) subject to monotonic tensile test.

Specimen	Loading protocol	$F_{po,0}$	$s_{Fpo,0}$
		kN	mm
TUD_MAT-28a	P0T	3.39	17.44
TUD_MAT-28b	P0T	3.38	19.90
TUD_MAT-28c	P0T	3.77	21.84
Average		**3.51**	**19.73**
Standard deviation		**0.22**	**2.21**
Coefficient of variation		**0.06**	**0.11**

Figure 80 shows the behaviour of *ties embedded in clay masonry* specimens (outer leaf configuration) subject to *monotonic compressive test* in terms of force versus tie's slip curve. The behaviour of the ties in compression was characterised by a linear behaviour up to the peak and a softening behaviour in the post-peak phase. The maximum force was reached at a slip of approximately 0.9 mm. In the post-peak phase, a softening behaviour was observed up to approximatively 10 mm slip. For slip values between 10 and 30 mm a residual force value equal to -1 kN was observed.

Figure 81 shows the crack pattern development during the monotonic test for specimen TUD_MAT-28e. In correspondence of the peak force, the buckling of the tie occurred. Afterwards, the deformation were mainly localised in the ties and the failure occurred due to buckling failure of the tie.

Table 47 lists the main experimental results for the monotonic compressive tests on ties in clay masonry specimens (inner leaf configuration). The specimens showed an average compressive load capacity of -2.51 kN, which occurred at a slip of -0.88 mm.

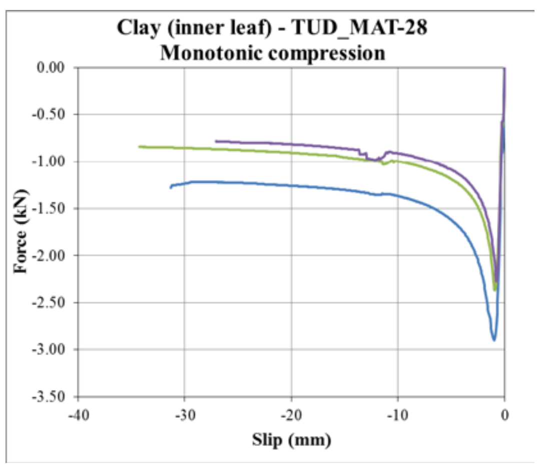

Figure 80 – Force-slip curves for ties embedded in clay masonry specimens (inner leaf configuration) subject to monotonic compressive test.

(a)

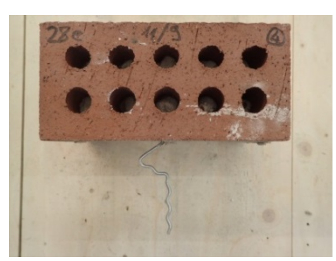

(b)

Figure 81 – Crack pattern of specimens TUD_MAT-28e: (a) buckling of the tie at the peak force level; (b) final deformed configuration.

Table 47 – Capacity of ties embedded in clay masonry specimens (inner leaf configuration) subject to monotonic compressive test.

Specimen	Loading protocol	$F_{c,0}$	$s_{Fc,0}$
		kN	mm
TUD_MAT-28d	P0C	-2.90	-0.96
TUD_MAT-28f	P0C	-2.37	-0.91
TUD_MAT-28g	P0C	-2.27	-0.79
Average		**-2.51**	**-0.88**
Standard deviation		**0.34**	**0.09**
Coefficient of variation		**0.13**	**0.10**

Figure 82 shows the behaviour of *ties embedded in clay masonry* specimens (inner leaf configuration) subject to *fully cyclic test* in terms of force versus tie's slip curve.
In tension, the pre-peak stage was characterised by an initial linear elastic stage followed by hardening branch up to the peak. The peak force was reached for slip value between 8 to 14 mm. The post-peak stage was described by brittle behaviour caused by the rupture of the tie.
In compression, the behaviour of the ties was characterised by a linear behaviour up to the peak and a softening behaviour in the post-peak phase. The maximum force in compression was reached at -0.4 mm slip approximatively. Afterwards, an exponential softening branch was observed. For slip in compression larger than 10 mm a zero residual force value was reached.

Figure 83 shows the crack pattern evolution during the fully cyclic test for specimen TUD_MAT-28m. The mechanisms in tension and compression were similar to the ones observed in the monotonic test. In the case of tensile loading, the cracks were concentrated in a cone of mortar surrounding the ties. In the case of compression loading, buckling of the tie was observed. The failure of the specimen was reached for tensile forces, which induced a brittle failure of the tie at the level of the clamp rather than in the connection with the mortar joint. These mechanisms could be caused by the presence of mortar dowels, which were present due to the perforation of the bricks, reducing the slip of the tie within the bed joint and thus generating tensile stresses in the tie itself.

Table 48 lists the main experimental results for the fully cyclic tests on ties in clay masonry specimens (inner leaf configuration). The specimens showed an average tensile load capacity of 3.40 kN, which occurred at a slip of 10.48 mm. The specimens showed an average compression load capacity of -1.27 kN, which occurred at a slip of -0.38 mm.

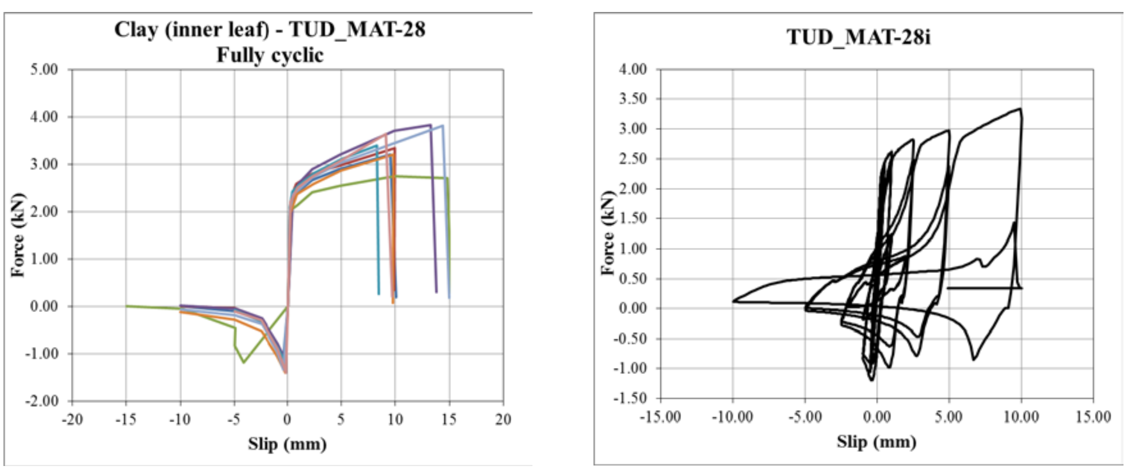

(a) (B)

Figure 82 – Force-slip curves for ties embedded in clay masonry specimens (inner leaf configuration subject to fully cyclic test: (a) backbone curve; (b) cyclic test.

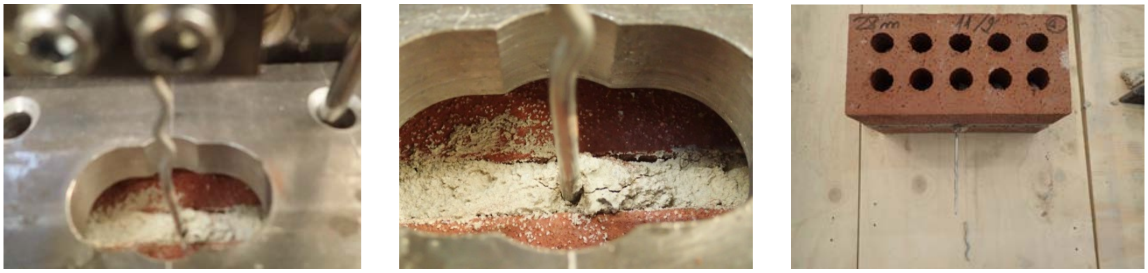

(a) (b) (c)

Figure 83 – Crack pattern of specimen TUD_MAT-28m: (a) initial buckling of the tie under the maximum compressive force; (b) cracks formation at the peak tensile force; (c) final deformed configuration.

Table 48 – Capacity of ties embedded in clay masonry specimens (inner leaf configuration) subject to fully cyclic test.

Specimen name	**Loading protocol**	$F_{po,2}$	$s_{Fpo,2}$	$F_{c,2}$	$s_{Fc,2}$
		kN	mm	kN	mm
TUD_MAT-28h	P2	3.21	9.34	-1.28	-0.54
TUD_MAT-28i	P2	3.34	9.95	-1.20	-0.39
TUD_MAT-28l	P2	2.75	9.91	-1.21	
TUD_MAT-28m	P2	3.83	13.26	-1.14	-0.38
TUD_MAT-28n	P2	3.42	8.07	-1.17	-0.35
TUD_MAT-28o	P2	3.21	9.82	-1.42	-0.34
TUD_MAT-28p	P2	3.81	14.40	-1.36	-0.49
TUD_MAT-28q	P2	3.63	9.13	-1.41	-0.20
Average		**3.40**	**10.48**	**-1.27**	**-0.38**
Standard deviation		**0.36**	**2.17**	**0.11**	**0.11**
Coefficient of variation		**0.11**	**0.21**	**0.09**	**0.29**

To analyse the cyclic response, Figure 84 show the force-slip curve for every cycle. Under pull-out displacements the specimen behaved linearly within the first two cycles (max slip 0.25mm).
The figure compare also the response for the two runs imposing 100% of the target slip and the followed runs imposing only 40% of the target slip. During the runs imposing only 40% of the target slip, a slight degradation of the capacity was observed. In both type of runs, the unloading was elastic.

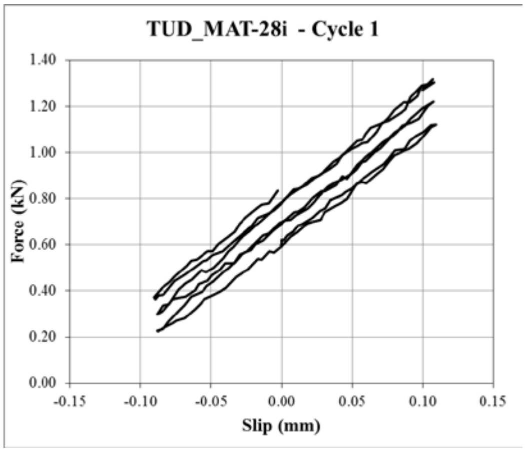

(a)

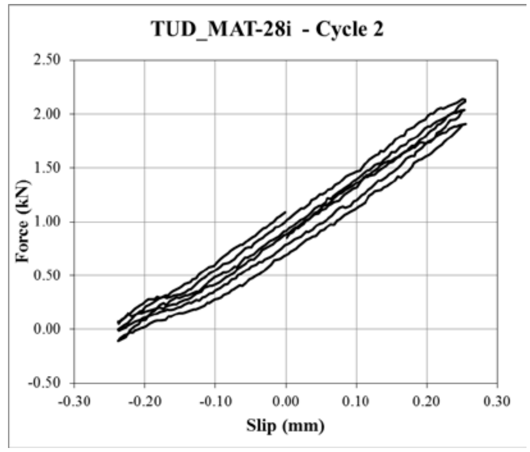

(b)

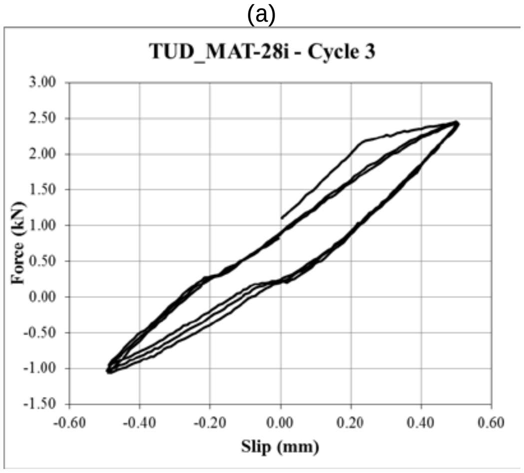

(c)

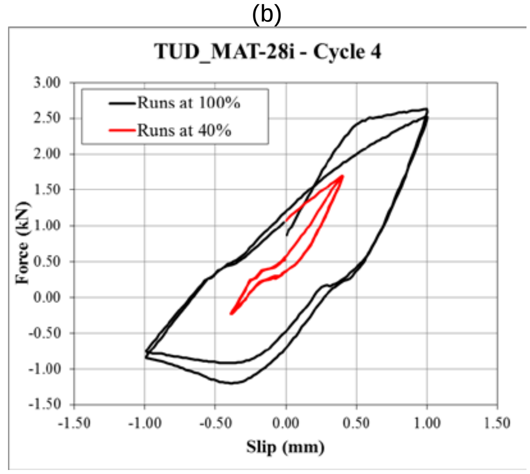

(d)

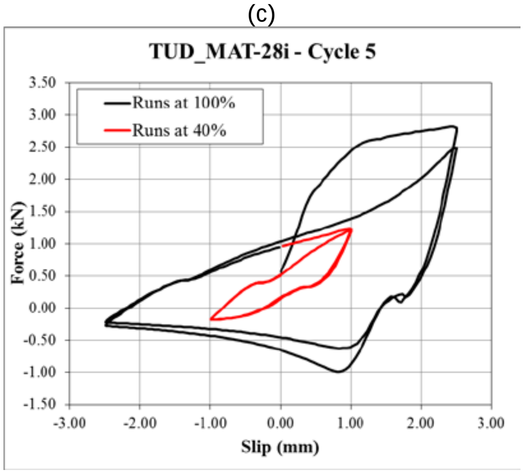

(e)

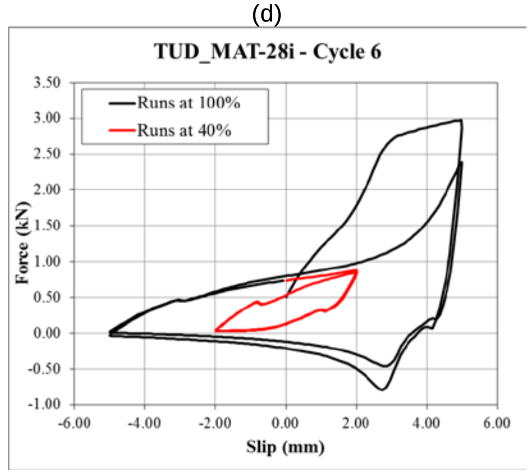

(f)

Figure 84 – Cyclic behaviour of tie embedded in clay masonry specimen (inner leaf configuration) subject to fully cyclic test: (a)-(f) Comparison between cycle at 100% and 40% of the target displacement.

Figure 85 and Table 49 show a comparison between the monotonic and the cyclic tests performed on ties embedded in clay masonry specimens (inner leaf configuration).
Considering the behaviour in tension, the tensile load capacity resulted nearly unaffected by the cyclic loading, while the corresponding slip value showed a variation of 50%. In both cases, the force-slip curve was characterised by an initial elastic branch followed by a hardening branch up to the peak and a brittle post-peak behaviour. The failure occurred in the ties rather than at the interface with the mortar bed joint. This mechanism could be caused by the presence of mortar dowels, which were present due to the perforation of the bricks, reducing the slip of the tie within the bed joint and increasing the tie's deformation
Considering the behaviour in compression, a reduction of approximatively 50% was observed in the case of cyclic tests for both the compressive load capacity and the corresponding slip value. The force-slip curve showed similar characteristics in the two types of tests. First, a linear elastic behaviour was observed till the peak. Second, a softening branch up to approximatively -10 mm slip was observed. Eventually, a plateau of constant residual force was reached. The residual force was approximatively -1 KN and zero for the case of monotonic and cyclic test, respectively.

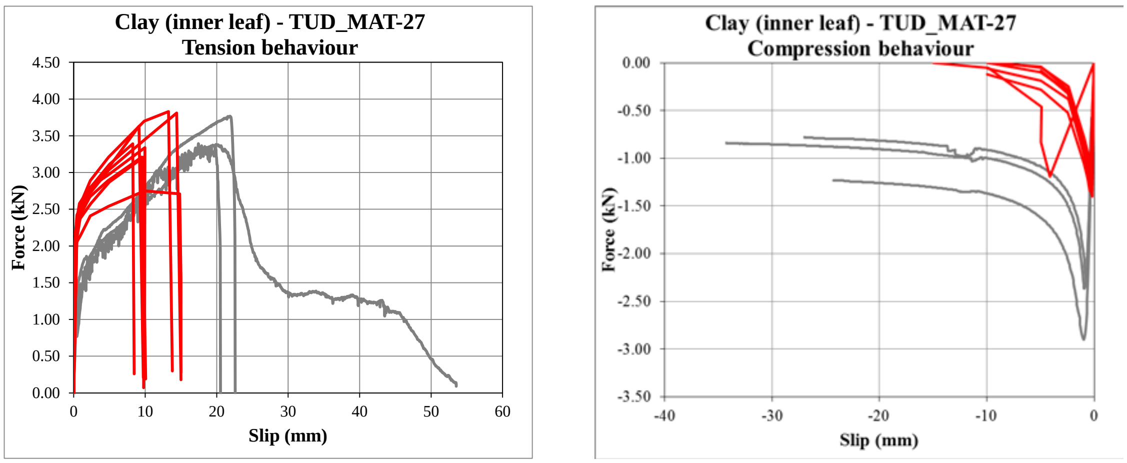

(a) (b)

Figure 85 – Comparison between monotonic and fully cyclic test on ties embedded in clay masonry specimens (inner leaf configuration): (a) tensile behaviour; (b) compressive behaviour.

Table 49 – Capacity of ties embedded in clay masonry specimens (inner leaf configuration).

Specimens	Loading protocol	F_{po}		s_{Fpo}		F_c		s_{Fc}	
			Average (C.o.V.)		Average (C.o.V.)		Average (C.o.V.)		Average (C.o.V.)
		kN	kN	mm	mm	kN	kN	mm	mm
TUD_MAT-28a	P0T	3.39	**3.51 (0.06)**	17.44	**19.73 (0.11)**				
TUD_MAT-28b	P0T	3.38		19.90					
TUD_MAT-28c	P0T	3.77		21.84					
TUD_MAT-28d	P0C					-2.90	**-2.51 (0.13)**	-0.96	**-0.88 (0.10)**
TUD_MAT-28f	P0C					-2.37		-0.91	
TUD_MAT-28g	P0C					-2.27		-0.79	
TUD_MAT-28h	P2	3.21	**3.40 (0.11)**	9.34	**10.48 (0.21)**	-1.28	**-1.27 (0.09)**	-0.54	**-0.38 (0.29)**
TUD_MAT-28i	P2	3.34		9.95		-1.20		-0.39	
TUD_MAT-28l	P2	2.75		9.91		-1.21		excluded	
TUD_MAT-28m	P2	3.83		13.26		-1.14		-0.38	
TUD_MAT-28n	P2	3.42		8.07		-1.17		-0.35	
TUD_MAT-28o	P2	3.21		9.82		-1.42		-0.34	
TUD_MAT-28p	P2	3.81		14.40		-1.36		-0.49	
TUD_MAT-28q	P2	3.63		9.13		-1.41		-0.20	
$(P_{P2}-P_{P0}) / P_{P0}$			**-0.03**		**-0.47**		**-0.49**		**-0.56**

13 Comparison with values proposed by standards

Eurocode 6 [1], it national annex [14] and NPR 9096-1-1:2012 [15] propose characteristics value of masonry properties to be used in the design procedure. In this section a comparison between experimental findings (derived in the first testing period) and the values proposed by these standards is presented.

13.1 Compressive strength of masonry

The compressive strength of masonry can be calculated by following Eurocode 6 and the national annex (Paragraph 3.6.1.2 [1], [14]):

$$f_{k,EC6} = K\ f_b^{\alpha}\ f_m^{\beta} \tag{17}$$

where f_b is the normalised mean compressive strength of the masonry unit, f_m is the compressive strength of mortar, and K, α, β are constants (Table NB-2 in [14]). The normalised mean compressive strength of the masonry unit f_b is determined by multiplying the measured value for the shape factor δ (Table B.1 in [3] or Table NB-A.1 in [14]).
Characteristic strength values of the compressive strength of masonry are also tabulated by the NPR 9096-1-1:2012 [15].
From the experiments, the characteristic compressive strength of masonry is calculated as [7]:

$$f_k = f_m^{'} - 1.645\sigma \tag{18}$$

where f'_m is the mean measured compressive strength and σ is the standard deviation.

Table 50 lists the characteristics compressive strength value of masonry. The characteristic values prescribed by the standards have been obtained adopting the strength value of mortar and bricks as declared by the producer (Appendix A).
For the calcium silicate masonry, the experimentally obtained characteristic strength values are closer to the estimates prescribed by the standards. For the clay masonry, the experiments provide a higher characteristic value with respect to the prescriptions. This difference can be correlated to the compressive strength of masonry unit, which declared value (25 MPa) is lower than the one found experimentally (45.81 MPa as reported in [15])

Table 50 – Characteristic values for the compressive strength of masonry.

			Calcium silicate	**Clay**
Declared compressive strength masonry mortar	f_m	MPa	5	5
Declared compressive strength masonry unit		MPa	16	25
Shape factor	δ		0.88	0.75
Normalized compressive strength masonry unit	f_b	MPa	14.0	18.8
Characteristic compressive strength masonry - Eurocode 6 and national annex (Eq. (17))	K		0.55	0.55
	α		0.65	0.65
	β		0.25	0.25
	$f_{k,EC6}$	MPa	5.44	7.27
Characteristic compressive strength masonry - NPR 9096-1-1:2012	$f_{k,NPR}$	MPa	5.44	7.27
Characteristic compressive strength masonry - Experiments	f_k	MPa	5.08	13.08

13.2 Elastic modulus of masonry

The national annex of Eurocode 6 [14] linearly correlates the elastic modulus of masonry to its compressive strength with a constant factor K_E = 700.

The characteristic value of the elastic modulus of masonry is correlated to the characteristic compressive strength in Table 51. The characteristics values from experiments are evaluate for both properties similarly to Eq. (18). Despite the estimate adopted for the elastic modulus, the ratio between stiffness and strength is approximatively equal to 400 for both masonry types. This estimate is 40% lower than the one prescribed by the national annex of the Eurocode 6 [14]. However, this relation is evaluated here only for a single strength class of masonry.

Table 51 – Ratio between the characteristic values of the elastic modulus and the compressive strength of masonry.

			Calcium silicate	**Clay**
National annex - Eurocode 6	K_E		700	700
Experiments	E_{1k} / f_k		474	367
	E_{2k} / f_k		428	429
	E_{3k} / f_k		449	456

13.3 Stress-strain relationship for masonry in compression

Both Eurocode 6 [1] and NPR 9998 [17] describes the typical stress-strain relationship for masonry in compression with a parabolic curve (Figure 86). Eurocode 6 suggests also that the non-linear behaviour start at 1/3 of the maximum compressive stress.
The proposed relationships are in line with the experiments as reported in Figure 11 and Figure 17. However, experimentally the non-linear behaviour is observed at stress level between 1/10 and 1/3 of the maximum stress.

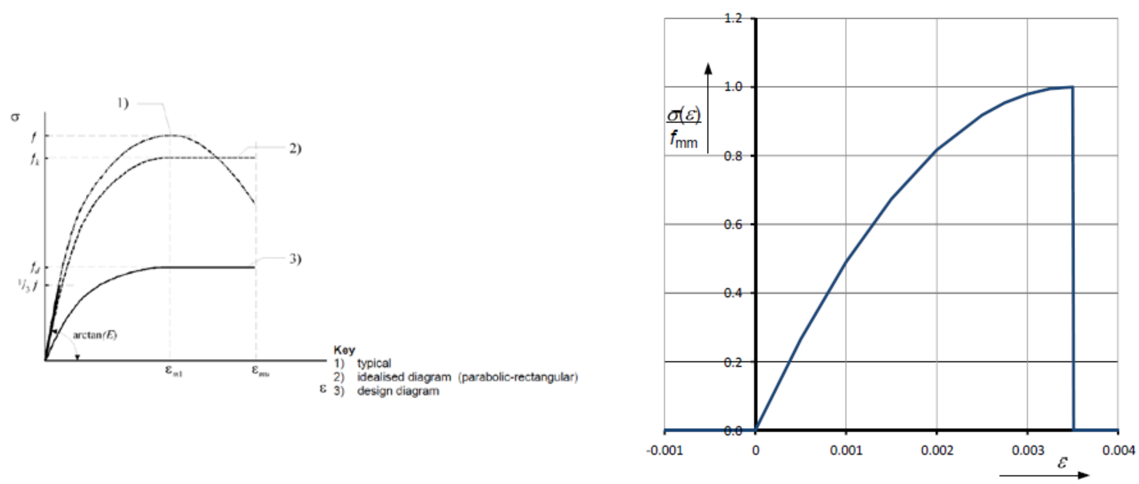

Figure 86 – Stress-strain relationship for masonry in compression: (a) Eurocode 6 (Figure 3.2 in [1]); (b) NPR 9998 (Figure 9.1 in [17]).

13.4 Out-of-plane flexural strengths of masonry

Eurocode 6 [1] reports characteristic value for the out-of-plane flexural strengths, while NPR 9096-1-1:2012 [15] prescribes minimum characteristic values on the basis of the exposure zone. From experiments, the characteristic value is determined by dividing the mean value for the factor 1.5 [10].

Table 52 lists the characteristic values for the out-of-plane flexural strengths. Both standards prescribe and orthotropic flexural strength ratio f_{x2k} / f_{x1k} of approximatively 4. Experimentally, a ratio equals to 3.6 and 2.9 is obtained for the calcium silicate and clay masonry, respectively.

Table 52 - Characteristic values for the flexural strength of masonry.

				Calcium silicate	**Clay**
Flexural strength with the moment vector parallel to the bed joint and in the plane of the wall	EC6	$f_{x1k,EC6}$	MPa	0.10	0.10
	NPR 9096-1-1:2012	$f_{x1,kNPR}$	MPa	0.20	0.20
	Experiments	f_{x1k}	MPa	0.14	0.27
Flexural strength with the moment vector orthogonal to the bed joint and in the plane of the wall	EC6	$f_{x2k,EC6}$	MPa	0.40	0.40
	NPR 9096-1-1:2012	$f_{x2k,NPR}$	MPa	0.79	0.79
	Experiments	f_{x2k}	MPa	0.51	0.75
Ratio f_{x2k} / f_{x1k}	EC6			4	4
	NPR 9096-1-1:2012			4	4
	Experiments			3.6	2.9

13.5 Initial shear strength of masonry

Eurocode 6 [1] reports characteristics value for initial shear strength of masonry, while NPR 9096-1-1:2012 [15] prescribes minimum characteristics values on the basis of the exposure zone. From experiments, the characteristic value of the initial shear strength is determined as the 80% of the mean measured value [12].

The characteristic initial shear strength values obtained by experiments are approximatively 40% lower than the one prescribed by the standards (Table 53).

Table 53 - Characteristic values for the initial shear strength of masonry.

			Calcium silicate	**Clay**
EC6	$f_{v0,EC6}$	MPa	0.15	0.20
NPR 9096-1-1:2012	$f_{v0k,NPR}$	MPa	0.20	0.20
Experiments	f_{v0k}	MPa	0.11	0.12

14 Summary and properties overview

In this report the characterisation of material and connection adopted in the large scale testing campaign are reported. The testing campaign selected as a case study a two-storey high terraced house characterised by: 1) cavity walls composed of an inner leaf in calcium silicate masonry and an outer leaf in clay masonry connected by masonry wall ties, 2) solid pre-fabricated concrete floor having a dry connection with the loadbearing masonry walls.

The material characterisation of masonry was performed by investigating its behaviour under compressive, bending and shear loading. For every type of test, both the maximum capacity of the masonry as well as the stress-strain relationship were investigated. To characterise the orthotropic behaviour of masonry, both compressive and out-of-plane bending tests were performed along two loading directions: one generating cracking parallel to the bed joints and one generating cracking perpendicular to the bed joints.
Table 54 and Table 55 show an overview of the material properties of both calcium silicate and clay masonry. The tests were performed in two periods: in the first construction period (March-April 2015) specimens for the material (MAT) and component tests (COMP) were built, while in the second period (September 2015) the construction of the assemblage took place and a limited number of material tests was repeated. The results of the second testing period are in line with the one obtained in the first period, as shown in Table 55. This result has been achieved thanks to the quality control procedure and by using materials from a single production batch.
The experimental results have been compared, in terms of characteristics value, with the analytical formulation available in standards, such as Eurocode 6 [1], it national annex [14] and NPR 9096-1-1:2012 [15]. A good agreement is found in terms of compressive strength, while an underestimation is observed for out-of-plane bending and shear properties. Due to the limited number of specimens adopted for every test, general conclusions cannot be drawn.

To characterise the connections present in the assemblage, friction tests on the floor-to-wall (dry) connection and test on wall ties connecting the two leaves of the cavity wall system were performed.
Table 56 lists the properties of the floor-to-wall connection together with the strength properties of masonry mortar and concrete. The frictional behaviour of the interface between the concrete floor and the masonry walls results similar to the one observed during shear tests on masonry.
Table 57 lists the properties of wall ties in terms of tensile and compressive load capacity as well as corresponding slip values. For the case of monotonic tensile loading, two level of lateral pre-compression were investigated. However, a direct correlation between the pre-compression stress and the tensile load capacity could not be established. Both monotonic and cyclic loading were performed, which revealed a lower capacity of the tie connection when fully cyclic loading is applied. On contrary, if the ties is only subject to cyclic tensile loading, no substantial variation was observed in comparison with the monotonic tension test.

Table 54 – Overview of mechanical properties for calcium silicate and clay masonry obtained in the first testing period.

Property	Symbol	Unit	Calcium silicate masonry			Clay masonry		
			Average	St. dev.	C.o.V.	Average	St. dev.	C.o.V.
Compressive strength of mortar	f_m	MPa	**6.59**	0.66	0.10	**6.11**	0.57	0.09
Flexural strength of mortar	f_{mt}	MPa	**2.79**	0.22	0.08	**2.43**	0.32	0.13
Flexural strength of masonry unit	f_{bt}	MPa	**2.74**	0.16	0.06	**4.78**	0.94	0.20
Elastic modulus of masonry unit	E_b	MPa	**8990**	3202	0.36	**7211**	3849	0.53
Compressive strength of masonry in the direction perpendicular to bed joints	f'_m	MPa	**5.93**	0.52	0.09	**14.73**	1.00	0.07
Elastic modulus of masonry in the direction perpendicular to bed joints	E_1	MPa	**3174**	467	0.15	**7728**	1287	0.17
	E_2	MPa	**5091**	1774	0.35	**6921**	1288	0.19
	E_3	MPa	**2746**	282	0.10	**8156**	1334	0.16
Poisson ratio of masonry in the direction perpendicular to bed joints	ν		**0.14**	0.01	0.07	**-**	-	-
Fracture energy in compression for loading perpendicular to bed joints	$G_{f\text{-}c}$	N/mm	**31.5**	5.1	0.16	**47.0**	4.8	0.10
Compressive strength of masonry in the direction parallel to bed joints	$f_{m,h}$	MPa	**7.55**	0.17	0.02	**7.53**	0.59	0.08
Elastic modulus of masonry in the direction parallel to bed joints	$E_{1,h}$	MPa	**2212**	660	0.30	**5030**	483	0.10
	$E_{2,h}$	MPa	**3583**	1668	0.47	**6526**	1589	0.24
	$E_{3,h}$	MPa	**2081**	864	0.42	**4676**	766	0.16
Fracture energy in compression for loading parallel to bed joints	$G_{f\text{-}c,h}$	N/mm	**43.4**	7.2	0.17	**31.4**	8.1	0.26
Masonry flexural strength with the moment vector parallel to the bed joints and in the plane of the wall	f_{x1}	MPa	**0.21**	0.05	0.25	**0.40**	0.11	0.26
Masonry flexural strength with the moment vector orthogonal to the bed joint and in the plane of the wall	f_{x2}	MPa	**0.76**	0.36	0.47	**1.12**	0.28	0.25
Masonry flexural strength with the moment vector orthogonal to the plane of the wall	f_{x3}	MPa	**0.40**	0.09	0.23	**0.61**	0.11	0.17
Flexural bond strength	f_w	MPa	**0.27**	0.12	0.43	**0.27**	0.15	0.54
Masonry (bed joint) initial shear strength	f_{v0}	MPa	**0.14**			**0.15**		
Masonry (bed joint) shear friction coefficient	μ		**0.43**			**0.87**		
Residual masonry (bed joint) initial shear strength	$f_{v0,res}$	MPa	**0.03**			**0.01**		
Residual masonry (bed joint) shear friction coefficient	μ_{res}		**0.54**			**0.74**		

Table 55 – Overview of mechanical properties for calcium silicate masonry in the first and second testing period

Property	Symbol	Unit	Calcium silicate masonry								
			First period (MAT/COMP)			Second period (BUILD)			All results		
			Avg.	St. dev.	C.o.V.	Avg.	St. dev.	C.o.V.	Avg.	St. dev.	C.o.V.
Compressive strength of mortar	f_m	MPa	**6.59**	0.66	0.10	**7.24**	0.60	0.08	**6.69**	0.69	0.10
Flexural strength of mortar	f_{mt}	MPa	**2.79**	0.22	0.08	**3.56**	0.18	0.05	**2.91**	0.36	0.12
Compressive strength of masonry in the direction perpendicular to bed joints	f'_m	MPa	**5.93**	0.52	0.09	**5.76**	0.59	0.10	**5.84**	0.54	0.09
Elastic modulus of masonry in the direction perpendicular to bed joints	E_1	MPa	**3174**	467	0.15	**3340**	800	0.24	**3264**	644	0.20
	E_2	MPa	**5091**	1774	0.35	**4536**	1888	0.42	**4788**	1768	0.37
	E_3	MPa	**2746**	282	0.10	**3005**	568	0.19	**2887**	460	0.16
Poisson ratio of masonry in the direction perpendicular to bed joints	ν		**0.14**	0.01	0.07	**0.18**	0.07	0.41	**0.16**	0.06	0.36
Fracture energy in compression for loading perpendicular to bed joints	$G_{f\text{-}c}$	N/mm	**31.5**	5.1	0.16	**21.8**	3.6	0.17	**26.2**	6.6	0.25
Flexural bond strength	f_w	MPa	**0.27**	0.12	0.43	**0.28**	0.08	0.29	**0.28**	0.10	0.36

Table 56 – Property of floor-to-wall connection (second period).

Property	Symbol	Unit	Avg.	St. dev.	C.o.V.
Compressive strength of mortar	f_m	MPa	**7.24**	0.60	0.08
Flexural strength of mortar	f_{mt}	MPa	**3.56**	0.18	0.05
Cubic compressive strength of concrete	f_{cc}	MPa	**74.7**	1.7	0.02
Initial shear strength of bed joint between concrete and CS brick	f^*_{v0}	MPa	**0.09**		
Shear friction coefficient of bed joint between concrete and CS brick	μ^*		**0.52**		
Residual initial shear strength of bed joint between concrete and CS brick	$f^*_{v0,res}$	MPa	**0.00**		
Residual shear friction coefficient of bed joint between concrete and CS brick	μ^*_{res}		**0.59**		

Table 57 – Overview of properties for ties embedded in calcium silicate and clay masonry.

Property	Symbol	Unit	Ties embedded in calcium silicate masonry			Ties embedded in clay masonry – outer leaf configuration			Ties embedded in clay masonry – inner leaf configuration		
			Avg.	St. dev.	C.o.V.	Avg.	St. dev.	C.o.V.	Avg.	St. dev.	C.o.V.
Monotonic tensile load capacity – lateral pre-compression 0.1 MPa	$F_{po,0}$	kN	**1.25**	0.10	0.08	**1.28**	0.80	0.63			
Slip corresponding to the monotonic tensile load capacity – lateral pre-compression 0.1 MPa	$s_{Fpo,0}$	mm	**10.26**	1.68	0.16	**4.92**	1.67	0.34			
Monotonic tensile load capacity – lateral pre-compression 0.3 MPa	$F_{po,0}$	kN	**1.40**	0.25	0.18	**2.76**	0.44	0.16	**3.51**	0.22	0.06
Slip corresponding to the monotonic tensile load capacity – lateral pre-compression 0.3 MPa	$s_{Fpo,0}$	mm	**8.42**	0.75	0.09	**5.43**	1.60	0.29	**19.73**	2.21	0.11
Monotonic compressive load capacity – lateral pre-compression 0.3 MPa	$F_{c,0}$	kN	**-1.09**	0.40	0.37	**-1.83**	0.14	0.08	**-2.51**	0.34	0.13
Slip corresponding to the monotonic compressive load capacity – lateral pre-compression 0.3 MPa	$s_{Fc,0}$	mm	**-0.94**	0.73	0.78	**-1.21**	0.23	0.19	**-0.88**	0.09	0.10
Cyclic tensile load capacity – lateral pre-compression 0.3 MPa	$F_{po,1}$	kN	**1.46**	0.25	0.17						
Slip corresponding to the cyclic tensile load capacity – lateral pre-compression 0.3 MPa	$s_{Fpo,1}$	mm	**9.53**	2.09	0.22						
Fully cyclic tensile load capacity – lateral pre-compression 0.3 MPa	$F_{po,2}$	kN	**1.02**	0.15	0.14	**3.03**	0.50	0.16	**3.40**	0.36	0.11
Slip corresponding to the fully cyclic tensile load capacity – lateral pre-compression 0.3 MPa	$s_{Fpo,2}$	mm	**12.87**	10.99	0.85	**5.87**	3.10	0.53	**10.48**	2.17	0.21
Fully cyclic compressive load capacity – lateral pre-compression 0.3 MPa	$F_{c,2}$	kN	**-0.36**	0.20	0.55	**-1.42**	0.07	0.05	**-1.27**	0.11	0.09
Slip corresponding to the fully cyclic compressive load capacity – lateral pre-compression 0.3 MPa	$s_{Fc,2}$	mm	**-0.83**	0.41	0.50	**-0.62**	0.40	0.64	**-0.38**	0.11	0.29

References

[1] EN 1996-1-1+A1 (2013). Eurocode 6 – Design of masonry structures – Part 1-1: General rules for reinforced and unreinforced masonry structures. Nederlands Normalisatie-instituit (NEN).

[2] Protocol for the construction of masonry, ver. 18-03-2015

[3] EN 1015-3 (1999). Method of test for mortar for masonry – Part 3: Determination of consistence of fresh mortar (by flow table). Nederlands Normalisatie-instituit (NEN).

[4] EN 1015-11 (1999). Method of test for mortar for masonry – Part 11: Determination of flexural strength of hardened mortar. Nederlands Normalisatie-instituit (NEN).

[5] NEN 6790 (2005). Technical principles for building structures - TGB 1990 - Masonry structures - Basic requirements and calculation methods. Nederlands Normalisatie-instituit (NEN).

[6] Jafari, S., Panoutsopoulou, L. and Rots, J.G. Tests for the characterisation of original Groningen masonry. Delft University of Technology. Final report 18 December 2015.

[7] EN 1052-1 (1998). Method of test masonry – Part 1: Determination of compressive strength. Nederlands Normalisatie-instituit (NEN).

[8] Van Mier, J.G.M. (1984) Strain Softening of concrete under multiaxial loading conditions, PhD thesis, Eindhoven University of Technology.

[9] Lourenco, P.B., De Borst, R. and Rots, J.G. (1997). A plane stress softening plasticity model for orthotropic materials. International Journal for Numerical Methods in Engineering 40(21), 4033-4057.

[10] EN 1052-2 (1999). Method of test masonry – Part 2: Determination of flexural strength. Nederlands Normalisatie-instituit (NEN).

[11] EN 1052-5 (2005). Method of test masonry – Part 5: Determination of bond strength by bond wrench method. Nederlands Normalisatie-instituit (NEN).

[12] EN 1052-3 (2002). Method of test masonry – Part 3: Determination of initial shear strength. Nederlands Normalisatie-instituit (NEN).

[13] EN 846-5 (2012). Methods of test for ancillary components for masonry – Part 5: Determination of tensile and compressive load capacity and load displacement characteristics of wall ties (couplet test). Nederlands Normalisatie-instituit (NEN).

[14] NEN-EN 1996-1-1+C1/NB (2011). National Annex to NEN-EN 1996-1-1+C1 Eurocode 6: Design of masonry structures – Part 1-1: General rules for reinforced and unreinforced masonry structures. Nederlands Normalisatie-instituit (NEN) (in Dutch).

[15] NPR 9096-1-1 (2012). Masonry structures – Simple design rules, based on EN 1996-1-1+C1. Nederlands Normalisatie-instituit (NEN) (in Dutch).

[16] Pavia rick centre, (2015). Report on Compression Tests of CS and Clay Bricks (V.7_5_15).

[17] NPR 9998 (2015). Assessment of building in case of erection, reconstruction and disapproval – Basic rules for seismic actions; Induced earthquakes. Normcommissie 351001 “Technische Grondslagen voor Bouwconstructies”. Draft version January 2015 (in Dutch).

Appendix A

This appendix reports the declaration of performance for the construction materials used during the experimental campaign.
Table A.1 and Table A.2 refers to the calcium silicate and clay bricks respectively.
Table A.3 and Table A.4 list the characteristic of mortars for calcium silicate and clay masonry, respectively.
Table A.5 reports the characteristics of the masonry wall ties.

Table A.1 – Declaration of performance of calcium silicate bricks (www.calduran.nl/producten/stenen/).

Wanddikte in mm	Type steen	Afmetingen (BxHxL) mm	Gewicht per stuk in kg	Druksterkte N/mm^2	Aantal per m^2 (incl. voeg)	Kg Metselfix per m^2 excl. morsverlies
55 (klamp)	Waalformaat	102x55x214	2	16	39,9	12,3
72 (klamp)	Amstelformaat	102x72x214	3	16	39,9	16,1
82 (klamp)	Maasformaat	102x82x214	3	16	39,9	18,4
102	Waalformaat	102x55x214	2	16	68,7	33,7
102	Amstelformaat	102x72x214	3	16	54,4	28,3
102	Maasformaat	102x82x214	3	16	48,5	26,1
150	Dubbel amstelformaat	150x72x214	4	16	54,4	42,5
150	Dubbel maasformaat	150x82x214	5	16	48,5	39,2

Table A.2 – Declaration of performance of clay bricks (Strating BV).

steenindustrie strating bv

gevestigd sinds 1883

(4) Fabrikant/Fabricant/
Hersteller/Manufacturer
Geimswijk 4
NL-9665 RR Oude Pekela
Tel +31 597 613920
Fax +31 597 613992
www.strating.nl

	PRESTATIEVERKLARING Nº	DÉCLARATION DES PERFORMANCES Nº	LEISTUNGSERKLÄRUNG Nº	DECLARATION OF PERFORMANCE Nº	WF-1
1	Producttype	Type de produit	Produkttyp	Product-type	Waalformaat (WF)
2	Identificatie	Identification	Identifikation	Identification	WF - *(2 - *(3 - *(4) - *(5
3	Beoogd gebruik: HD-producten voor gebruik in onbeschermde metselwerkmuren, kolommen en scheidingswanden	Usage prévu: Briques HD pour utilisation dans murs, poteaux et cloisons en maçonnerie non-protégée	vorgesehener Verwendungszweck: HD-Ziegel für die Verwendung in Wänden, Stützen und Trennwänden aus nicht geschütztes Mauerwerk	Intended use: HD-Unprotected masonry in masonry walls, columns and partitions	HD
6	Het systeem voor de beoordeling en verificatie van de prestatiebestendigheid van het bouwproduct	Le système d'évaluation et de vérification de la constance des performances du produit de construction	System zur Bewertung und Überprüfung der Leistungsbeständigkeit des Bauprodukts	System of assessment and verification of constancy of performance of the construction product	2+
7	De aangemelde instantie n° , heeft de volgende taken uitgevoerd: Initiële inspectie van de productie-installatie en productiecontrole in de fabriek en permanente bewaking, beoordeling en evaluatie van de productiecontrole in de fabriek en heeft een conformiteitscertifcaat van de productiecontrole in de fabriek afgeleverd met nummer:	L'organisme notifié n° , a réalisé une inspection initiale de l'établissement de fabrication et du contrôle de la production en usine, une surveillance, une évaluation et une appréciation permanentes du contrôle de la production en usine et a délivré le certificat de conformité du contrôle de la production en usine n°:	Die notifizierten Stelle N° hat die Erstinspektion des Werks und der werkseigenen Productionskontrolle, die laufende Überwachung, Bewertung und Evaluierung der werkseigenen Produktionskontrolle vorgenommen und hat die Konformitätsbescheinigung für die werkseigene Produktionskontrolle ausgestellt mit Nummer:	Notified Body N° performed the initial inspection of the manufacturing plant and of the factory production control, performed the continuous surveillance, assessment and evaluation of the factory production control and issued the certificate of conformity of the factory production control number	0957 IKOB-BKB BV 0957-CPD-0614

9	Aangegeven prestatie/dimensie/norm	Performances déclarées:	Erklärte Leistung:	Declared performance:			
L	Lengte	Longeur	Länge	Length	210	mm	
B	Breedte	Largeur	Breitte	Width	100	mm	
H	Hoogte	Hauteur	Höhe	Hight	50	mm	
	Maattolerantie categorie	Tolérances dimensionelles category	Grenzabmaße	Dimensional tolerances	T1		EN 771-1:2011
	Maatspreidingscategorie	Rangée catégorie	Maßspanne	Range category	NPD		
	Verschijningsvorm	Configuration	Form und Ausbildung	Configuration	1		
	Vlakheid	Planéité	Planheit	Flatness	NPD		
	Planparalleliteit	Planparallélisme	Planparallelität	Plane parallelism	NPD		
	Gemiddelde druksterkte	Résistance à la compression moyenne	Mittlere Druckfestigkeit	Mean compressive strength	≥ 25	N/mm², ⊥, cat I	
	Genormaliseerde druksterkte	Résistance à la compression normalisée	Normierte Druckfestigkeit	Normalized compressive strength	NPD	N/mm²	
	Bruto droge volumieke massa	Masse voluminique apparente sèche	Bruto Trockenrohdichte	Gross dry density	NPD	kg/m³	
	Tolerantie bruto droge volumieke massa	Tolérances masse voluminique apparente sèche	Grenzen bruto Trockenrohdichte	Tolerances	NPD		
	Hechtsterkte	Adhérance	Verbundfestigkeit	Bond strength	0,15	N/mm²	
	Thermische geleiding	Conductivé thermique	Wärmeleitfähigkeit	Thermal conductivity	NPD	W/m,K	
	Dampdoorlatendheid	Perméabilité à la vapeur d'eau	Wasserdampfdurchlässigkeit	Water vapor diffusion coefficient	50/100	µ	
	Duurzaamheid inzake vriezen en dooien: Vorst/dooiweerstand	Durabilité contre gel/dégel: resistance au gel/dégel	Dauerhaftigkeit: Frostwiderstand	Darability against freeze/thaw: freeze/thaw resistance	F2		
	Vrijwillige wateropname	Absorption d'eau	Wasseraufnahme	Waterabsorption	≤ 10%	% m/md	
	Initiële wateropname	Absorption d'eau initial	Anfängliche Wasseraufnahme	Initial rate of waterabsorption	NPD	kg/m²,min	
	Gehalte actieve oplosbare zouten	Teneur au sels solubles actifs	Gehalt an aktiven löslichen Salzen	Active soluble salts content	S2		
	Gehalte oplosbaar sulfaat	Teneur au sulfate solubles	Gehalt an lösliches Sulfat	Soluble sulphate content	≤ 0,10	% m/md	
	Brandreactie (Euroklasse)	Réaction au feu (Euroclass)	Brandverhalten (Euroklasse)	Reaction to fire (Euroclass)	A1		
	Gevaarlijke componenten	Substances dangereuses	Gefährliche Substanzen	Dangerous substances	NL-BBK		

10	De prestaties van het in de punten 1 en 2 omschreven product zijn conform de in punt 9 aangegeven prestaties. Deze prestatieverklaring wordt verstrekt onder de exclusieve verantwoordelijkheid van de in punt 4 vermelde fabrikant. Ondertekend voor en namens de fabrikant door:	Les performances du produit identifié aux points 1 et 2 sont conformes aux performances déclarées indiquées au point 9. La présente déclaration des performances est établie sous la seule responsabilité du fabricant identifié au point 4. Signé pour le fabricant et en son nom par:	Die Leistung des Produkts gemäß den Nummern 1 und 2 entspricht der erklärten Leistung nach Nummer 9. Verantwortlich für die Erstellung dieser Leistungserklärung ist allein der Hersteller gemäß Nummer 4. Unterzeichnet für den Hersteller und im Namen des Herstellers von:	The performance of the product identified in points 1 and 2 is in conformity with the declared performance in point 9. This declaration of performance is issued under the sole responsibility of the manufacturer identified in point 4. Signed for and on behalf of the manufacturer by:

G.J.E. Hoogerduijn Strating, Oude Pekela 31.01.2014

*(2) : P; M
*(3) : V; L; A; W
*(4) : 0001,....,9999
*(5) : 00,....,99

Table A.3 – Declaration of performance for calcium silicate masonry mortar (www.remix.nl)

1. Unieke identificatie	**Sakrete Brickfix**	**Nr. RV001 – 2013-11-05**
2. Aanduiding	**M5 type G (voor algemene toepassing) conform NEN-EN 998-2: 2010**	
3. Toepassing	**Metselmortel voor binnen- en buitentoepassing**	
4. Naam en contactadres fabrikant	**Remix Droge Mortel BV** **Hoofdstraat 41 NL-9531 AB Borger** **Postbus 3 NL-9530 AA Borger**	
5. Naam en contactadres gemachtigde	geen	
6. Systeem voor de beoordeling en verificatie van de prestatiebestendigheid	systeem 2+	
7. Activiteit van de aangemelde certificatie-instantie zoals vereist in de geharmoniseerde norm	De aangemelde certificatie-instantie Kiwa BMC B.V. (identificatienummer 0620) heeft onder systeem 2+ de initiële inspectie van de productie-installatie en van de productiecontrole in de fabriek uitgevoerd en zal tevens de permanente bewaking, beoordeling en evaluatie van de productiecontrole op zich nemen. Op basis daarvan is het conformiteitscertificaat voor de productiecontrole in de fabriek verstrekt.	
8. Europese Technische beoordeling	niet van toepassing	
9. Aangegeven prestaties		
Essentiële kenmerken (NEN-EN 998-2)	**Prestaties**	**Europees beoordelingsdocument**
5.4.1 druksterkte	M5	NEN-EN 998-2:2010
5.4.2 Hechtsterkte (kruisproef)	≥ 0,3 N/mm² (tabelwaarde)	
5.2.2 chloridegehalte	< 0,1 M.-%	
5.6 brandklasse	A1	
5.3.3 waterabsorptie	≤ 0,40 kg/(m²*min0,5)	
5.4.4 waterdampdoorlaatbaarheid	15/35 (tabelwaarde)	
5.4.6 warmtegeleidbaarheid	≤ 0,82 W/(m*K) P = 50% ≤ 0,89 W/(m*K) P = 90% (tabelwaarden)	
5.4.7 duurzaamheid	NPD	
vrijkomende gevaarlijke bestanddelen	NPD	

10. De prestaties van het in de punten 1 en 2 omschreven product zijn conform de in punt 9 aangegeven prestaties. Deze prestatieverklaring wordt verstrekt onder de exclusieve verantwoordelijkheid van de in punt 4 vermelde fabrikant.

Borger, 5 November 2013

Getekend: AGAR Holding BV

Mr. R.M.P.P. Reef
Algemeen directeur

Remix Droge Mortel BV is een werkmaatschappij van Agar Holding BV.

Table A.4 – Declaration of performance for clay masonry mortar (Remix BV).

Name	BM-2
Compressive strength	M5
Compositions	Cement: 1.2 Kg/m³ Hydrated lime: 0.5 kg/m³ Sand: 1.5 kg/m³:

Table A.5 – Declaration of performance of masonry wall ties (www.gb.nl).

GB-Spouwverankering

UNI-L spouwanker

Artikel Informatie

Spouwmaat mm	D mm	L mm	Inlegdiepte buitenblad mm	Inlegdiepte binnenblad mm	Art. nr. (VD)	Art. nr. RVS 304	Art. nr. RVS 316
55 +/- 15	Ø 3,6	170	45-75	40-80	32502	37102	37372
85 +/- 15	Ø 3,6	200	45-75	40-80	32512	37112	37374
115 +/- 15	Ø 3,6	230	45-75	40-80	32522	37122	37376
145 +/- 15	Ø 3,6	260	45-75	40-80	325320	371320	37378
175 +/- 15	Ø 3,6	290	45-75	40-80	325420	371420	37380
115 +/- 15	Ø 4	230	45-75	40-80	32524	37124	37324
145 +/- 15	Ø 4	260	45-75	40-80	32534	371340	37334
160 +/- 15	Ø 4	275	45-75	40-80	+	371345	37336
175 +/- 15	Ø 4	290	45-75	40-80	32544	371440	37344
205 +/- 15	Ø 4	320	45-75	40-80	32554	371445	37354
115 +/- 15	Ø 5	230	45-75	40-80	32526	-	-
145 +/- 15	Ø 5	260	45-75	40-80	32536	-	-
175 +/- 15	Ø 5	290	45-75	40-80	32546	37162	37362
205 +/- 15	Ø 5	320	45-75	40-80	32556	37164	37364
235 +/- 15	Ø 5	350	45-75	40-80	32566	37166	37366
285 +/- 15	Ø 5	400	45-75	40-80	32576	37168	37368

Technische tekening

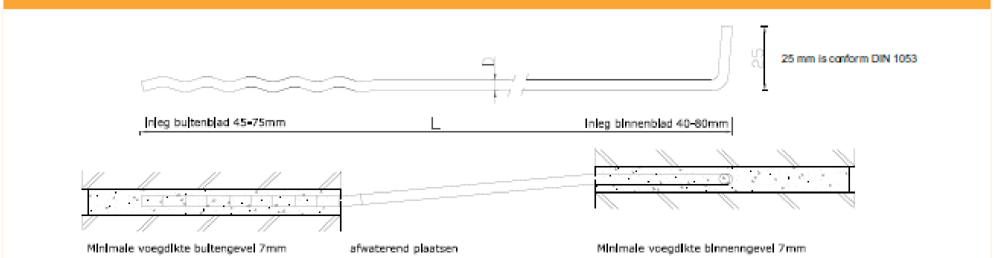

Sterktewaarden

Treksterkte

	Frep (karakteristieke waarde)	Fu;d (rekenwaarde)
Binnenblad, verankering ≥ 40 mm	2,0 kN	1,4 kN
Buitenblad, verankering ≥ 45 mm	1,7 kN	1,2 kN

Fu;d volgt uit $F_{u;d} = \frac{F_{rep}}{\gamma_m}$ γ_m = materiaalfactor 1,4 (als het anker op trek belast is)

Druksterkte (rekenwaarde)

Spouwbreedte max (mm)	Fu;d Ø 3,6 mm	Fu;d Ø 4 mm	Fu;d Ø 5 mm
70	0,50 kN	0,66 kN	-
90	0,44 kN	0,61 kN	-
110	0,40 kN	0,56 kN	1,12 kN
120	0,38 kN	0,53 kN	1,08 kN
130	0,36 kN	0,50 kN	1,03 kN
140	0,34 kN	0,48 kN	0,99 kN
150	0,32 kN	0,45 kN	0,94 kN

Spouwbreedte max (mm)	Fu;d Ø 3,6 mm	Fu;d Ø 4 mm	Fu;d Ø 5 mm
160	0,30 kN	0,43 kN	0,90 kN
170	0,28 kN	0,40 kN	0,86 kN
180	0,26 kN	0,38 kN	0,82 kN
190	0,25 kN	0,36 kN	0,78 kN
220	-	0,34 kN	0,70 kN
250	-	-	0,55 kN
300	-	-	0,41 kN